COUMARIN ALDEHYDE CHEMOSENSORS

FOR SELECTIVE RECOGNITION OF NEUROTRANSMITTERS

A Dissertation

presented to

the Faculty of the Graduate School

at the University of Missouri-Columbia

In Partial Fulfillment

of the Requirements for the Degree

Doctor of Philosophy

---

by

KENNETH S. HETTIE

Dr. Timothy E. Glass, Dissertation Supervisor

May 2014

The undersigned, appointed by the dean of the Graduate School, have examined the dissertation entitled

COUMARIN ALDEHYDE CHEMOSENSORS FOR SELECTIVE RECOGNITION OF NEUROTRANSMITTERS

presented by Kenneth S. Hettie,

a candidate for the degree of doctor of philosophy

and hereby certify that, in their opinion, it is worthy of acceptance.

_____

Dr. Timothy Glass

_____

Dr. Kent Gates

_____

Dr. Michael Harmata

_____

Dr. Sheila Grant

ACKNOWLEDGEMENTS

Many thanks to the members of my graduate committee: Drs. Gates, Harmata, and Grant for your thoughtful guidance, patience, and accommodations throughout the doctoral process. Additional thanks goes to Drs. Lever, Glaser, and Gillis for various means of support.

Thank you to Alexander Jurkevic and Xin “Alice” Liu for assistance with fluorescence microscopy experiments. You were both an invaluable part of the process and I enjoyed working with you very much.

Thank you to the Glass Group members: Chris, Shana, Jae, Jamie, Jamison, Shaohui, Chun, Yuksel, Chad, Xiaole, Patrick, Nick, Selina, C.W., Kang, Tam, and Le. Good luck to you all in the future. I would especially like to acknowledge Dr. Glass for many hours spent with me brainstorming, trouble-shooting, and mentoring throughout numerous struggles in research and life alike. The ability to work alongside Dr. Glass has been a privilege and honor.

Lastly, thank you to my wife, Jess, my parents, Bill and Shelley Hettie, and to the rest of my family who has shown tremendous support and encouragement.

TABLE OF CONTENTS

LIST OF FIGURES

LIST OF TABLES

ABSTRACT

Here, we present a series of fluorescent sensors based on the coumarin-3-aldehyde scaffold intended to sense primary amine neurotransmitters. Discussed are the major design considerations, syntheses, initial UV/Vis and fluorescence titrations, and fluorescence microscopy studies in living cells.

NeuroSensor 521 was developed as a turn-on molecular sensor for norepinephrine and dopamine. It was designed to bind with lower affinity in order to monitor dynamic changes in neurotransmitter concentrations and was validated in both live and fixed cells. The sensor selectively bound to norepinephrine- over epinephrine-containing chromaffin cells producing prominent punctate fluorescence which is indicative of uptake into secretory granules.

The NeuroSensor 521 model was used to produce 17 benzene- or thiophene-based derivatives which differed only at the coumarin C4-substituent. The substituents ranged from very electron-donating to very electron-withdrawing and modulated the fluorescence of the fluorophore by changing the E_{HOMO} levels and thereby the ability of various analytes to quench the fluorescence by photoinduced electron transfer (PET). A thorough computational analysis was bolstered by experimental fluorescence titrations.

Lastly, a near-infrared (NIR) sensor was developed for the turn-on fluorescent sensing of serotonin, a known fluorescence-quenching analyte. The electron-rich sensor gave a fluorescence increase upon titration with serotonin and was shown to bind norepinephrine in chromaffin granules giving punctate fluorescence with an excitation of 633 nm and an emission of 710 nm.

CHAPTER ONE

Introduction

1.1 Fluorescent Sensors

Fluorescent chemosensors are abiotic supramolecular devices or "hosts" that transform chemical information into measurable analytical signals via interactions with an analyte or "guest" (Figure 1-1).[1] The intracellular detection of biologically important guests requires that fluorescent chemosensors exhibit selectivity, sensitivity, and solubility in aqueous environments.[2]

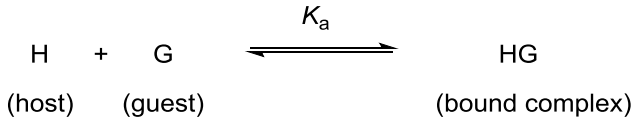

Figure 1-1. Equilibrium of host-guest binding

Fluorescent chemosensors bind to the analyte via non-covalent interactions (i.e. hydrophobic interactions, hydrogen bonding, metal coordination, electrostatic interactions, etc.) or reversible covalent bond formation.[1, 3] Sensors possess a receptor, an optical reporter, and a signal transduction mechanism that communicates between the two (Figure 1-2).

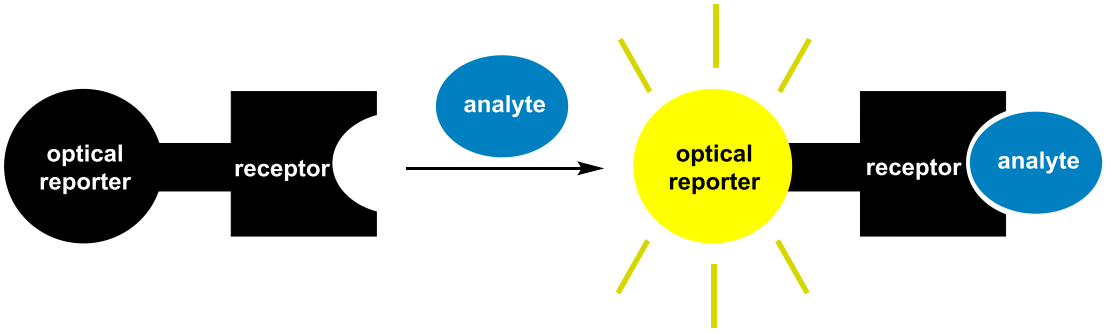

Figure 1-2. Binding of an analyte guest to a chemosensor host

Signal transduction mechanisms exclusive to fluorescence sensing include internal charge transfer (ICT), photoinduced electron transfer (PET), and Förster resonance energy transfer (FRET).[4] PET and ICT, in particular, have been widely employed for amino acid, diamine, and amine chemosensors.[3b]

1.2 Signal Transduction Mechanisms

1.2.1 Internal Charge Transfer (ICT)

For internal charge transfer mechanisms, the receptor is directly conjugated to the pi system of the fluorophore. Electrons are transferred across the pi system from a donor group to an acceptor group. The energy of the ICT state is determined by the interaction of the solvent and/or the bound guest molecule with the donor/acceptor groups.[3a] Chemosensors using an ICT mechanism have been developed for numerous biological analytes including amines, saccharides, and metal ions (Figure 1-3).[5,6,7,8]

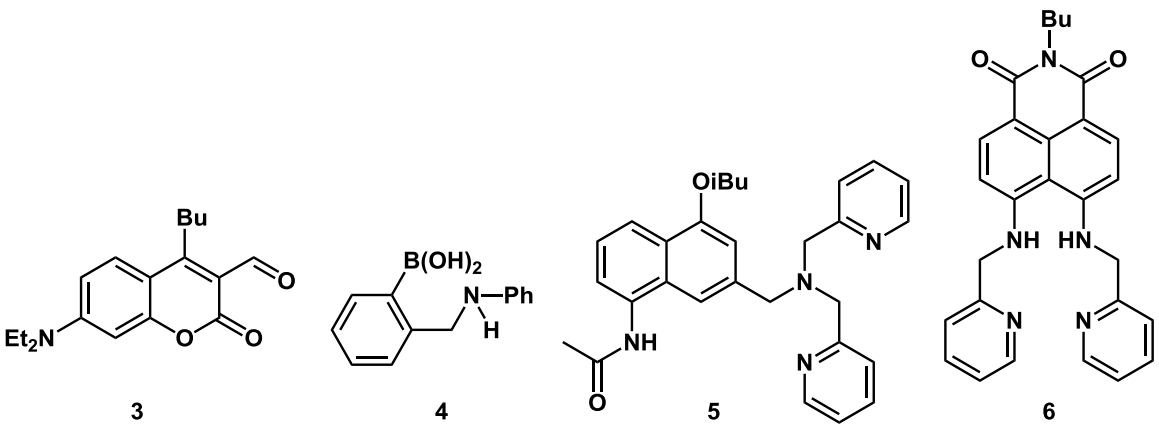

Figure 1-3. Sensors that use an ICT signal transduction mechanism

1.2.2 Photoinduced Electron Transfer (PET)

Photoinduced electron transfer requires two non-conjugated components: a fluorophore and either an electron-donating group or an electron-withdrawing group.[9] Two methods, acceptor-PET (a-PET) and donor-PET (d-PET), will be described later in detail. The literature is replete with chemosensors based on the PET transduction mechanism (Figure 1-4). [9-10 11]

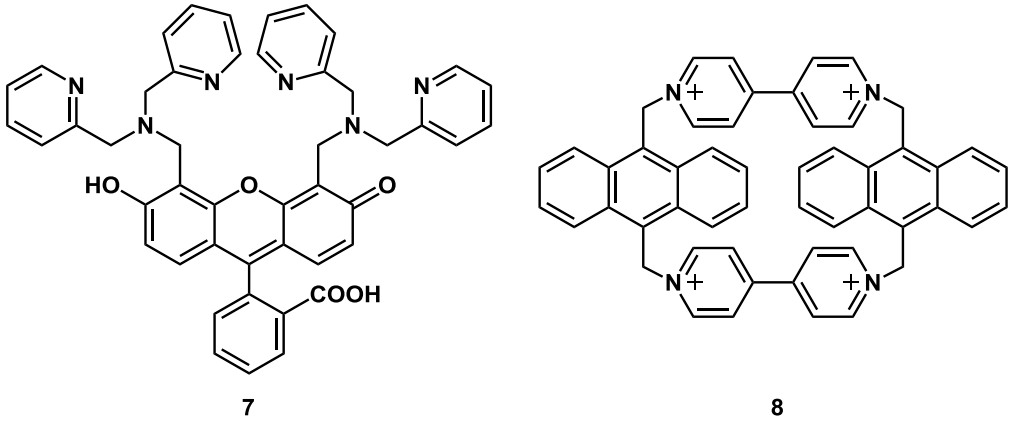

Figure 1-4. Sensors that use a PET signal transduction mechanism

1.2.3 Förster Resonance Energy Transfer (FRET)

FRET involves the transfer of energy from an excited donor fluorophore to an acceptor fluorophore in its ground state (Figure 1-5).[12] For FRET to occur between a linked donor-acceptor pair, two criteria must be met: i) there must be significant spectral overlap between the fluorescence of the donor and the absorbance of the acceptor; ii) the pair must have an optimal distance of separation known as the "Förster distance" which is usually ~20-60 Å and is defined as the distance at which the resonance energy transfer is 50% efficient.[13]

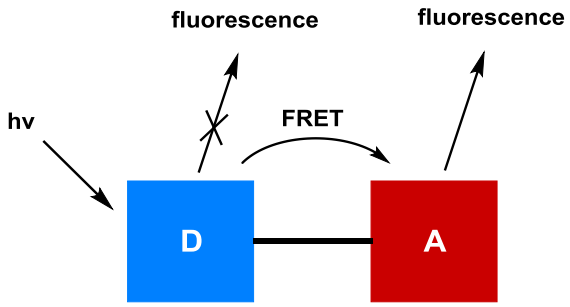

Figure 1-5. FRET mechanism between a linked donor (D) and accepter (A) pair

FRET-based sensors have been used widely in biological studies, especially for the evaluation of protein folding and protein-protein interactions. The donor-acceptor pairs can either be fluorescent proteins, or proteins tagged with fluorophores. Due to the distance-dependence of the FRET efficiency, both spatial and temporal information can be gleaned.[12] Other experiments have included placing a conformationally-sensitive protein between a FRET pair. Experimental

results coupled with mathematical analysis can elucidate a signaling pathway's negative feedback or biostability. [2, 14]

1.3 Neurotransmitters

1.3.1 Background

Neuronal communication involves the transmission of chemical messengers or neurotransmitters from one neuron to the next across the synaptic cleft. The neurotransmitters packaged in high millimolar concentrations in intracellular compartments called vesicles.[15,16] One commonality of many small molecule neurotransmitters is the presence of an amine functional group (Figure 1-6). The amine can be used as a recognition unit for molecular sensors.

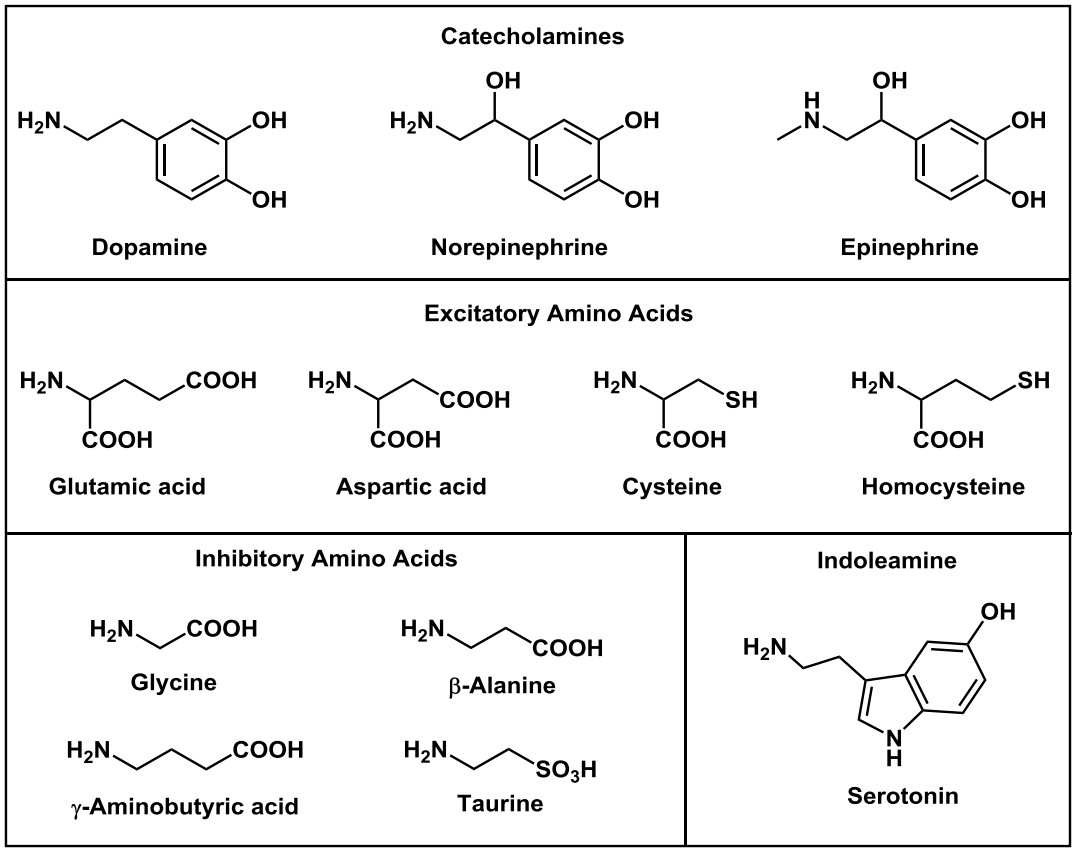

Figure 1-6. Structures of various amine neurotransmitters

The neurosecretory vesicles are acidic compared to the cytosol (pH ~5.5 and 7.2, respectively) which is important to the accumulation and retention of amine neurotransmitters.[17,18,19,20] Most neurotransmitters are taken up into the vesicle against a proton or electrochemical gradient. Catecholamines, for example, utilize the vesicular monoamine transporter (VMAT) protein which exchanges protons in the vesicle for neurotransmitters (Figure 1-7). V-ATPase uses ATP to pump protons into the vesicular lumen. The protons accumulate and lower the pH within the vesicle. VMAT exchanges protons for catecholamines until a large gradient has been built against the cytosol.

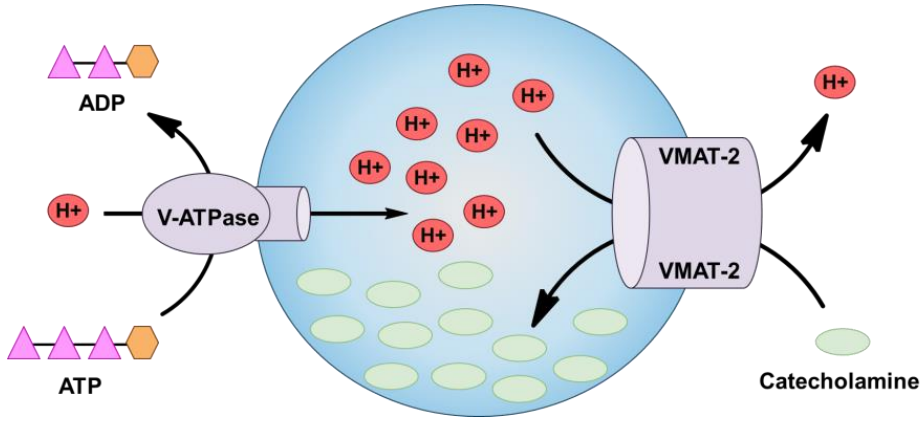

Figure 1-7. Catecholamine uptake into secretory vesicles. V-ATPase uses ATP to pump protons into the vesicle while VMAT-2 exchanges the protons for catecholamines.

Synaptic small dense-core vesicles (SDCV) and large dense-core vesicles (LDCV or chromaffin granules) are the two morphologically distinct types of neurosecretory vesicles that mediate regulated secretion in neurons. Approximately 21,600 – 30,000 LDCVs account for over 30% of the total chromaffin cell volume.[21] In general, synaptic SDCVs primarily contain classical neurotransmitters, namely acetylcholine (ACh), γ-aminobutyric acid (GABA), and glutamate. In contrast, synaptic LDCVs primarily contain adenosine triphosphate (ATP), calcium, catecholamines, chromogranins, neuropeptide Y (NPY), and opioid peptides. More specifically, the synaptic LDCVs within chromaffin cells of the adrenal medulla synthesize, sequester, and release the catecholamines norepinephrine (noradrenaline) and epinephrine (adrenaline) in high concentrations (0.5-1.0 M).[15,16]

Dopamine β-hydroxylase (DBH) is a hallmark protein of noradrenergic cells that is responsible for the synthesis of norepinephrine (Figure 1-8).[22] DBH is specifically

expressed in norandrenergic neurons and chromaffin cells of the adrenal medulla and catalyzes the oxidative hydroxylation of dopamine to form norepinephrine. The enzyme phenylethanolamine N-methyltransferase (PNMT) is responsible for the subsequent conversion of norepinephrine to epinephrine.

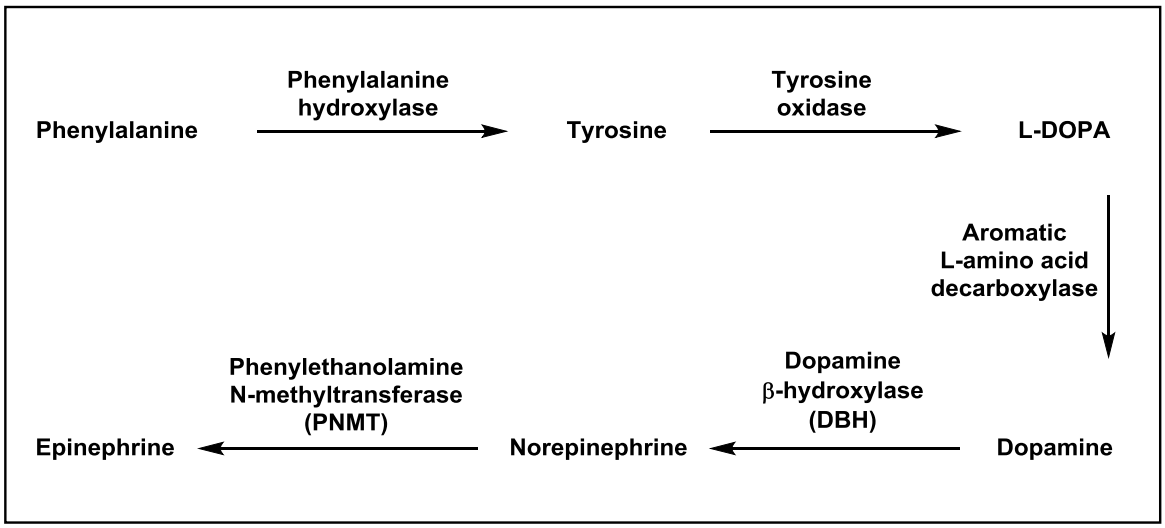

Figure 1-8. Synthetic pathway for catecholamine neurotransmitters

PNMT is specifically expressed in chromaffin cells of the adrenal medulla and catalyzes the N-methylation of norepinephrine to form epinephrine. PNMT serves as the classical specific enzyme marker in enzyme assays to differentiate two putative subpopulations of chromaffin cells of the adrenal medulla: epinephrine- and norepinephrine-containing chromaffin cells. Traditionally, chromaffin cells expressing PNMT (termed andrenergic) primarily store and secrete epinephrine, whereas chromaffin cells lacking PNMT (termed norandrenergic) primarily store and

secrete norepinephrine. In addition to the traditional immunocytochemical PNMT enzymatic assay, the conventional protocol that entails the physical separation and isolation of chromaffin cells by centrifugation through density gradients permits the similar ascription to chromaffin cells phenotypes (epinephrine- and norepinephrine-containing).[23] Both the traditional PNMT enzymatic assay and the conventional physical isolation protocol and their associated mutually exclusive epinephrine- and norepinephrine-containing designation amongst chromaffin cells results in the misrepresentation of catecholamine stores in chromaffin cells.

Cyclic voltammetry and liquid chromatography analyses distinguish three subpopulations of chromaffin cells based on epinephrine:norepinephrine ratios of total catecholamine stores.[23,24,25,26] Chromaffin cells that store and release ≥80% epinephrine or norepinephrine are similarly designated as epinephrine- or norepinephrine-containing chromaffin cell subpopulations, respectively, and account for approximately 75% of all chromaffin cells. The third subpopulation amongst chromaffin cells store and secrete both epinephrine and norepinephrine between 20% – 80% epinephrine:norepinephrine and accounts for approximately 25% of all chromaffin cells. Therefore, all chromaffin cells traditionally obtained and designated as epinephrine-containing and norepinephrine-containing by means of conventional physical separation or traditional PNMT assay do contain variable amounts of their norepinephrine and epinephrine counterpart, respectively.

The catecholamines serve as the principal neurotransmitters in the sympathetic nervous system and are critical to many physiological and cognitive

functions.[15,16,27,28] Dopamine helps regulate attention, arousal, cognition, reward, and motor activity in the central nervous system. Abnormalities in dopaminergic biosynthesis and impaired neurotransmission are linked to many neurodegenerative and psychiatric disorders that include bipolar disorder, depression, Tourette's syndrome, schizophrenia, and Parkinson's disease.[29,30,31] The gradual loss of dopamine producing neurons and concomitant loss of dopamine input to forebrain motor structures eventually leads to the classical debilitating motor symptoms such as resting tremor, muscular rigidity, and bradykinesia.[32] Due to the high prevalence and devastating effects of these neurological disorders, a significant physical, emotional, and financial toll is placed on Americans today (Figure 1-9).

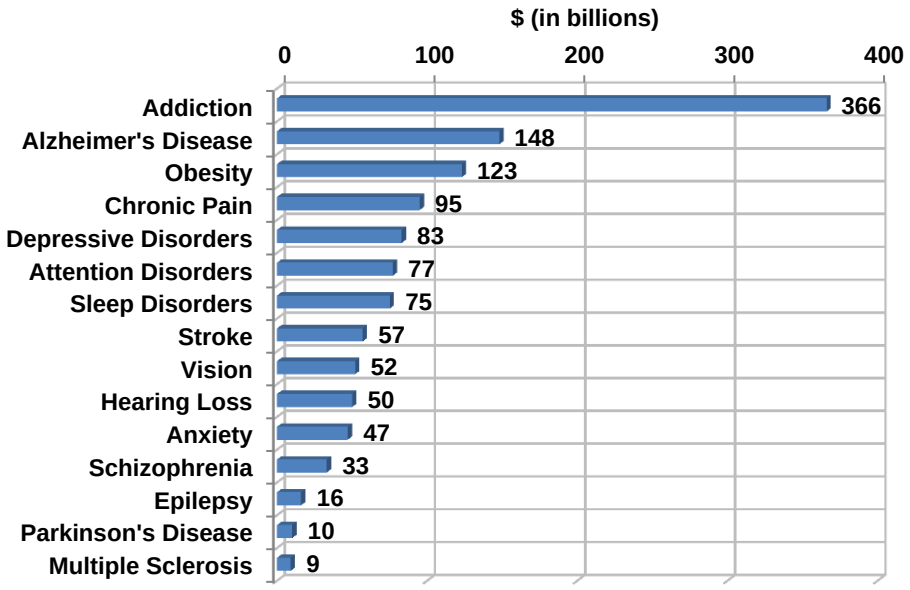

Figure 1-9. Annual national economic burden of brain-related disorders as of 2007 (in billions). Sources include: Neuroinsights, Office of Nat'l Drug Policy, Nat'l Institute of Diabetes, Alz Assoc., Duke University, American Psych. Association, Harvard, Nat'l Sleep Found., American Stroke Assoc., Prevent Blindness America, CDC, Journal of Clinical Psych, Epilepsy Foundation, Cost of Brain Disorders Europe. Obtained from http://scienceprogress.org/2007/10/brain-tech-is-here/.

Similarly, norepinephrine regulates many critical functions that include attention, memory, learning, emotion, and autonomic and cardiovascular function (*e.g.*, heart rate and blood pressure). In the periphery, norepinephrine increases heart rate, cardiac contractility, vascular tone, renin-angiotensin system activity, and renal sodium reabsorption. Norepinephrine deficiency is characterized by severe deficits in autonomic regulation of cardiovascular function that leads to orthostatic hypotension and cardiovascular disease. Extreme abnormalities of norepinephrine concentration levels lead to several diseases such as neuroblastoma, ganglioneuroblastoma, ganglioneuroma, paraganglioma, and diabetes mellitus ketoacidosis.[33] Most importantly, dysregulated biosynthesis and neurotransmission of norepinephrine has been widely implicated in the pathophysiology of both Parkinson's disease and attention-deficit hyperactivity disorder (ADHD).

1.3.2 Conventional Detection Methods

Conventional methods for the detection of small molecule neurotransmitters include autofluorescence, histochemical staining, electrochemistry, and fluorescence tracers.

Autofluorescence

The catecholamines and serotonin contain aromatic groups which are observed in the UV/Vis spectral range. The respective absorption and emission bands for these analytes are at 290 nm and 340 nm for serotonin,[34] 280 nm and 317 nm for norepinephrine,[35] 280 nm and 317 nm epinephrine, and 279 nm and 315 nm for

dopamine.[36] Basifying from pH 5 to 10 causes the absorbance to shift to the red and the fluorescence to decrease. The fluorescence quenching of catecholamines is attributed to their oxidation in alkaline solutions (Figure 1-10).

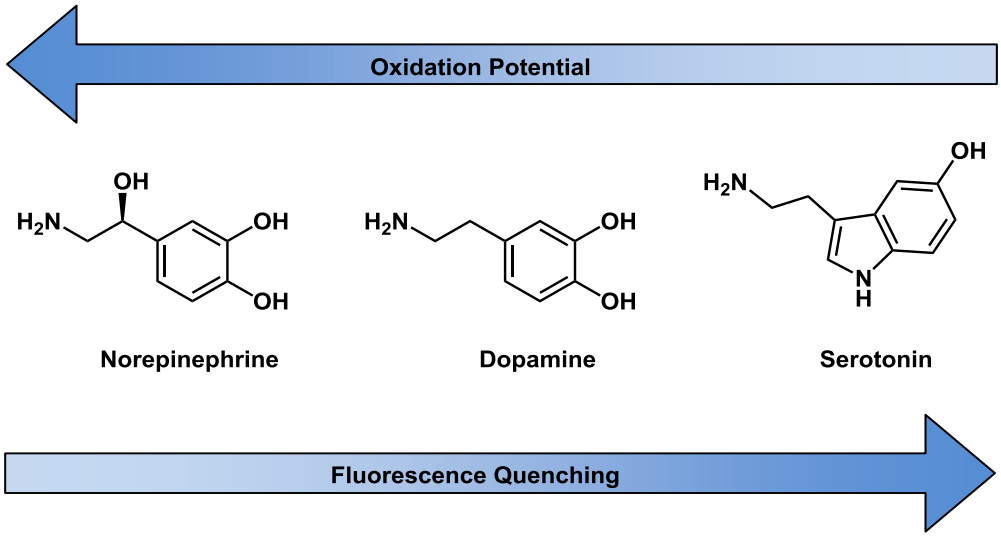

Figure 1-10. Relationship between catecholamine oxidation potential and fluorescence quenching

Histochemical Staining

Histochemistry involves the identification of the chemical constituents in cells and tissues and can be both qualitative and quantitative in nature.[37] This technique typically involves isolation, fixation, and sectioning of a tissue followed by treatment with a stain or indicator and observation with microscopy. Using this method, it was determined that neurotransmitters and peptides were colocalized in rat and monkey brainstem tissue.[38] It has also been used to monitor the localization of exogenous dopamine and serotonin in nematodes.[39]

Electrochemistry

Electrochemical methods, which may include potentiometry, coulometry, or voltammetry, are also useful in neurochemistry for several reasons: i) action potentials are required for neuronal exocytosis, ii) many neurotransmitters can be detected oxidatively (*e.g.* dopamine, acetylcholine, norepinephrine, serotonin, glutamic acid, and GABA), iii) high temporal resolution enables evaluation of biological events oftentimes occurring on a millisecond timescale (*e.g.* synaptic firing), and iv) small electrodes can monitor very localized regions.[40] Electrochemical methods have been used to measure dopamine content in individual synaptic vesicles (carbon-fiber microelectrodes (CFM)),[41] assess the differences in the regulation of dopamine versus serotonin (CFM),[42] and obtain measurements of both the membrane capacitance as well as the released transmitter (patch amperometry, Figure 1-11).[43]

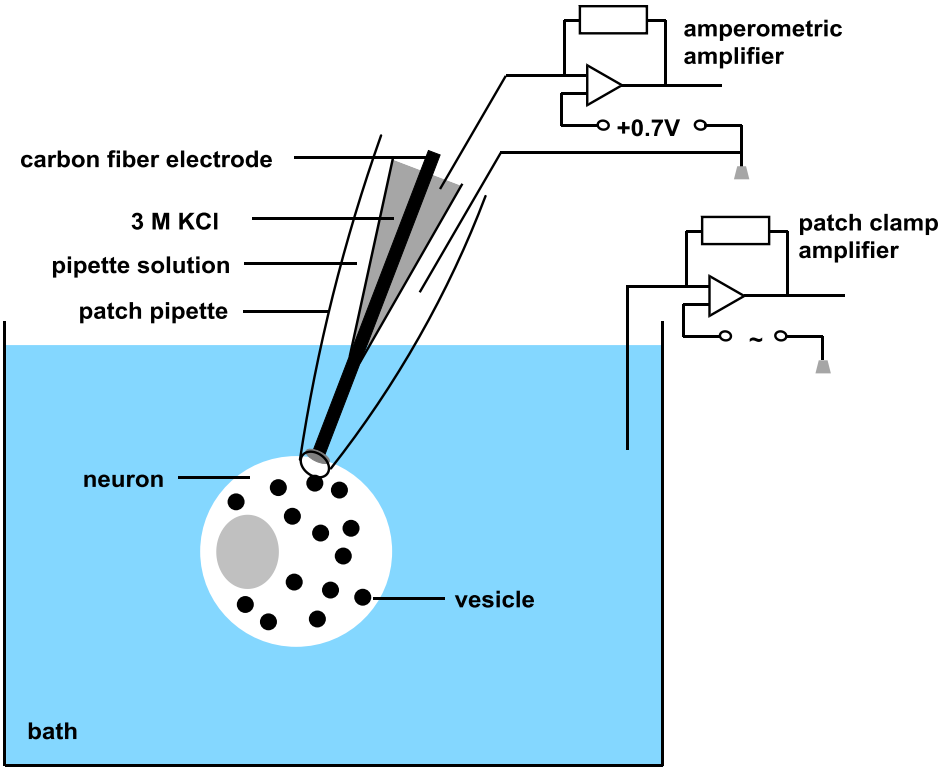

Figure 1-11. Patch amperometry configuration

As mentioned previously, the oxidation of neurotransmitters at neutral pH enables facile detection via electrochemical methods. Catecholamines, in particular, oxidize to quinones and can give cyclized derivatives (Figure 1-12). The oxidized catecholamines tend to quench fluorescence which will be addressed in Chapter 3.

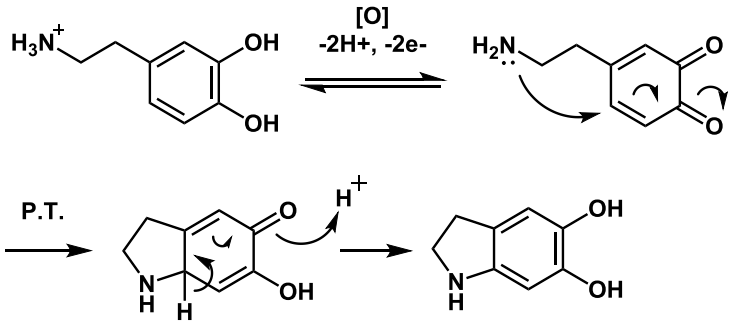

Figure 1-12. Oxidation and cyclization of dopamine. P.T. = proton transfer.

Tracers

Tracers called "fluorescent false neurotransmitters" (FFNs) have been developed by the Sames group as neurotransmitter mimics.[44] The sensors are taken up into the vesicle by the vesicle monoamine transporter, VMAT2. Using these sensors, they discovered that the number of vesicle fusion and firing events was dependent upon the frequency of stimulation applied.[44a] Application of electrical stimulus resulted in destaining of the striatal mouse brain slices. pH-sensitive versions were also developed and enabled quantification of vesicular pH, as well as visualization of enhanced background fluorescence upon stimulation indicating release of the vesicular contents into the synaptic cleft.[44b, 44c]

1.3.3 Molecular Recognition Methods

Other methods for neurotransmitter detection using molecular recognition include bioorganic receptors, inclusion complexes, and boronic acid-based receptors.

Bioorganic receptors

There are several examples of bioorganic receptors for neurotransmitters in the literature.[45,46,47,48,49,50] One example includes target-binding aptamers with appended pH-sensitive fluorophores. The fluorescence changes upon analyte-binding due to the slightly altered pH of the microenvironment. [51] Another strategy has been to encapsulate target-binding enzymes in quantum dot (QD) hydrogels (Figure 1-13).[52] When dopamine was added to one such QD hydrogel, it bound to the enzyme and caused a decrease in fluorescence due to dopamine oxidation to its quinone derivative. Pitfalls of this method include the limited use with aqueous media due to changes in gel porosity and reduced enzymatic activity upon dehydration of the gel.

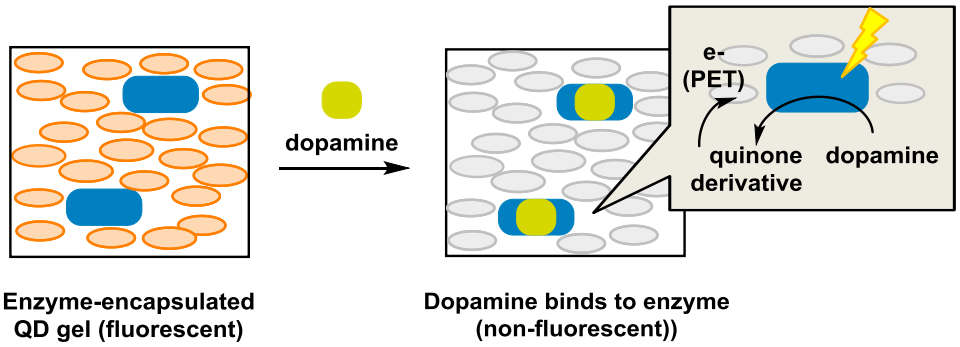

Figure 1-13. Dopamine sensing using enzyme-encapsulated QD hydrogels

Inclusion Complexes

Inclusion complexes, which may include calixarenes, cucurbiturils, cyclodextrins, porphyrins, and other macrocycles have also been developed for the detection of neurotransmitter analytes.[53,54,55,56,57]

Cucurbituril CB7 was developed to evaluate how the fluorescence properties of 4',6-diamidino-2-phenylindole (DAPI), a fluorescent dye, change as it binds inside the cavitand (Figure 1-14A).[57] A competition study was conducted where CB7 was complexed with various analytes before DAPI is added. The DAPI displaces the alternate analytes which induces a fluorescence increase at 470 nm. This permits determination of binding constants which was shown to be very high for dopamine (1×10^5 M^{-1}).

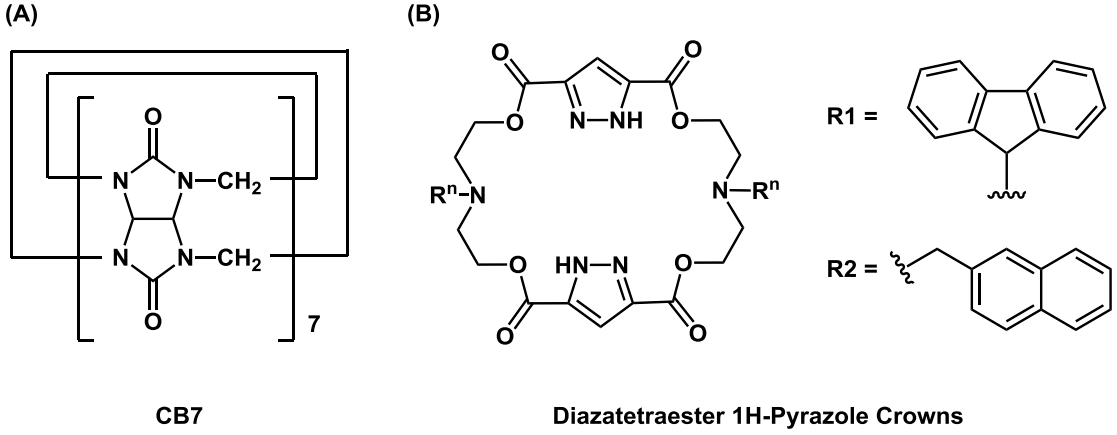

Figure 1-14. Macrocyclic sensors for dopamine: a) Structure of CB7, and b) diazatetraester 1H-pyrazole crowns.

Other examples of macrocyclic binding to neurotransmitters are diazatetraester 1H-pyrazole crowns for the detection of amphetamines and dopamine (Figure 1-

14B).[55] The R^1-substituted and R^2-substituted crowns bound to dopamine with affinities of 5.6 x 10^5 M^{-1} and 3.8 x 10^7 M^{-1}, respectively. Molecular modeling calculations suggested stabilizing hydrogen bonding between the protonated ethylamine in dopamine and the esters and/or pyrazoles of the crown as well as between the catechol of dopamine and the carbonyl oxygens of the crown. A drawback of this work were the titration conditions (70:30 water/ethanol) which do not realistically exemplify the efficacy of detection in physiological environments.

Boronic Acid Receptors

Neurotransmitters containing catechol moieties (*e.g.* dopamine, norepinephrine, and epinephrine) can be detected via the diol using boronic acid receptors. Yoon and coworkers, for example, developed a fluorescent chemosensor composed of imidazolium, pyrene, and boronic acid components (Figure 1-15).[58] The boronic acid of the receptor reversibly forms a boronate with the diol in pH 7.4 buffer/MeCN (95:5) and quenches the fluorescence upon binding by over 6-fold. The excimer emission at 470 nm was dominant over the monomer peak at 355 nm.

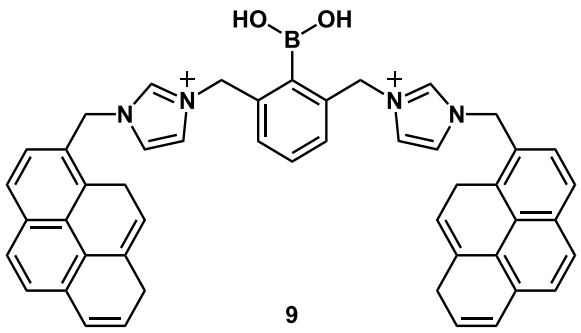

Figure 1-15. a) Turn-off fluorescent pyrene-based boronic acid receptor for catechols[58]

Our group developed a ditopic sensor for dopamine that binds to the analyte amine *and* boronic acid.[59] This sensor will be discussed further in Chapter 2, but it should be noted that it, too, gave a "turn-off" fluorescence response when bound to dopamine.

CHAPTER TWO

Coumarin Aldehyde Sensors

2.1 Coumarin Aldehyde with Tethered Boronic Acid

Our group has labored toward creating fluorescent sensors for neurotransmitters based on the coumarin aldehyde scaffold.[60,61] The sensor is composed of a coumarin fluorophore, an amine-binding aldehyde unit and an alkyl or aryl C4 substituent that either modulates binding by providing a secondary interaction with the analyte or modulates fluorescence by altering the electronic properties of the molecule (Figure 2-1).

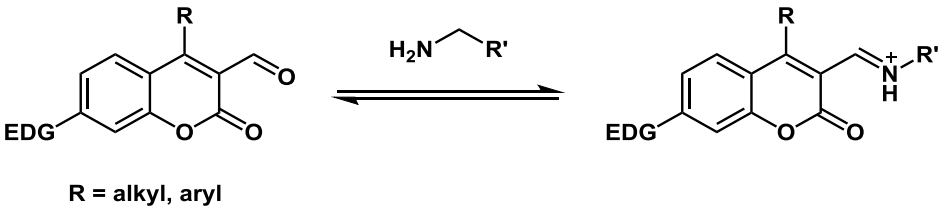

Figure 2-1. Reversible binding of coumarin aldehyde sensors to primary amine analytes

The sensor functions by an ICT signal transduction mechanism where an electron-donating group (EDG) at the coumarin 7-position donates charge through the pi system to the electron acceptor at the 3-position. When the primary amine of the analyte binds to the aldehyde of the sensor, an iminium ion is formed which creates a better,

positively-charged acceptor. This induces a bathochromic shift in absorbance. By using an excitation wavelength corresponding to the bound sensor, a fluorescence increase can be observed in response to analyte addition.

Compound **10** was first developed as a selective fluorescent sensor for dopamine and norepinephrine (Figure 2-2).[59] The sensor aldehyde and boronic acid reversibly bind to the analyte amine and diol, respectively. Epinephrine is the only catecholamine neurotransmitter that cannot bind because it possesses a secondary amine which cannot form imines with aldehydes.

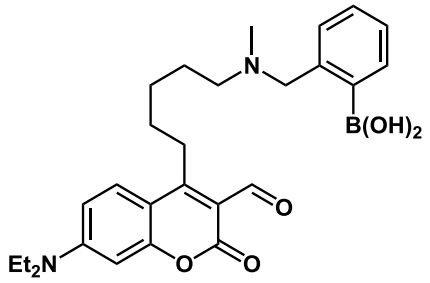

10

Figure 2-2. Fluorescent molecular sensor for dopamine and norepinephrine.

The sensor demonstrated strong binding toward dopamine and norepinephrine (3400 M^{-1} and 6500 M^{-1}, respectively) and weak binding toward other primary amine analytes that lack a catechol group like glutamic acid and lysine (6.8 M^{-1} and 4.0 M^{-1}, respectively). As indicated previously, binding to the analyte induced a bathochromic shift in the absorbance by ~35 nm (Figure 2-3). The sensor, however, was quenched by all catecholamine analytes indicating that the bound species in each case was not emissive. For practical applications, the substantially high binding constants to

norepinephrine and dopamine prohibit the monitoring of dynamic changes in neurotransmitter concentrations as the sensor will be almost completely in its bound state.

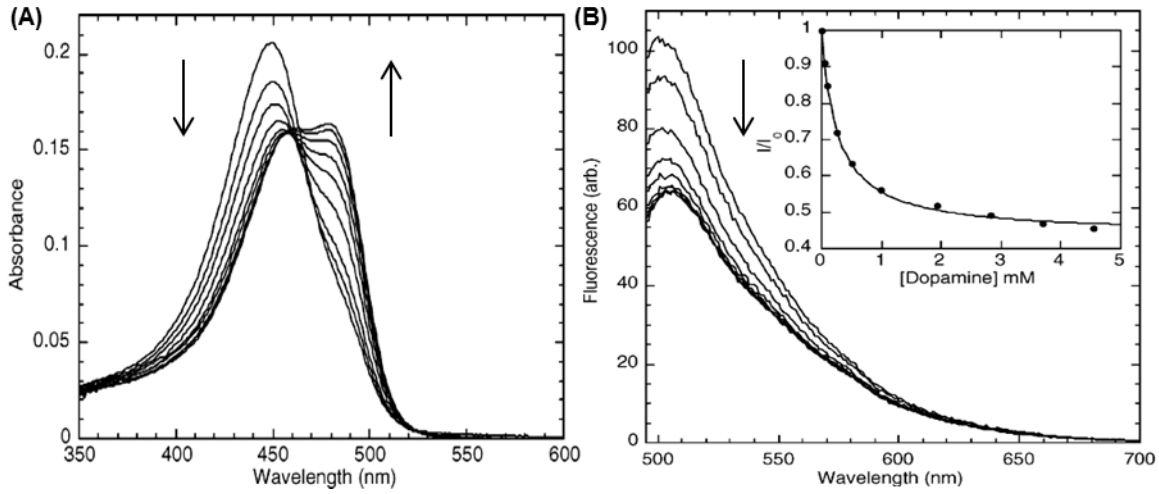

Figure 2-3. (A) UV/Vis and (B) fluorescence spectra of compound **8** (10 μM) with dopamine in buffer (100 mM $Na_2S_2O_3$, 50 mM HEPES, 20 mM NaCl, pH 7.0). λ_{ex} = 484 nm. λ_{em} = 500 nm. Inset is the fit to a binding isotherm.

2.2 NeuroSensor 521

2.2.1 Design

To afford, a turn-on fluorescence response to catecholamines, NeuroSensor 521 (NS521) was developed (Figure 2-4). This sensor was altered to have only one binding site as opposed to sensor **10** which possessed two. Here, only the aldehyde group would associate with the analyte amines which would still induce a bathochromic shift upon analyte binding due to the formation of the iminium ion. Instead of a boronic acid group, a *p*-methoxyphenyl moiety was incorporated to modulate the fluorescence properties of the coumarin such that it would not be

quenched by the catechol group. It was anticipated that the lack of a boronic acid recognition unit would lower the affinity of NS521 for catecholamines relative to sensor **10**, but given the extremely high concentration of catecholamines in the secretory vesicles, a lower binding constant was not a concern. In fact, it would permit a more reversible binding interaction so that both increases and decreases in neurotransmitter content could be observed.

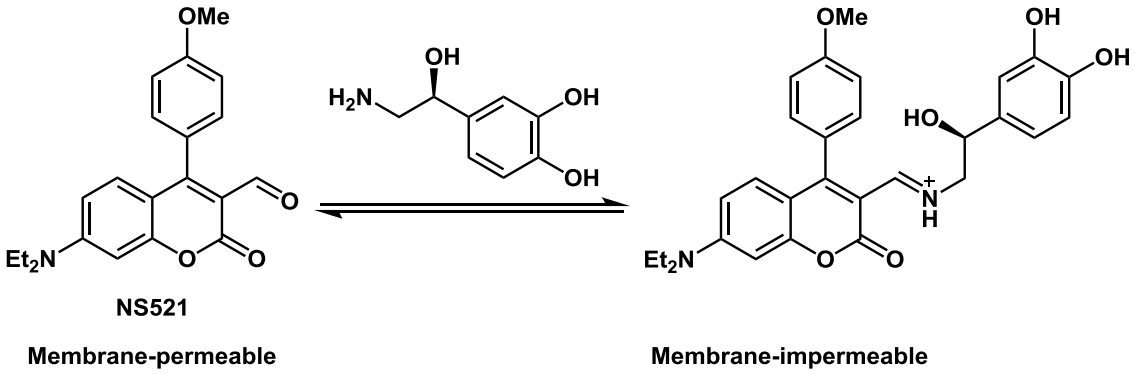

Figure 2-4. Equilibrium of norepinephrine binding to NS521

Another key design parameter involves the net charges of the bound and unbound sensor. When unbound, NS521 is neutrally-charged and membrane-permeable. However, upon binding, the positively-charged iminium ion that is created causes the bound species to become membrane-impermeable. This strategy allows the sensor to enter into the secretory vesicles, bind to the neurotransmitter, and then become trapped due to its cationic state (Figure 2-5). The fluorescence within the vesicle should increase as more of the bound sensor accumulates.

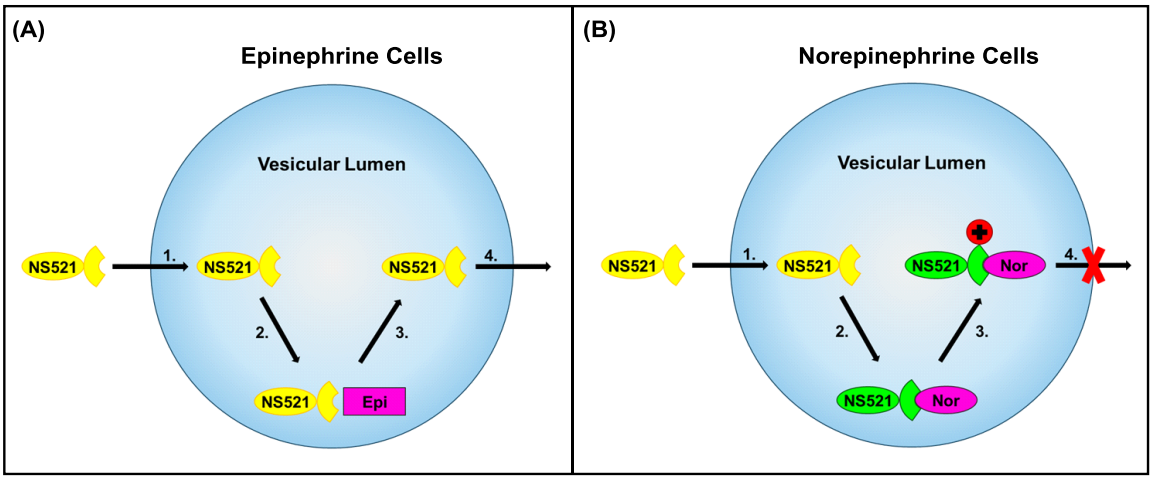

Figure 2-5. Mechanism of selective binding and accumulation of NS521 within norepinephrine-enriched secretory vesicles. (A) Step 1. NS521 enters secretory vesicular lumen. Step 2. NS521 does not bind to epinephrine (Epi) and does not fluoresce. Step 3. NS521 does not form a charged complex. Step 4. NS521 translocates across vesicular membrane and exits vesicle. (B) Step 1. NS521 enters secretory vesicular lumen. Step 2. NS521 selectively labels norepinephrine (Nor) and fluoresces. Step 3. NS521-Nor complex is protonated. Step 4. Charged complex cannot translocate across vesicular membrane and accumulates.

2.2.2 Synthesis

NS521 was synthesized in two steps from commercially available starting materials (Figure 2-6). Compound **11** was tosylated followed by a Suzuki coupling with *p*-methoxyphenylboronic acid (**12**) in a one-pot reaction to afford compound **13**. Treatment with the Vilsmeier reagent formylated the coumarin at the 3-position to produce NS521.

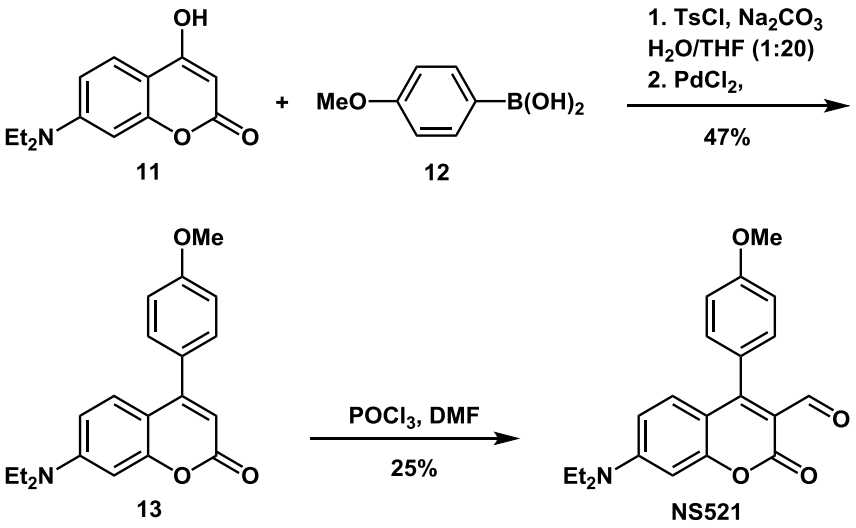

Figure 2-6. Synthesis of NS521

2.2.3 Titrations

NS521 was screened with various relevant amines via absorption and fluorescence spectroscopy. As observed with other sensors in this series,[2] NS521 binds to all primary amines via iminium ion formation, which produces a red shift in absorption from 448 to 488 nm (Figure 2-7). In fluorescence mode, exciting the sensor at 488 nm and adding norepinephrine produced a marked 5.3-fold increase in fluorescence. Table 2-1 summarizes binding and spectroscopic data for the interaction of NS521 and a number of relevant amines. As observed with other sensors in this series,[2] all primary amines bind with low binding affinity and high fluorescence enhancements. Interestingly, catacholamines such as norepinephrine and dopamine have 10-fold higher binding constants than other alkyl amines such as glycine. As with other sensors in the class, NS521 does not interact with secondary amines such as epinephrine.

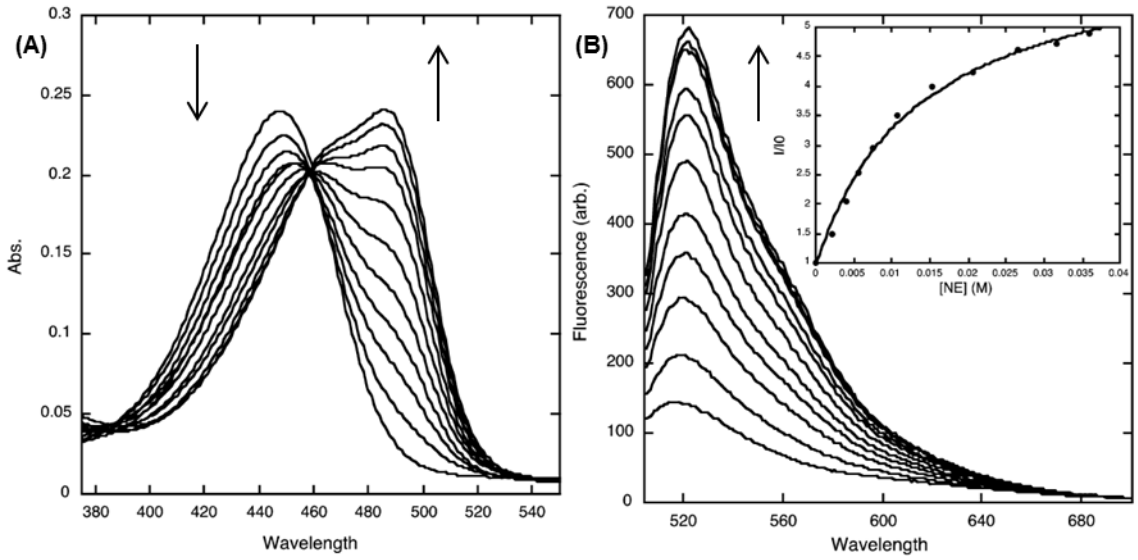

Figure 2-7. (A) UV/Vis and (B) fluorescence spectra of NS521 (10 µM in 25 mM HEPES, 50 mM $Na_2S_2O_3$, pH 5.0) with norepinephrine (λ_{ex} = 488 nm). Inset is the fit to a single-site binding isotherm.

The data in Table 2-1 indicates that the maximum fluorescence response of the catecholamines is lower than that of generic amines such as glutamate. The quantum yield for NS521 was determined both alone and bound to glutamate and norepinephrine. The 3-fold difference in the latter two quantum yields is due to the quenching nature of the catechol group, which can undergo photoinduced electron transfer (PET) to the coumarin fluorophore. Taken together, these data suggest that NS521 will bind more strongly to catecholamines in a cell, but with lower overall fluorescent enhancements.

In a neuroendocrine cell, the concentration of catecholamines (0.5 − 1.0 M) in secretory vesicles is at least an order of magnitude greater than the concentration of other biogenic primary amines.[18,19,20] Thus, the moderate selectivity of NS521 for catecholamines over other biogenic amines coupled with the relatively high

concentrations of catecholamines in secretory vesicles was expected to overcome the lower fluorescence response from the catecholamine. In addition, the unique spectral properties of NS521 allow for monitoring the unbound and bound states using 440 and 488 nm excitation, respectively.

Table 2-1. Binding constants (K_a) and spectroscopic parameters for the binding of NS521 to various analytes

Amine Guest	K_a (M^{-1})[a]	I_{sat}/I_0[b]	Φ_{fl}[c]
Epinephrine	0	nd	nd
Norepinephrine	78	5.4	0.0033
Dopamine	112	3.0	nd
Glutamate	10	7.8	0.0095
Lysine	11	15.1	nd
Glycine	8	11.1	nd
None			0.0053

[a] Binding constants (K_a) were measured by fluorescence spectroscopy, λ_{ex} = 488 nm, λ_{em} = 521 nm. Error in K_a values are ±10% based on triplicate titrations. [b] I_{sat} = fluorescence intensity at saturation taken from the theoretical fit to the binding isotherm. [c] Quantum yields (Φ_{fl}) were calculated using fluorescein as a fluorescence standard (Φ_{fl} = 0.850). nd = not determined.

2.2.4 Cell Studies

From the titration data, it appeared that NS521 could be used to selectively detect dopamine and norepinephrine over epinephrine. Thus, we chose to demonstrate the utility of our method through the selective labeling and direct visualization of norepinephrine in secretory vesicles to distinguish norepinephrine- from epinephrine-enriched populations of chromaffin cells. Chromaffin cells were separated into norepinephrine- and epinephrine-enriched fractions by

centrifugation on a Percoll gradient.[62,63] Both populations were independently incubated with a 0.1 μM solution of NS521 at 37 °C for 30 min and then washed to remove excess sensor and plated. The cells were examined by confocal fluorescence microscopy using 488 nm excitation (Figure 2-8).

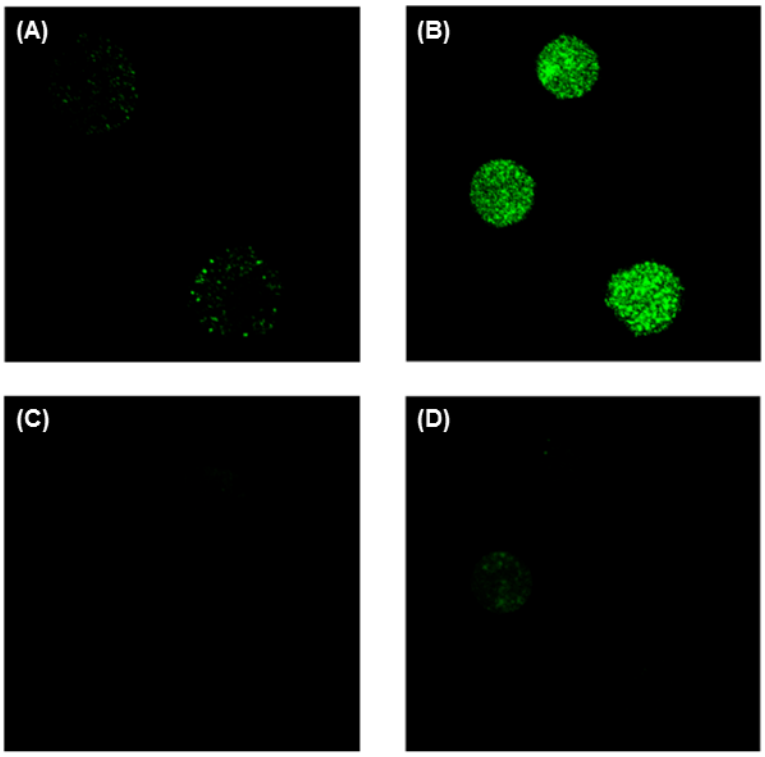

Figure 2-8. Incubation of NS521 (0.1 μM) with chromaffin cells. Epinephrine-enriched cells: (A) λ_{ex} = 488 nm and (C) λ_{ex} = 440 nm. Norepinephrine-enriched cells: (B) λ_{ex} = 488 nm and (D) λ_{ex} = 440 nm.

The norepinephrine-enriched cell population showed strong, punctate fluorescence compared to the epinephrine-enriched cell population, which only showed marginal fluorescence (Figure 2-8A,B). The punctate fluorescence pattern is consistent with secretory vesicles in chromaffin cells. These results indicate that the

sensor is able to enter the vesicle and bind to norepinephrine selectively over epinephrine, as anticipated. The low fluorescence response observed within the epinephrine-containing chromaffin cells was attributed to the binding of NS521 to the low concentration of norepinephrine present in these vesicles. Next, the cells were excited at 440 nm to selectively excite any potential unbound sensor, although some excitation of bound sensor is expected at this wavelength (Figure 2-8C,D). Weak fluorescence was observed in both cell populations, though again more in the norepinephrine-enriched population. These data suggest that little sensor remains in the epinephrine-enriched cell population.

This result supports the notion that NS521 accumulates in vesicles, which is not surprising for a neutral compound that forms a charged complex upon interaction with the target analyte. The charged complex presumably cannot cross the vesicle membrane and thus becomes trapped (Figure 2-5).[4] Thus, the higher fluorescence in the norepinephrine-containing cells is a result of the high concentration of primary catecholamine in the vesicles, which causes accumulation of the sensor in these vesicles. Lacking significant concentrations of primary catecholamines, the epinephrine-containing cells do not accumulate the sensor and show lower fluorescence. The overall low background fluorescence is remarkable given the rather promiscuous binding of NS521 to primary amines. Here the rather low affinity of the sensor for binding amines actually confers an advantage for selective labeling of high concentrations of primary amine analytes in secretory vesicles.

To further validate the selective labeling of norepinephrine-containing vesicles, we labeled fixed cells using an antibody against phenylethanolamine *N*-methyltransferase (PNMT), an enzyme that converts norepinephrine to epinephrine. Antibody labeling was visualized with a Cy3-conjugated secondary antibody.[23] It has been shown that epinephrine-enriched cell populations give the highest level of PNMT staining, while norepinephrine-enriched populations gave lower staining (ca. 20% of that with epinephrine-enriched cells). For this experiment, three populations of chromaffin cells (norepinephrine-enriched, epinephrine-enriched, and mixed) were stained with NS521 and fixed in 4% paraformaldehyde. The fixed cells were stained with the anti-PNMT and secondary antibodies (Figure 2-9). The top row of Figure 2-9 shows that the NE-enriched cell population stains brightly with NS521 and weakly with the fluorescent antibody while the opposite is true for the EP-enriched cell population (second row). Indeed the mixed population of cells (third row, Figure 2-9) contained cells with staining patterns consistent with both NE-enriched cells (circled in green) and EP-enriched cells (circled in red).

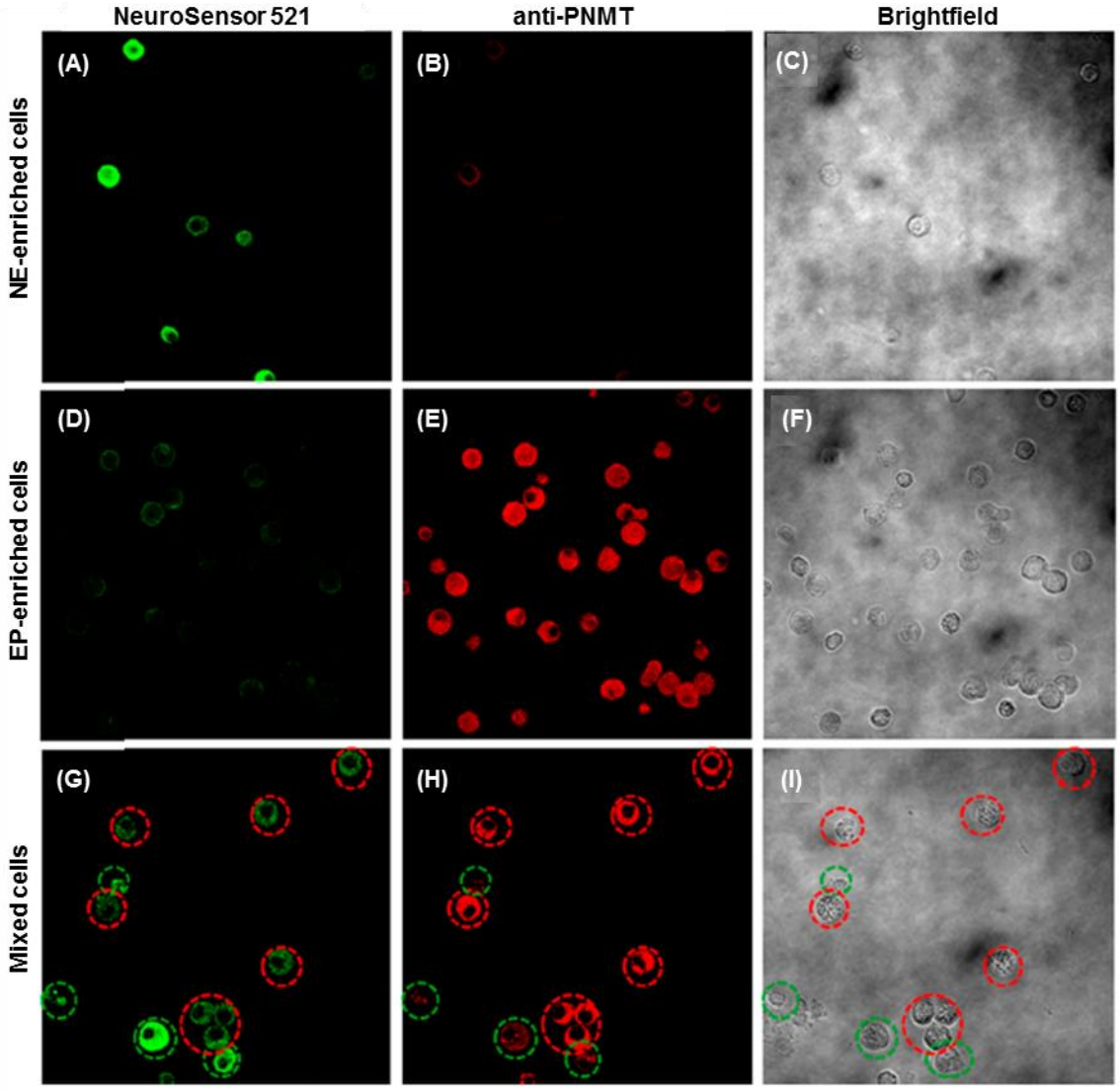

Figure 2-9. Immunohistochemical staining of chromaffin cells. All cells were stained with NS521 (1 µM), fixed (4% formaldehyde), and incubated with an anti-PNMT antibody followed by a Cy3-anti-rabbit antibody. Norepinephrine-enriched (NE) cells (A-C) visualized at (A) 525 nm, (B) 585 nm, and (C) bright field. Epinephrine-enriched (EP) cells (D-F) visualized at (D) 525 nm (E), 585 nm, and (F) bright field. Mixed cells (G-I) visualized at (G) 525 nm, (H) 585 nm, and (I) bright field. Cells circled in green indicate NE cells, and cells circled in red indicate EP cells.

The fluorescence emission in the images shown in Figure 2-9 were quantified using ImageJ.[64] EP-enriched cells show an increased anti-PNMT staining compared to NS521 (Figure 2-10A). Conversely, the NE-enriched cells showed an increased

staining by NS521 compared to the anti-PNMT. As expected, the mixed cell population contained cells which fell into both categories. The average fluorescence intensity ratio of 585 nm vs 525 for epinephrine-enriched cells was 6 times of that of norepinephrine-enriched cells (Figure 2-10B).

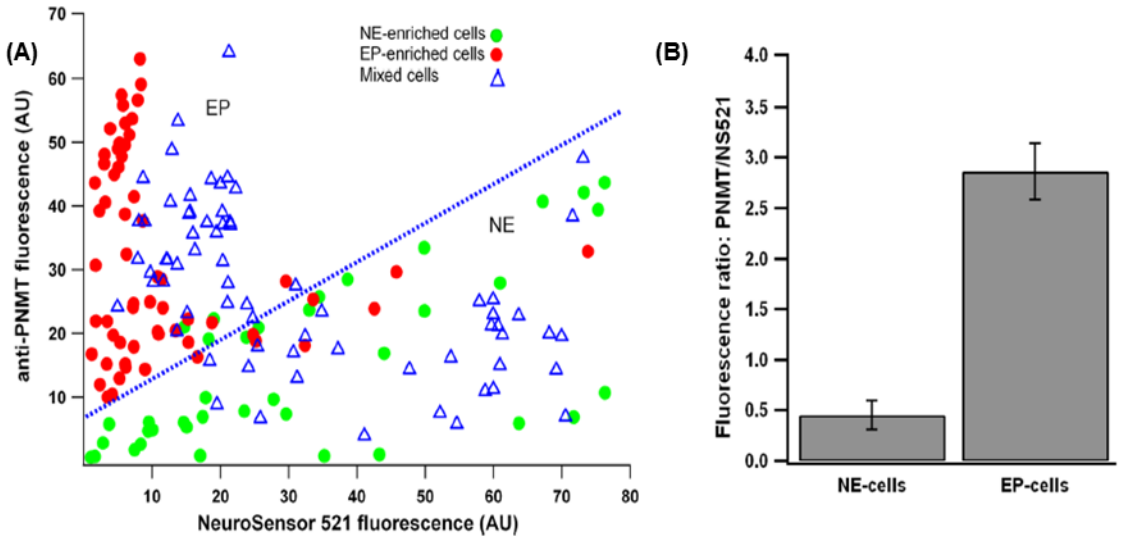

Figure 2-10. Quantification of cell fluorescence from the cell populations from Figure 2-9. (A) Fluorescence intensity at 585 nm plotted on the Y-axis and fluorescence intensity at 525 nm plotted on the x-axis. Each point represents an individual cell. EP cells fall above the blue line, and NE cells fall below the blue line. (B) The average ratio of fluorescence intensity at 585 nm vs 525 nm for NE and EP cells.

In conclusion, NS521 was developed as a turn-on sensor for primary amines. It binds catecholamines such as norepinephrine more tightly than other biogenic amines such as glutamate, and it has no apparent affinity for secondary amines such as epinephrine. This selectivity was demonstrated in chromaffin cells where the norepinephrine-containing cells were stained preferentially over epinephrine-containing cells under identical conditions. Furthermore, the fluorescence is not

affected by fixation. NS521 represents a convenient method to selectively stain norepinephrine and dopamine in neurosecretory vesicles.

CHAPTER THREE

PET-Modulated Fluorescent Sensors

3.1 a-PET vs. d-PET

Photoinduced electron transfer (PET) between a fluorophore and a pendant electron-donating or accepting group has been widely exploited in fluorescence sensing.[9] Two schools exist: acceptor-PET (a-PET) and donor-PET (d-PET) (Figure 3-1). Acceptor-PET occurs when the excited fluorophore behaves as the electron-acceptor. An electron from the fluorophore is excited into a higher energy state. However, it is unable to fluoresce back down to the ground state because an electron from a donor is placed into the temporarily vacant ground state which means the excited electron must relax via some other non-radiative process.

By contrast, donor-PET occurs when the fluorophore acts as the electron-donor. Here, an electron from the fluorophore is excited into a higher energy state, but instead of fluorescing back down to its ground state, it transfers into the LUMO of a pendant acceptor group. Again, this prohibits fluorescence emission.

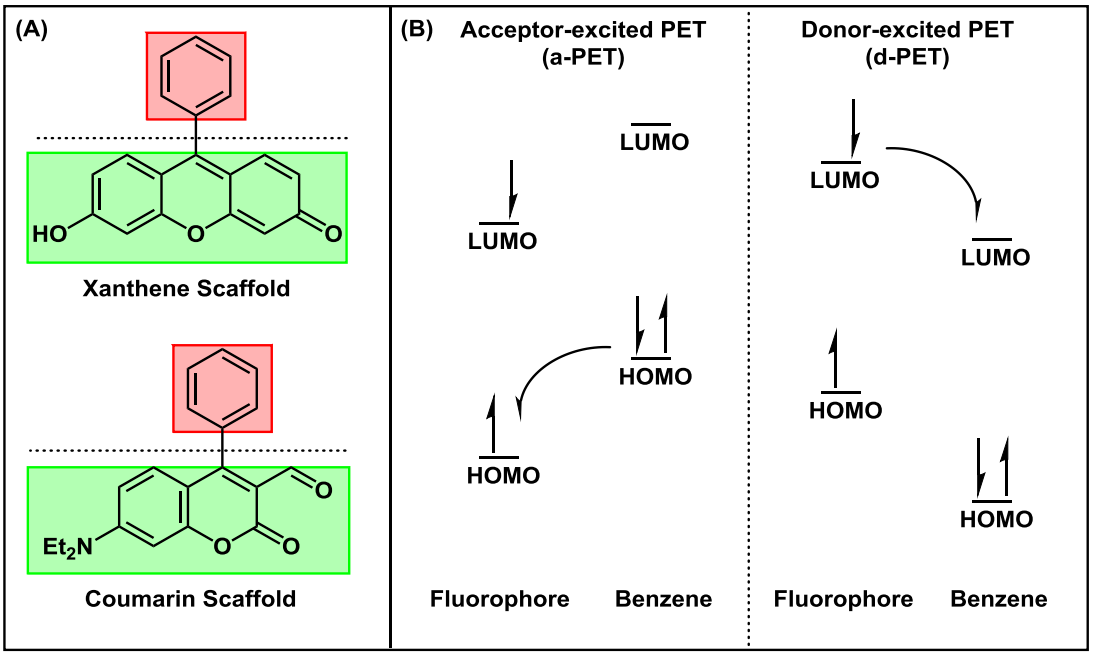

Figure 3-1. (A) Orthogonal pi-systems capable of PET. (B) Molecular orbitals describing acceptor-excited PET (a-PET) and donor-excited PET (d-PET).

3.2 Previous Work

Several research groups have exploited these electron transfer mechanisms in order to optimize the fluorescence output or to create fluorescence switches.[65,66,67,68] For example, Nagano demonstrated the orthogonal pendant benzene moiety of fluorescein can quench fluorescence via a PET mechanism by developing xanthene-based TokyoGreens, fluorescein derivatives that lack or replace the ortho-substituted carboxylic acid group. [67]

The researchers designed and synthesized various derivatives of TokyoGreen where the electron density of the benzene moiety was tuned in a fine manner through the introduction of methyl and methoxy groups. Furthermore, they demonstrated that the extent of PET quenching in TokyoGreens can be increased or decreased by altering the

electron density of the pendant aryl moiety (Figure 3-2). Modifying the pendant aryl moiety of fluorescein did not alter the absorption and emission maxima relative to fluorescein, indicating the ground-state interaction between the benzene moiety and the xanthene moiety of the TokyoGreen derivatives was minimal and that the two moieties were conjugatively uncoupled.

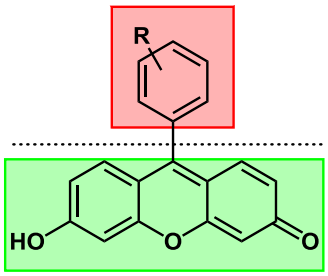

R =

2-Me	2-Me-4-OMe
2,4-DiMe	2-OMe-5-Me
2,5-DiMe	2,4-DiOMe
2-OMe	2,5-DiOMe

Figure 3-2. Selected TokyoGreen derivatives

To describe these systems in a quantitative fashion, the rate of electron transfer (k_{ET}) between the excited state fluorophore (scaffold) and the pendant aryl moiety was determined from the free energy change for electron transfer (ΔG_{ET}) using the Marcus equation. In turn, ΔG_{ET} values were determined from the Rehm-Weller equation using experimentally-measured oxidation and reduction potentials of the platform components.[66,69,70] The data could then be used to calculate the fluorescence quantum yields (Φ_{fl}) of the derivatives. Most importantly, Nagano demonstrated a direct relationship between the experimentally determined quantum yield and the calculated energy of the highest occupied molecular orbital (E_{HOMO}) of the corresponding pendant aryl moiety. This relationship greatly facilitates the *a priori* determination of

fluorescence output. However, to be truly quantitative, it was necessary to have experimentally determined oxidation potential of the unsubstituted scaffolds (fluorophores). Thus, only the xanthene and BODIPY scaffolds have undergone quantitative evaluation. However, the method has been used for qualitative assessment of fluorescence properties based on platforms consisting of modified scaffolds.[67, 68, 71,]

Recently, we developed NS521 as a turn-on fluorescent sensor for the catecholamines norepinephrine and dopamine (Figure 3-3). NS521 derives from the coumarin-3-aldehyde scaffold, wherein the aldehyde group associates with the analyte primary amine group via reversible iminium ion formation.[5, 72] The coumarin aldehyde fluoresces from an internal charge transfer (ICT) state. Formation of the iminium ion stabilizes the ICT state and shifts the wavelength of absorbance from 448 nm to 488 nm, allowing the bound and unbound forms of the sensor to be independently monitored by appropriate selection of the excitation wavelength.

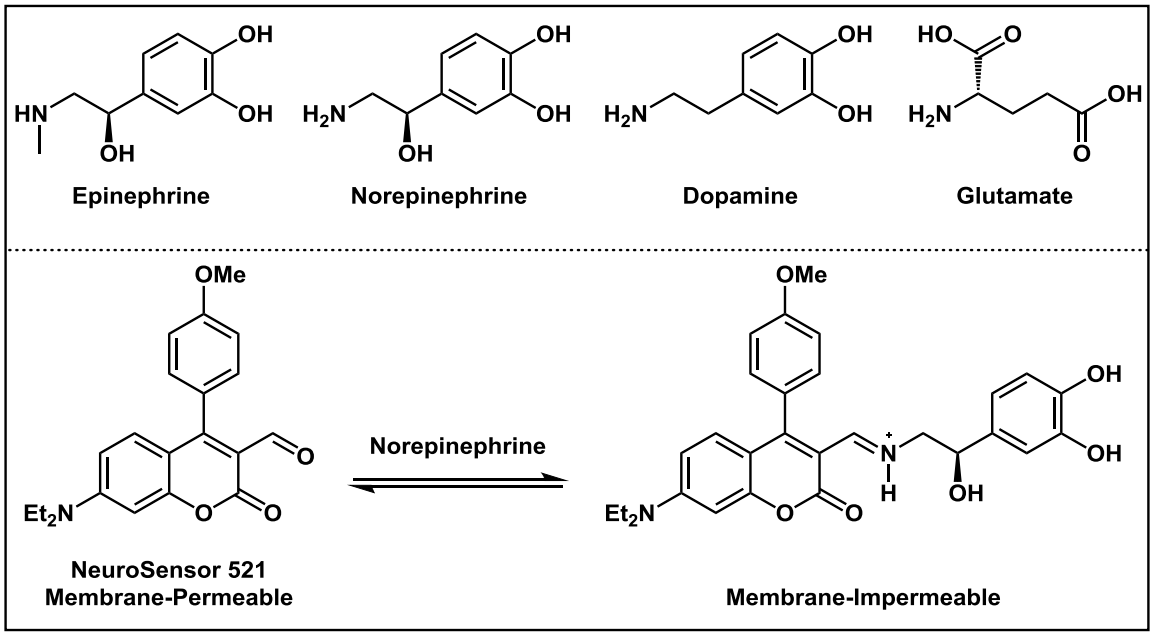

Figure 3-3. Structures of select neurotransmitters. Structure of NS521 and formation of the iminium ion upon interaction with norepinephrine.

In principle, the aldehyde group of NS521 can interact with any intracellular free primary amine. However, the low binding affinities of NS521 toward free primary amines (~10 M^{-1}) coupled with the low concentration of intracellular free primary amines (5 mM) translates into extremely weak associations and thus, NS521 remains largely unassociated upon exposure to typical cells. However, specialized neurons sequester and package individual primary-amine neurotransmitters (*e.g.*, glutamate, norepinephrine, dopamine, and serotonin) in secretory vesicles at extremely high concentrations (300 mM – 1 M) within an acidic environment (~pH 5).[17,18,19,20,73,74,75]

We envisaged that the neutral NS521 would diffuse into the secretory vesicles of such specialized cells and only bind with the primary amine neurotransmitter due to the extremely high concentration of the bioanalyte. In turn, the resultant imine form of NS521 would become protonated to form a charged complex due to the acidic

environment within secretory vesicles and become membrane-impermeable (Figure 2-4). As a result, the sensor would accumulate inside the secretory vesicles and allow for clear visualization of the neurotransmitter with low background. NS521 was initially validated in chromaffin cells and demonstrated selective detection of norepinephrine, allowing discrimination between norepinephrine- and epinephrine-enriched cell populations.[61]

Since the fluorescent imaging of neurons, neurotransmitters, and events surrounding synaptic firing is an increasingly active area of research, the potential applications of such sensors are profuse. Fluorescent sensors would enable research in neuroscience by providing both the imaging of primary-amine neurotransmitters (especially for neurotransmitters such as dopamine that tend to quench fluorescence) and the continuous monitoring of primary-amine neurotransmitter trafficking. Therefore, we sought to establish a model by which sensors could be rationally designed for the purposes of neuroimaging. Since the NS521 platform consists of a fluorophore (scaffold) with a pendant orthogonal aromatic group, we designed various NS521 analogues and applied Nagano's method to this unique sensor system to evaluate the photophysical interaction between the platform components.

Here, we report a series of benzene- and thiophene-substituted sensors based on the coumarin-3-aldehyde scaffold. The photophysical properties, binding affinities, and fluorescence responses toward glutamate, norepinephrine, and dopamine, were experimentally determined. DFT calculations provided the energy of the highest occupied molecular orbital (E_{HOMO}) values of the pendant aryl substituents (calculated at

the B3LYP/6-31G(d) level of theory), which were fine-tuned through the introduction of various electron-withdrawing and -donating groups. In conjunction with the Marcus theory of electron transfer, oxidation and reduction potential values strictly derived from the calculated molecular orbital energy values of the fluorophore allowed for calculation of the fluorescence properties of the sensors. Good agreement between the calculated and experimentally determined fluorescence properties was found only in the case of the benzene-substituted sensors.

3.3 NS521 Derivatives

3.3.1 Design

To systematically investigate the directly linked intramolecular PET in this system, a series of benzene- and thiophene-substituted derivatives based on the coumarin-3-aldehyde scaffold were prepared (Figure 3-4A). Substituents on the C4 aryl groups were chosen to cover a wide range of calculated E_{HOMO} values (Figure 3-4B). The primary difference between the two classes of aryl moieties is the dihedral angle of the pendant aryl moiety with respect to the plane of the coumarin aldehyde scaffold. The thiophene class was determined to maintain a smaller dihedral angle (72.1°) compared to the benzene class (82.3°) based on geometry-optimized structures. For the purpose of discussion, it is noted that the only *ortho*-substituted derivative (**1h**) was determined to have a larger dihedral angle (89.3°).

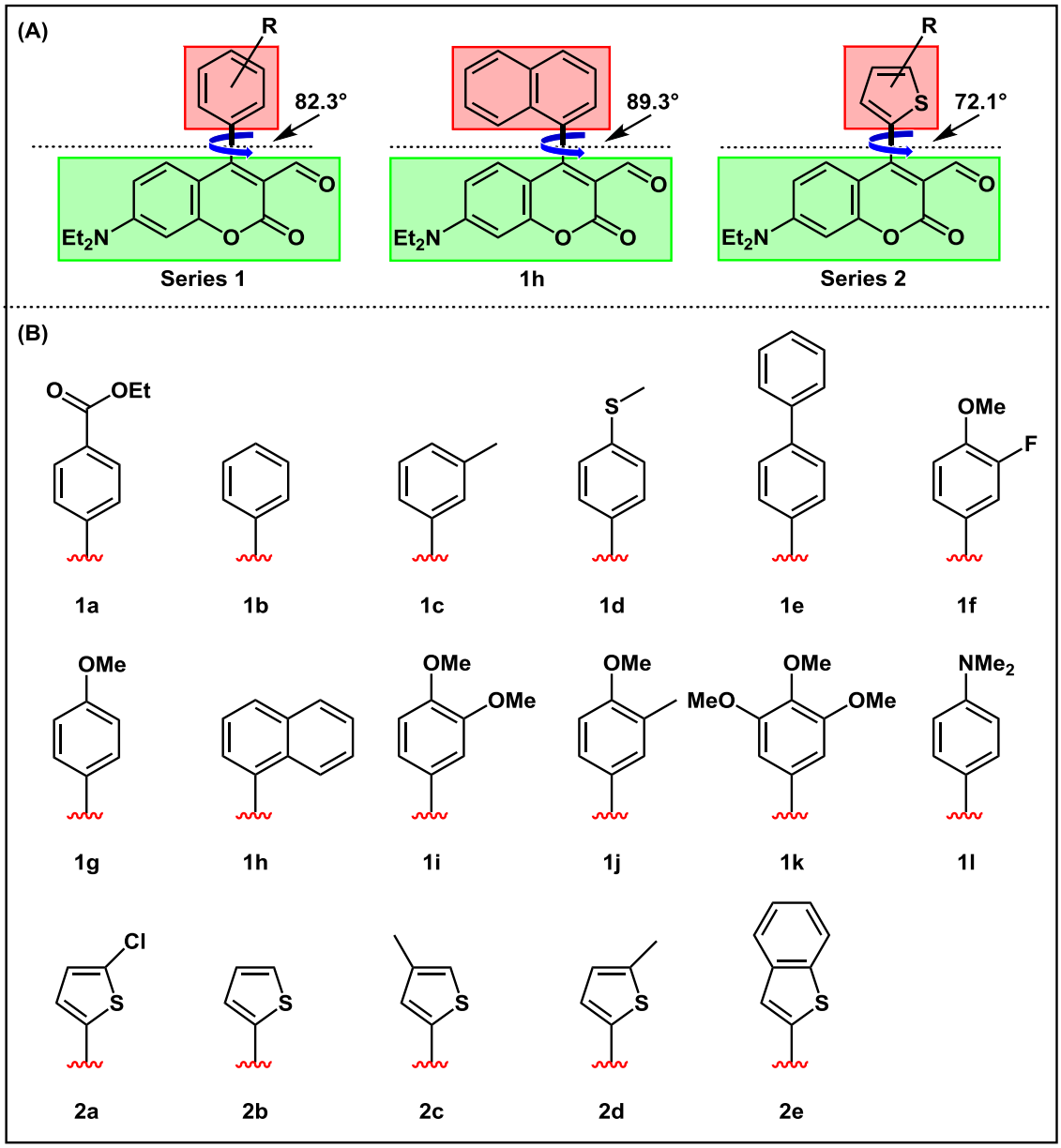

Figure 3-4. Structures of the NS521 analogues used in this study: (A) General structures of Series 1 (benzene) and Series 2 (thiophene) derivatives accompanied by calculated bond angles; (B) Structures of the benzene-based (**1a-l**) and thiophene-based (**2a-e**) aryl moieties at the C4-position of the coumarin aldehyde scaffold.

3.3.2 Synthesis

The sensors were prepared as shown in Figure 3-5. The synthesis of the benzene-based sensors (**1a-l**) and the benzothiophene sensor (**2e**) was achieved through a

single Suzuki coupling reaction with compound **14** to provide the final products. The thiophene-based sensors (**2a-d**) were synthesized in two steps from compound **16**, via tosylation and coupling followed by formylation under Vilsmeier conditions.

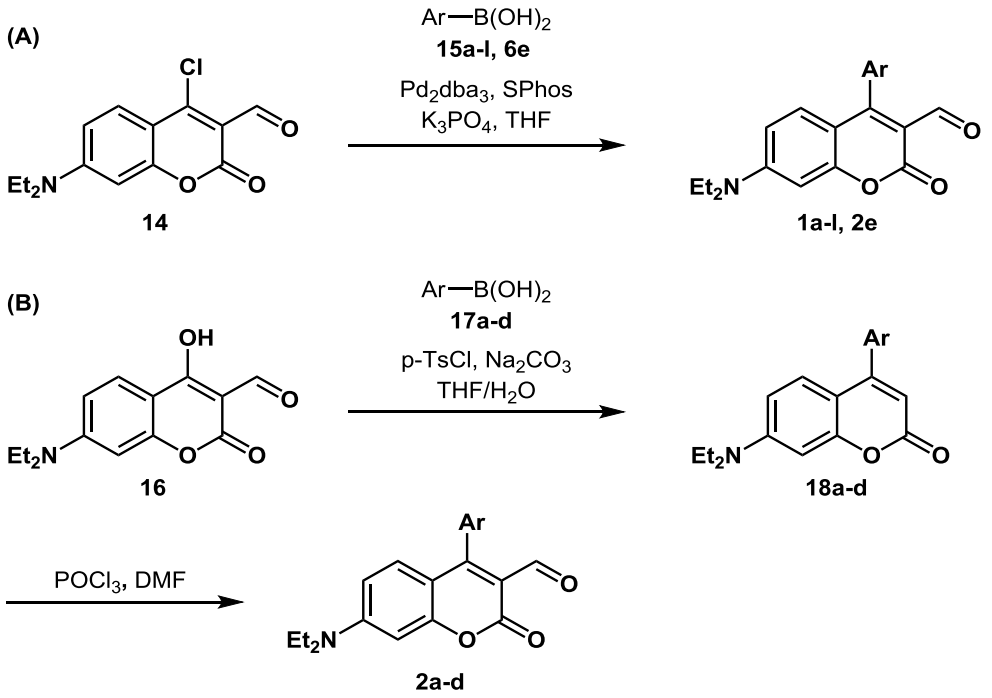

Figure 3-5. Synthesis of (A) benzene- and (B) thiophene-substituted NS521 derivatives.

3.3.3 Titrations

Spectroscopic Properties

The sensors were titrated with glutamate as a representative amine and the absorption and fluorescence spectra recorded in buffer at pH 5 to mimic the acidic interior of the secretory vesicle. Representative spectral changes for sensors **1b** and **2b** upon binding with analyte are shown in Figure 3-6. As observed with other sensors in this series, interaction with a primary amine produces a red shift in

absorption. For the series 1 sensors, the absorption of the bound species shifted from approximately 448 nm to 488 nm. Similarly, the emission maxima of the series 1 sensors were red-shifted to approximately 520 nm upon binding, giving these sensors spectroscopic properties that conveniently match that of fluorescein. For the series 2 sensors, the absorbance shifts from approximately 467 nm to 502 nm upon interaction with glutamate and the emission shifts from approximately 522 to 540 nm, which is 20 nm longer in wavelength than the absorbance values for the series 1 sensors. The absorbance maxima, fluorescence emission, and fluorescence quantum yield (Φ_{fl}) of the unbound and bound sensors were measured in buffer at pH 5.0 and tabulated in Tables 3-1 and 3-2 along with the E_{HOMO} and E_{LUMO} values calculated using standard methods.

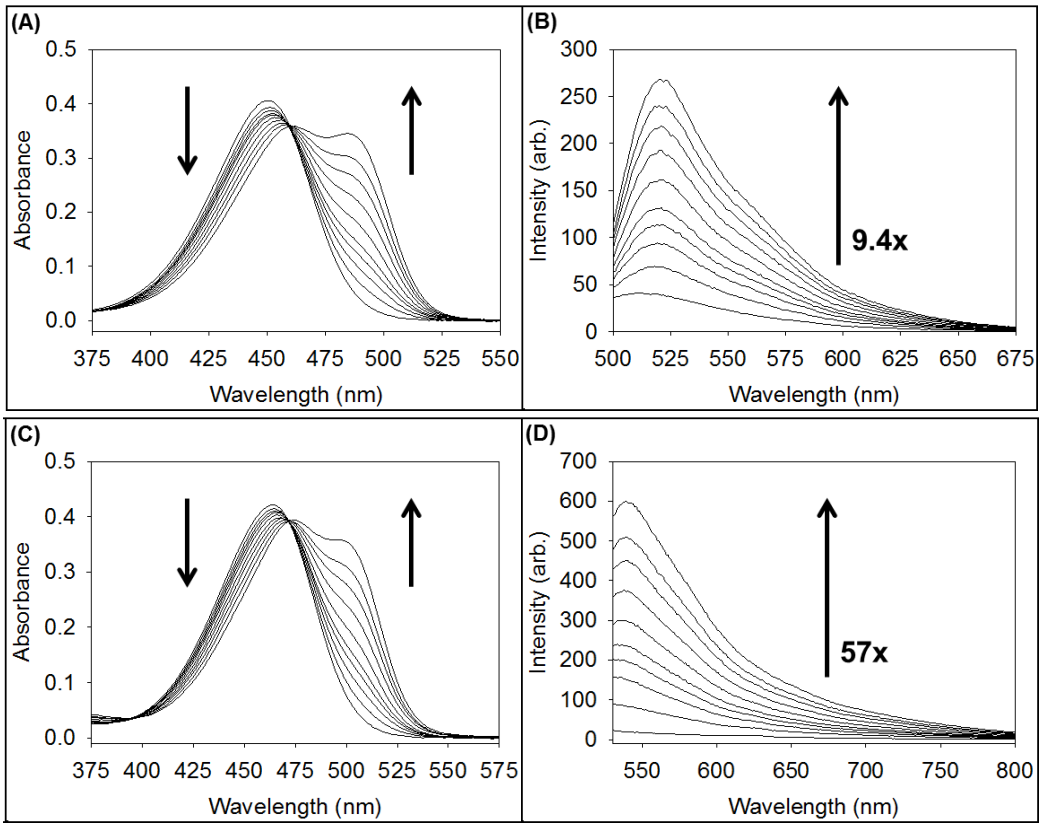

Figure 3-6. (A) UV/Vis and (B) fluorescence spectra of sensor **1b** (10 µM) with aliquots of 500 mM glutamate in buffer (25 mM HEPES, 50 mM $Na_2S_2O_3$, pH = 5.0, 37 °C). Excited at 488 nm. (C) UV/Vis and (D) fluorescence titration of sensor **2b (**10 uM**)** with aliquots of 500 mM glutamate in buffer (25 mM HEPES, 50 mM $Na_2S_2O_3$, pH = 5.0, 37 °C). Excited at 515 nm.

Table 3-1. Photophysical properties of series 1 sensors

	Absorbance[a]		Emission[a]		Quantum Yield[a,b]		Energy Values[c,d]	
	Unbound	Bound[e]	Unbound[f]	Bound[e,g]	Unbound[f]	Bound[e,g]	E_{HOMO}	E_{LUMO}
Benzene-Based Moiety	λ_{max} (nm)	λ_{max} (nm)	λ_{max} (nm)	λ_{max} (nm)	pH 5.0	pH 5.0	hartrees	hartrees
[h]4-Carbethoxy (1a)	456	493	534	534	0.0054	0.0100	-0.2561	-0.0422
Phenyl (1b)	452	488	505	520	0.0072	0.0128	-0.2463	0.0036
3-Methyl (1c)	452	488	505	522	0.0069	0.0102	-0.2354	-0.0054
4-Methylthio (1d)	453	488	504	522	0.0067	0.0101	-0.2240	-0.0170
[h]4-Biphenyl (1e)	452	488	517	529	0.0085	0.0150	-0.2222	-0.0248
3-Fluoro-4-methoxy (1f)	453	489	504	526	0.0063	0.0097	-0.2222	-0.0018
(NS521) 4-Methoxy (1g)	452	488	505	521	0.0055	0.0095	-0.2151	0.0040
Naphthalene (1h)	456	494	505	521	0.0078	0.0126	-0.2127	-0.0352
3,4-Dimethoxy (1i)	452	488	503	522	0.0047	0.0094	-0.2109	0.0077
4-Methoxy-3-methyl (1j)	452	488	502	522	0.0050	0.0093	-0.2106	0.0089
3,4,5-Trimethoxy (1k)	452	489	505	522	0.0036	0.0090	-0.2085	0.0112
4-Dimethylamino (1l)	451	488	505	521	0.0002	0.0009	-0.1844	0.0134

[a]Measured in buffer (1.0 µM sensor, 25 mM HEPES, 50 mM $Na_2S_2O_3$, pH = 5.0, 37 °C). [b]Calculated by using fluorescein as a fluorescence standard (Φ_{fl} = 0.85). [c]Calculated E_{HOMO} and E_{LUMO} values of the aryl moiety. [d]Data were calculated with DFT B3LYP/6-31G(d) using Gaussian 09W Rev. A.02. [e]Bound sensor solutions contain 500 mM glutamate. [f]Excited at 473 nm. [g]Excited at 488 nm. [h]Sensors **1a** and **1e** were adjusted to 5% and 30% DMSO, respectively.

Table 3-2. Photophysical properties of series 2 sensors

	Absorbance[a]		Emission[a]		Quantum Yield[a,b]		Energy Values[c,d]	
	Unbound	Bound[e]	Unbound[f]	Bound[e,g]	Unbound[f]	Bound[e,g]	E_{HOMO}	E_{LUMO}
Thiophene-Based Moiety	λ_{max} (nm)	λ_{max} (nm)	λ_{max} (nm)	λ_{max} (nm)	pH 5.0	pH 5.0	hartrees	hartrees
2-Chlorothiophene (2a)	472	506	527	544	0.0019	0.0030	-0.2332	-0.0223
Thiophene (2b)	462	502	522	539	0.0022	0.0038	-0.2328	-0.0076
3-Methylthiophene (2c)	465	502	522	540	0.0028	0.0041	-0.2268	-0.0026
2-Methylthiophene (2d)	467	502	521	540	0.0029	0.0042	-0.2216	-0.0045
Benzothiophene (2e)	472	506	542	545	0.0039	0.0046	-0.2162	-0.0236

[a]Measured in buffer (5.0 µM sensor, 25 mM HEPES, 50 mM $Na_2S_2O_3$, pH = 5.0, 37 °C). [b]Calculated by using rhodamine B as a fluorescence standard (Φ_{fl} = 0.31). [c]Calculated E_{HOMO} and E_{LUMO} values of the aryl moiety. [d]Data were calculated with DFT B3LYP/6-31G(d) using Gaussian 09W Rev. A.02. [e]Bound sensor solutions contain 500 mM glutamate. [f]Excited at 473 nm. [g]Excited at 515 nm.

Binding Affinities

The association constants (K_a) of each sensor toward glutamate, norepinephrine and dopamine are listed in Tables 3-3 and 3-4 for series 1 and 2, respectively. The interaction between coumarin aldehydes and primary amines is a covalent reaction and, in principle, would be best represented as an equilibrium constant (K_{eq}). However, because most supramolecular interactions are measured in terms of association constant, we have adopted that convention here for the sake of comparison and ease of use. Tables 3-3 and 3-4 also list maximum fluorescent enhancements (I_{sat}/I_0), which are the fluorescence intensities at saturation (as determined by the fit to a one-site binding isotherm) relative to the fluorescence intensities of the unbound sensors. These data give the maximum possible fluorescence response and are useful in comparing the spectroscopic properties of the fully bound sensor to the unbound state as well as to other sensors.

Glutamate binds to all derivatives with the same relatively low affinity (5 – 10 M^{-1}). This result is consistent with other coumarin aldehyde sensors, which appear to bind all primary alkyl amines with similar low affinity.[5,72] Surprisingly, the catecholamines bind roughly an order of magnitude better. Moreover, there is a clear trend toward better binding to sensors with more electron-rich aromatic groups in the C4-position. There appears to be subtle contact between the catechol group and the C4-aromatic, which increases with electron density on the C4-aromatic residue. Interestingly, the thiophene-based sensors demonstrated slightly lower overall affinity than the benzene-based sensors and the electronic structure of

the thiophene does not appear to influence the binding constant of catecholamines. Although these binding constants are modest, they should suffice for cell imaging purposes because catecholamines are present at high concentrations (0.5 – 1 M) in secretory vesicles compared to the concentrations of typical amines present in a cell (5 mM) and would promote binding. Indeed, even glutamate is thought to be present in concentrations as high as 300 mM in vesicles of glutamatergic neurons.[74] Given that NS521 appears to accumulate in vesicles (*vide supra*), it is possible that some of the sensors described here could be used to image glutamate as well as catecholamines.

Table 3-3. Association constants (K_a) for the binding of series 1 sensors to various analytes[a]

	Amine Guest					
	Glutamate		Norepinephrine		Dopamine	
Benzene-Based Moiety	K_a (M^{-1})[b]	I_{sat}/I_0[c]	K_a (M^{-1})[b]	I_{sat}/I_0[c]	K_a (M^{-1})[b]	I_{sat}/I_0[c]
[d]**4-Carbethoxy (1a)**	7.0	4.7	81.5	1.8	107.5	1.1
Phenyl (1b)	9.4	10.5	68.7	6.6	68.1	3.2
3-Methyl (1c)	9.2	10.0	68.4	6.6	74.1	3.2
4-Methylthio (1d)	8.4	9.8	68.8	6.5	87.1	3.1
[d]**4-Biphenyl (1e)**	13.8	6.2	148.8	2.6	203.3	1.6
3-Fluoro-4-methoxy (1f)	9.0	9.3	70.2	6.4	92.9	3.1
(NS521) 4-Methoxy (1g)	9.6	7.8	77.8	5.4	112.1	3.0
Naphthalene (1h)	10.1	6.8	103.7	4.3	170.0	2.9
3,4-Dimethoxy (1i)	10.2	6.6	107.2	4.1	177.5	2.7
4-Methoxy-3-methyl (1j)	10.3	6.4	136.0	3.9	192.1	2.4
3,4,5-Trimethoxy (1k)	10.3	5.6	159.1	2.6	205.1	1.6
4-Dimethylamino (1l)	10.2	1.7	160.0	1.2	206.2	1.1

[a]Measured in buffer (1.0 μM sensor, 25 mM HEPES, 50 mM $Na_2S_2O_3$, pH = 5.0, 37 °C). [b]K_a measured by fluorescence spectroscopy. Excited at 488 nm. [c]I_{sat} = fluorescence intensity at saturation taken from the theoretical fit to a one-site binding isotherm. [d]Sensors **1a** and **1e** were adjusted to 5% and 30% DMSO, respectively.

Table 3-4. Association constants (K_a) for the binding of the series 2 sensors to various analytes[a]

	Amine Guest					
	Glutamate		Norepinephrine		Dopamine	
Thiophene-Based Moiety	K_a (M^{-1})[b]	I_{sat}/I_0[c]	K_a (M^{-1})[b]	I_{sat}/I_0[c]	K_a (M^{-1})[b]	I_{sat}/I_0[c]
2-Chlorothiophene (2a)	5.9	34	69.2	21	84.0	12
(NS539) Thiophene (2b)	7.3	57	65.2	48	43.6	25
3-Methylthiophene (2c)	7.4	51	63.6	38	51.1	23
2-Methylthiophene (2d)	6.1	48	58.7	32	54.6	22
Benzothiophene (2e)	5.2	30	49.6	17	49.3	9.5

[a]Measured in buffer (5.0 µM sensor, 25 mM HEPES, 50 mM $Na_2S_2O_3$, pH = 5.0, 37 °C). [b]K_a measured by fluorescence spectroscopy. Excited at 515 nm. [c]I_{sat} = fluorescence intensity at saturation taken from the theoretical fit to a one-site binding isotherm.

Fluorescence Enhancements

Upon analyte addition, the fluorescence enhancements for the series 1 sensors were very good: as high as an 11-fold increase for glutamate and a 6.6-fold increase for norepinephrine. As the absorbance maximum shifts to the red upon interaction with the analyte, selective excitation of the red wavelength produces a fluorescence increase upon binding. In addition, the fluorescence quantum yields of the bound sensors were higher than those for the unbound sensors. Thus, the observed fluorescence enhancements are due to the selective excitation wavelength used and an increase in fluorescence quantum yield upon binding. Indeed, better enhancements might be possible by judicious choice of excitation wavelength; however, we chose to use 488 nm because this wavelength is commonly available for imaging applications. The catecholamines can quench by PET, which is reflected in a lower fluorescence quantum yield for the dopamine- and norepinephrine-bound sensors compared to sensors bound to glutamate. However, useful enhancements

are seen even for those quenching analytes (Tables 3-3 and 3-4). It should be noted that sensors **1a** and **1e** required a DMSO cosolvent due to solubility issues, so the spectroscopic properties of these two sensors are not directly comparable to the others in this series.

The fluorescence response of the series 2 sensors to the primary amine analytes was markedly higher than the fluorescence response of the series 1 sensors: as high as 57-fold for glutamate and 48-fold for norepinephrine. The difference in fluorescence response can be attributed to a lower initial fluorescence baseline. From Table 2, the quantum yields of the unbound thiophene derivatives are lower than those for the unbound benzene derivatives; however, the change in quantum yield between bound and unbound state were similar to the series 1 sensors. The major difference in the case of the series 2 sensors is that they were excited at 515 nm to mimic a common laser line rather than exciting at the absorption maxima (~502 nm). At this higher excitation wavelength, the unbound derivative hardly absorbs, resulting in an overall low background that contributes to the very high fluorescence enhancements seen in Table 3-4.

3.3.4 Computational Analysis

Optimized models of the benzene-based sensors clearly indicate that the pendant aryl moiety is nearly perpendicular to the plane of the coumarin aldehyde scaffold (Figure 3-4A). The modeling results are supported by the fact that all of the benzene-based sensors (except **1h**) have approximately the same absorbance and

emission maxima, indicating that the ground-state interaction between the pendant aryl moiety and the coumarin aldehyde scaffold was similar in all of them. The E_{HOMO} and E_{LUMO} values of the coumarin aldehyde scaffold were calculated to be -0.2109 and -0.0805 hartrees, respectively (Figure 3-7). The calculated E_{LUMO} values of the pendant aryl moiety of the benzene-based sensors (summarized in Table 1) are significantly higher than the calculated E_{LUMO} values of the coumarin aldehyde fluorophore, indicating that a d-PET process is not operative. In contrast, the calculated E_{HOMO} values of the pendant aryl moiety are in the same range as the calculated E_{HOMO} value of the coumarin aldehyde fluorophore, suggesting an a-PET mechanism can modulate the fluorescence properties of the coumarin. Thus, the C4-aryl moiety can be used to control the fluorescence properties of the coumarin aldehyde fluorophore.

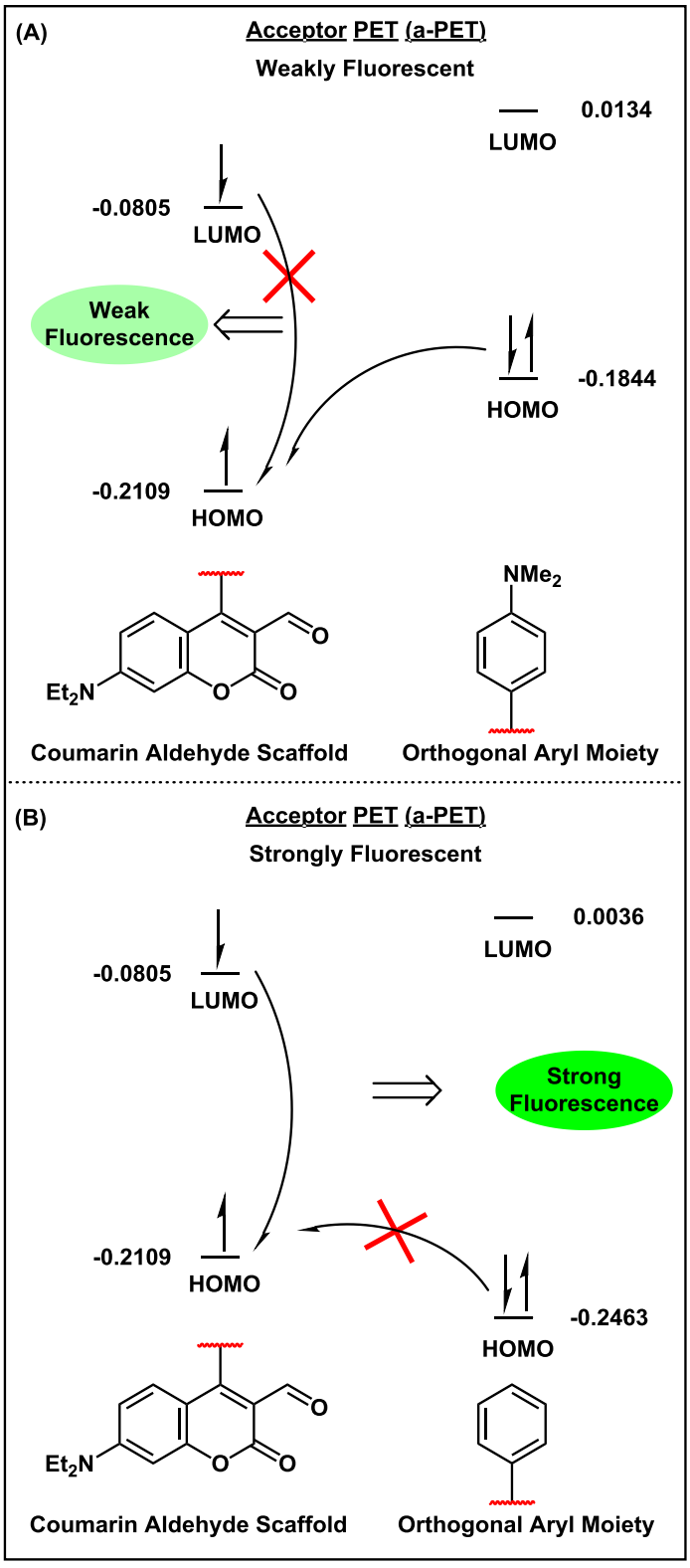

Figure 3-7. Frontier orbital energy diagram of the PET process. (A) a-PET results in weak fluorescence. (B) Loss of a-PET quenching results in strong fluorescence.

This analysis also explains the differential fluorescence response of the sensors to the various analytes (Table 3-3). In all cases, dopamine and norepinephrine produce a lower fluorescence response than glutamate does. The calculated E_{HOMO} values of the catecholamines (Table 3-5) indicate that these analytes should act as PET quenchers, with dopamine being a better PET quencher than norepinephrine. Indeed, this expectation was borne out from the observed fluorescence enhancements. Further, the calculated E_{HOMO} value of serotonin is significantly higher than the E_{HOMO} values for both catecholamines, indicating that serotonin should be a considerably better PET quencher of the coumarin aldehyde fluorophore. Indeed, serotonin completely quenches the fluorescence response of all sensor derivatives upon binding (data not shown).

Table 3-5. Calculated E_{HOMO} and E_{LUMO} values for select neurotransmitters[a]

Neurotransmitter	E_{HOMO}	E_{LUMO}
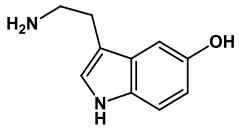 **Serotonin**	-0.1890	-0.0022
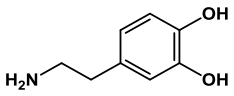 **Dopamine**	-0.2025	-0.0028
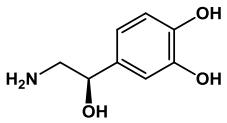 **Norepinephrine**	-0.2078	-0.0082

[a] E_{HOMO} and E_{LUMO} values (hartrees) of the corresponding aryl moiety calculated with DFT B3LYP/6-31G(d) using Gaussian 09W Rev. A.02.

PET Process in Series 1 Sensors

As can be seen in Table 3-1, a wide range of fluorescence quantum yields was observed with the more electron rich pendant aryl moieties giving much stronger quenching. Interestingly, the quantum yields of the bound species are uniformly higher than the unbound species. The iminium ion formed upon binding has a lower calculated E_{HOMO} value (-0.3373 hartrees) than the aldehyde (-0.2109 hartrees) and thus, would be subject to stronger quenching by the C4-aromatic group. However, this quenching effect is more than offset by the formation of the iminium ion which stabilizes and rigidifies the ITC state resulting in an overall increase in quantum yield upon binding.

To evaluate the photophysical interaction between the pendant aryl moiety and the coumarin aldehyde scaffold, the relationship between the quantum yield for the unbound and bound series 1 sensors and the calculated E_{HOMO} values of the corresponding benzene moiety was plotted and fit to the Marcus equation on the basis of the calculated E_{HOMO} values (Figure 3-8). The calculated free energy change for electron transfer (ΔG_{ET}) values, a prerequisite for fluorescence analysis in terms of the Marcus theory, were obtained as per the Rehm-Weller equation. In turn, the calculated free energy change for electron transfer (ΔG_{ET}) values were derived, in part, from the oxidation and reduction potential values using an established linear correlation between the molecular orbital energy values (E_{HOMO} and E_{LUMO}) and the experimentally measured oxidation and reduction potential values.[76] The experimentally determined quantum yields aligned with the fitted curves quite well,

indicating that the sensor platform fits the model of a directly linked donor-acceptor system. In the case of compound **1h** having the 1-naphthyl group, both the unbound and bound quantum yields of **1h** are higher than theory would predict. However, this difference is attributed to the greater rigidification of the fluorophore (*vide infra*) because the C4-naphthyl moiety is closer to 90° from the plane of the fluorophore (Figure 3-4A).

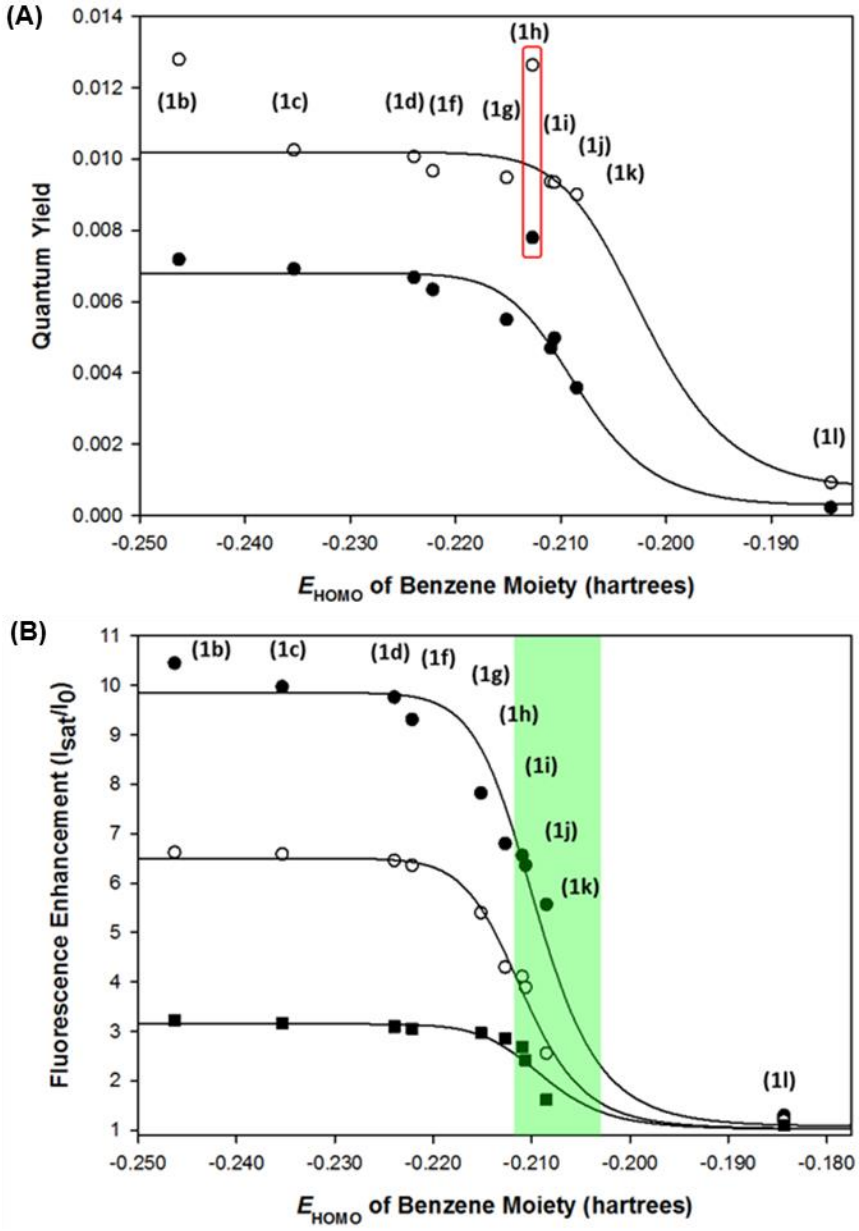

Figure 3-8. Comparison of photophysical properties of series 1 sensors. (A) Relationship between the calculated E_{HOMO} values of the pendant aryl moiety and the fluorescence quantum yields for series 1 sensors (●) unbound and (○) bound with glutamate. The red box highlights naphthalene derivative. (B) Relationship between the calculated E_{HOMO} values of the pendant aryl moiety and the fluorescence enhancement for series 1 sensors with (●) glutamate, (○) norepinephrine, and (■) dopamine. The shaded region identifies derivatives with selective fluorescent responses. The curves represent the best fit to the Marcus equation.

Because the absorbance maxima of the series 1 sensors were similar in both unbound and bound forms, the differences in fluorescent enhancement (I_{sat}/I_0) from Table 3-3 are due entirely to variations in quantum yield between the two forms. Thus, these maximum fluorescence changes were plotted versus the calculated E_{HOMO} values (Figure 3-8B) and the same trends were observed as when plotting just the quantum yield. Indeed, compound **1h**, which was an outlier in Figure 6A, falls in line with the other derivatives in such a plot, indicating that the effect of the naphthyl group on the quantum yield was similar in both the bound and unbound states. Interestingly, the fluorescence enhancement for the series 1 sensors toward glutamate, norepinephrine, and dopamine followed a similar relationship, indicating that quenching analytes such as dopamine can quench all the sensors to the same degree.

From this type of analysis, it is possible to identify sensors that would give selective turn-on fluorescent responses. For example, compounds in the green region of Figure 3-8B should give a good response to glutamate, but much weaker response to dopamine and norepinephrine. Of the sensors tested here, compound **1k** appears to be the best glutamate-selective sensor. Taken together, these results support the notion that an a-PET process modulates the fluorescence properties of the sensor platform and establishes a method for the rational design of selective sensors for primary amine neurotransmitters by variation of the C4-substituent.

Variation in Quantum Yields for the Series 2 Sensors

Calculations indicated that the thiophene substituents have more π-overlap with the fluorophore than the phenyl groups of the series 1 sensors. This overlap causes the absorbance and emission of the series 2 sensors to be at longer wavelengths. Indeed, the trends indicated that the more electron-rich thiophenes display higher wavelengths of excitation and emission. However, the quantum yields of the thiophene derivatives were lower than that of most of the series 1 sensors. This low quantum yield effect has been observed in other directly linked donor-acceptor systems (platforms) and has sometimes been attributed to PET quenching from the thiophene.[77]

The calculated E_{HOMO} and E_{LUMO} values of the series 2 sensors (Table 3-2) indicate that the a-PET mechanism is not operational in these derivatives. For the series 2 sensors, the quantum yields trend upward as the group becomes more electron rich (Figure 3-9). It should be noted that for the chlorothiophene derivative (**2a**), it is possible that quenching due to the heavy atom effect of the chlorine may contribute to an anomalously low quantum yield for this sensor. Regardless, it is clear that PET quenching does not explain the low quantum yield of the thiophene derivatives.

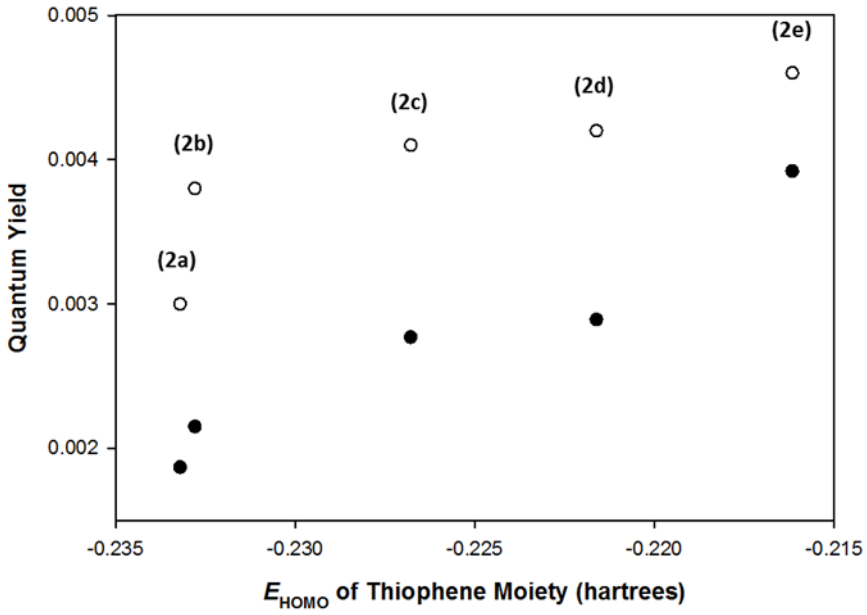

Figure 3-9. Relationship between the calculated E_{HOMO} values of the pendant aryl moiety and the fluorescence quantum yields for series 2 sensors (●) unbound and (○) bound with glutamate.

If one compares the quantum yield of the naphthalene derivative (**1h**) to the other benzene derivatives (*e.g.*, **1b**) and the thiophene derivatives (*e.g.*, **2b**), the sensors in which the C4-group is more perpendicular and thereby, more rigid, have higher fluorescence quantum yields than those where the C4-group is more in plane with the coumarin aldehyde scaffold and thereby, less rigid (Figure 3-4A). These results indicate that twisting of the aryl-fluorophore bond in the excited state leads to non-radiative decay processes and lowers the quantum yield of the fluorophore.[78,79]

Summary of the Fluorescence Responses

The fluorescence enhancements for the series 1 and 2 sensors upon binding to glutamate, norepinephrine, and dopamine are summarized in Figure 3-10 and Figure 3-11, respectively. It should be noted that sensor **1g** (NS521) does not have the highest fluorescence response of the series 1 sensors. However, we chose to utilize sensor **1g** in our initial work because it struck a good balance between high fluorescence responses and good binding affinity toward norepinephrine and dopamine that would provide selective labeling and imaging in cellular studies.

Overall, compared to the benzene-based series 1 sensors, the thiophene-based series 2 sensors provided only subtle differences in binding constants. However, the fluorescence enhancements for the thiophene-based series were considerably larger than the fluorescence enhancements for the benzene-based series. Of this series, sensor **2b** had the highest fluorescence enhancements due to a high ratio of quantum yields between the unbound and bound sensor as well as high binding affinities toward the primary-amine analytes. Given the high fluorescence enhancements and red-shifted fluorescence properties observed for compound **2b** (Table 3-3), we named this compound NeuroSensor 539 (NS539) and pursued cell imaging studies.

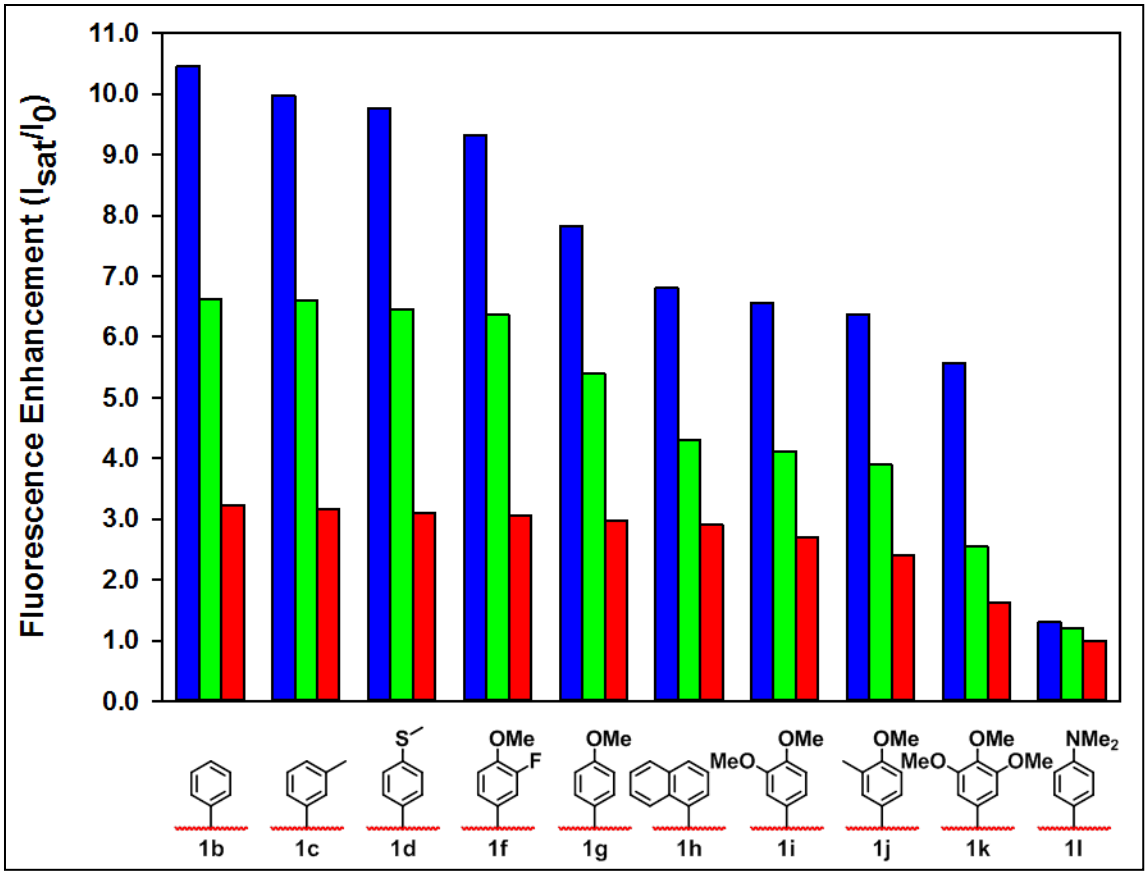

Figure 3-10. The fluorescence enhancements of series 1 derivatives toward glutamate (blue ■), norepinephrine (green ■), and dopamine (red ■).

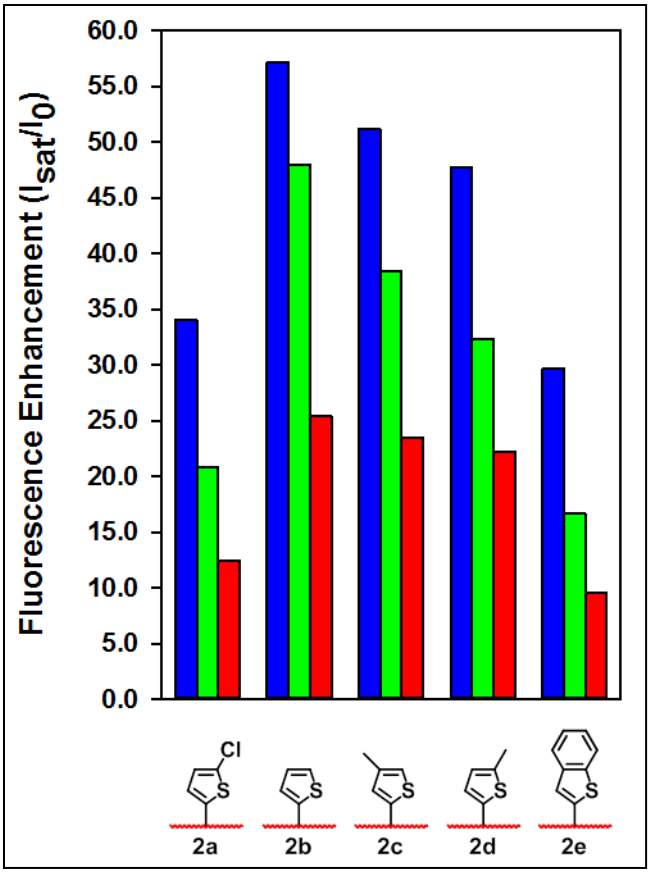

Figure 3-11. The fluorescence enhancements of series 2 derivatives toward glutamate (blue ■), norepinephrine (green ■), and dopamine (red ■).

3.3.5 Cell Studies

Norepinephrine- and epinephrine-secreting chromaffin cells were isolated from bovine adrenal glands, separately incubated with NS539 (**2b**, 10 µM), and imaged using confocal fluorescence microscopy. The live cells were imaged at 458 nm which would excite any potential unbound sensor and at 514 nm which would excite the bound sensor.

Excitation of the epinephrine cells at 514 nm provided marginal fluorescence response, indicating that the sensor is not binding to epinephrine (Figure 3-12B) as expected since epinephrine is a secondary-amine neurotransmitter (Figure 3-3).

Indeed, excitation at 458 nm gave no fluorescence, indicating that the unbound neutral sensor does not remain inside the cell (Figure 3-12A).

However, the norepinephrine-enriched cells exhibited strong punctate fluorescence upon excitation at 514 nm (Figure 3-12E). Exciting the norepinephrine-enriched cells at the wavelength associated with the unbound sensor (λ_{ex} = 458 nm) similarly provided no measurable fluorescence response (Figure 3-12D). The results indicate that the NS539 only accumulates within secretory vesicles upon binding to norepinephrine, as previously seen with NS521.[61] The ratio of the mean corrected total cell fluorescence intensity of norepinephrine- over epinephrine-enriched cells was approximately 27-fold (Figure 3-12G). These results validate NS539 as an excellent sensor for cellular imaging of primary-amine neurotransmitters with very low background.

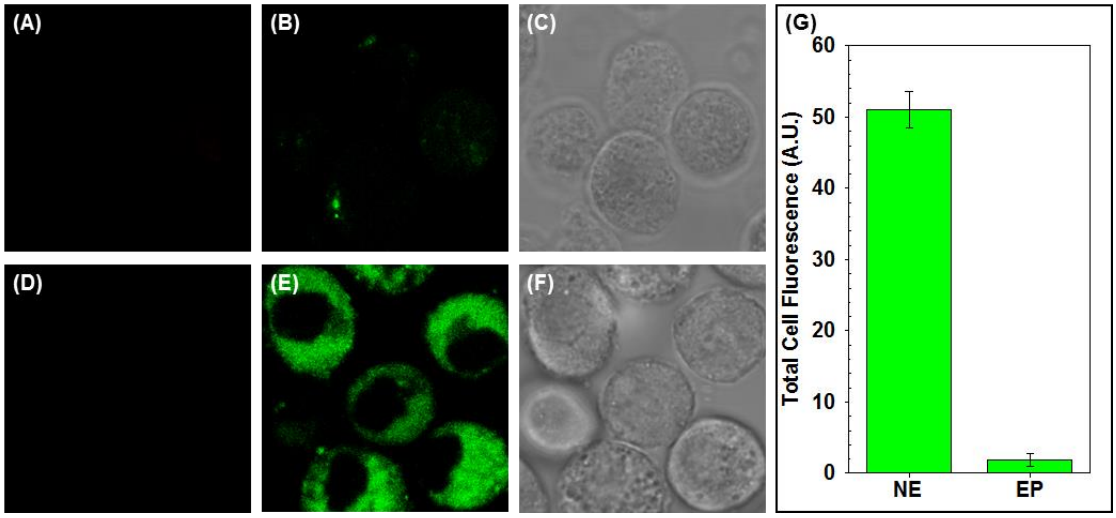

Figure 3-12. Incubation of NS539 (**2b**, 10 μM) with chromaffin cells. Epinephrine-enriched cells (A-C): (A) λ_{ex} = 458 nm; (B) λ_{ex} = 514 nm; (C) brightfield image. Norepinephrine-enriched cells (D-F): (D) λ_{ex} = 458 nm; (E) λ_{ex} = 514 nm; (F) brightfield image. Fluorescence was visualized using a 535-590 nm bandpass filter. (G) The mean corrected total cell fluorescence intensity for norepinephrine- and epinephrine-enriched (NE and EP, respectively) cells was 51.0 ± 2.6 and 1.86 ± 0.98 respectively. Error bars represent standard deviation (*n* = 6).

These data suggest that the coumarin-3-aldehyde scaffold and pendant aryl-based moiety comprise a platform that constitutes a new directly linked donor-acceptor system when the pendant aryl moiety is benzene-based, and thus, perpendicular to the plane of the fluorophore. The benzene-substituted series of sensors operates via an a-PET mechanism, which allows one to predict both the fluorescence quantum yields and the fluorescence responses toward primary-amine neurotransmitters based on DFT calculations.

The results provide a rational design strategy for the development of turn-on fluorescent sensors for primary-amine neurotransmitters based on the coumarin-3-aldehyde scaffold. The thiophene-substituted series of sensors did not follow the same trend based on PET quenching, indicating that the π-system of the

thiophene is more conjugated with the π-system of the fluorophore. However, due to favorable excitation/emission profiles, the thiophene sensors gave far superior fluorescence enhancements upon binding analytes.

Based on these studies, NeuroSensor 539 was identified as a good candidate for biological imaging studies by demonstrating enhanced spectral and photophysical properties. The efficacy of NeuroSensor 539 was validated by selectively labeling and imaging norepinephrine in secretory vesicles of live chromaffin cells using longer excitation wavelengths that provided lower background.

CHAPTER FOUR

Near-Infrared Sensing of Neurotransmitters

4.1 Near-Infrared Sensing

Near-infrared (NIR) bioimaging has become increasingly popular in recent years.[80,81,82] The NIR region of the electromagnetic spectrum is typically considered between 650-900 nm and is preferred for biological imaging due to the excellent tissue penetration of long-wavelength light and low phototoxicity to cells (Figure 4-1).[83] Also, the excitation and emission wavelengths of NIR sensors are far longer than those of autofluorescing molecules and tissues (*e.g.* flavins, nicotinamide, adenine dinucleotide, collagen, elastin, porphyrins, and etc.).[84,85]

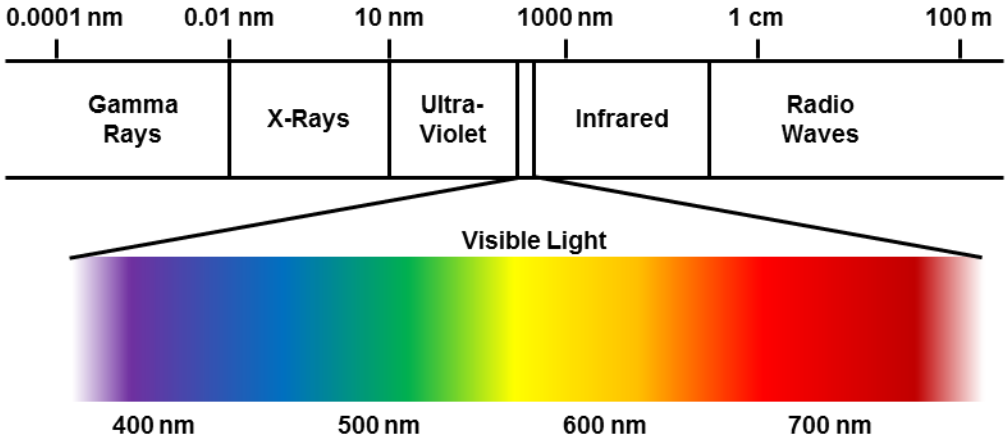

Figure 4-1. The electromagnetic spectrum

NIR molecular sensors have extended pi-systems and have been made from cyanines, BODIPYs, squaraines, and porphyrins, to name a few (Figure 4-2).[81] For practical uses, the sensors need to have high quantum yields, large stokes shifts, modular syntheses for facile alteration, and high photostability. There is still a need for better molecular sensors that fit these criteria as there are only a few FDA-approved NIR dyes for *in vivo* bioimaging (*e.g.* indocyanine green, methylene blue).[82,86] Moreover, there is now a strong movement to incorporate NIR indicators into therapeutic delivery systems to enable monitoring of drug release at target sites.[87]

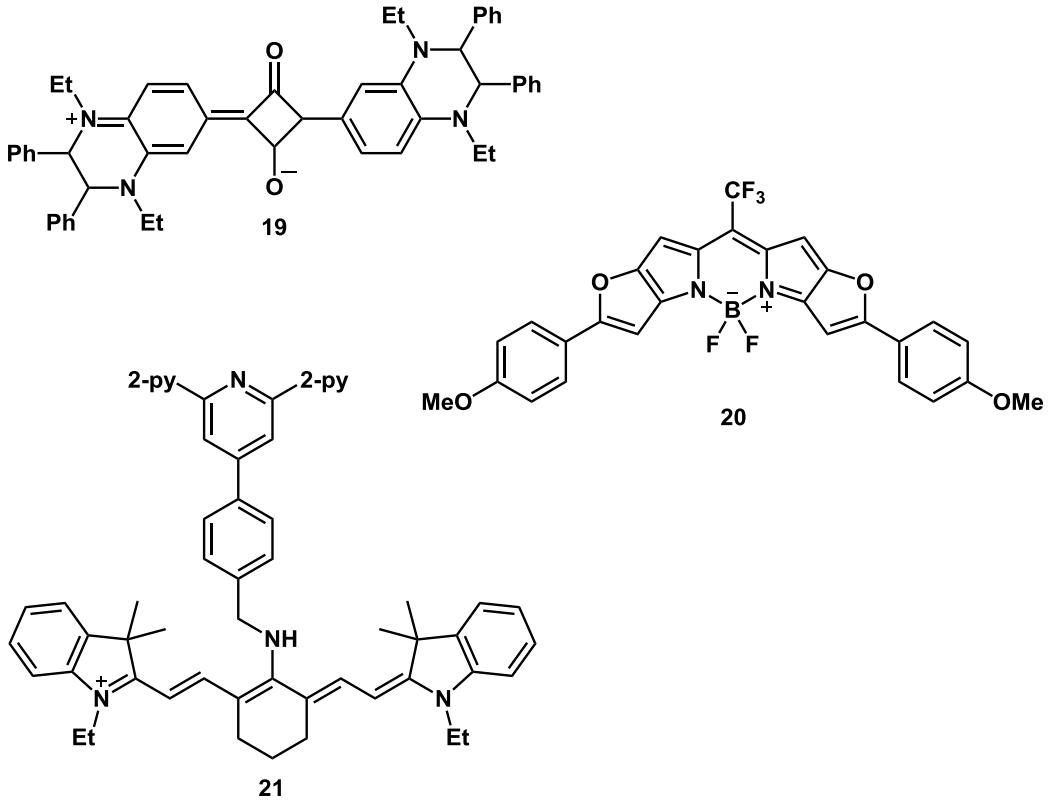

Figure 4-2. NIR dyes for bioimaging

We aim to develop a NIR sensor for serotonin. Serotonin contains an aromatic indole moiety and absorbs light at ~325 nm. Therefore, it is necessary to have a high-wavelength absorbing and emitting fluorescent sensor in order to avoid background fluorescence from the analyte itself and to be more compatible with biological samples. It is important to note that fluorescence sensing of serotonin is difficult as the electron-rich indole can easily quench fluorophores via photoinduced electron transfer (PET).

4.2 Previous Work

The detection of serotonin is mainly achieved through analytical methods that include chromatographic and electrochemical techniques. Chromatographic techniques allow for selective detection of intracellular concentrations of serotonin, but require sample preparation unsuitable for preserving intact cells.[88,89] Electrochemical techniques such as amperometry and cyclic voltammetry are non-destructive approaches allowing for selective detection of serotonin that relay quantitative and temporal information, but provide crude spatial information.[90,91,92,93]

^{11}C and ^{18}F radioligands are developed as *in vitro* and *in vivo* noninvasive tracers based on positron emission tomography for imaging the serotonergic system in the human brain by targeting the 5-HT family of receptors (*e.g.*, 5-HT_{1A}) or the membrane-bound human serotonin transporter (SERT) protein.[94] The majority of radioligand tracers that are designed to interact with 5-HT receptors act as antagonists to label receptor populations that allow for quantification and imaging of receptor distribution. SERT-specific positron emission tomography radioligands are designed as substrates for the

SERT protein in order to colocalize with serotonin within secretory vesicles and represent an optical approach for labeling secretory vesicles that contain serotonin through colocalization. As optical tracers, neither 5-HT receptor targeting nor SERT-specific radioligands directly label serotonin.

Fluorescence-based technologies remain a compelling approach to selectively detect and image serotonin.[47, 95] In recent years, fluorescence-based approaches for monitoring serotonin interactions have included multi-photon excitation of intracellular serotonin,[96] label-based fluorescent immunoassays,[97,98] and fluorescent sensors such as amplifying fluorescent polymers (AFPs).[99] However, the current fluorescence-based approaches either suffer from high background fluorescence, or do not represent practical approaches toward *in vivo* and *ex vivo* analyses because the approaches represent inapplicable bioorganic models or do not provide a fluorescence turn-on response due to the photophysical tendency of the electron-rich indoleamine moiety to quench the fluorescence response of the fluorophore through photoinduced electron transfer (PET).

A water-soluble fluorescence-based molecular sensor permits a unified approach in the selective recognition and visualization of serotonin *in vivo* and *in vitro* analyses that limits interference with native neuronal functions. Moreover, a fluorescence-based turn-on molecular sensor possessing spectroscopic properties capable of fluorescence emission in the near infrared (NIR) spectral region (i.e., a wavelength emission greater than 600 nm) would be particularly advantageous by minimizing background from

biological analytes (i.e., riboflavin), reducing photodamage to biological samples, and allowing for greater tissue penentration.

4.3 NeuroSensor 715

4.3.1 Design

Here we report NeuroSensor 715 (NS715), a near-IR fluorescence-based turn-on molecular sensor for the selective recognition and sensing of serotonin based on a modified coumarin aldehyde scaffold with a design that capitalizes on the relationship between fluorescence response and DFT computational analyses and entails exclusively modifying the electron density of the fluorophore and corresponding E_{HOMO} and E_{LUMO} values. NS715 can be divided into two distinct moieties from the viewpoint of fluorescence: i) the modified coumarin aldehyde scaffold (fluorophore) and ii) the pendant thiophene moiety situated at the 4-position of the coumarin core (C4-position) (Figure 4-3).

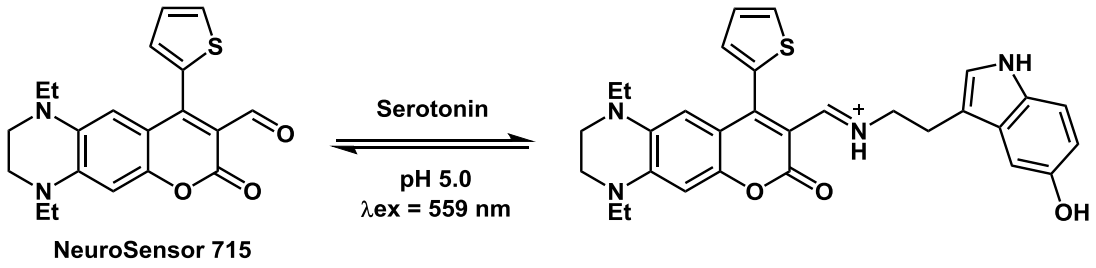

Figure 4-3. Reversible covalent interaction between NeuroSensor 715 and serotonin

NS715 features an aldehyde recognition element at the 3-position of the coumarin core (C3-position) that associates with the analyte amine via iminium ion formation. The modified coumarin aldehyde scaffold derives from the electron-rich 1,2,3,4-tetrahydroquinoxaline (THQ) framework. Ethyl groups situate the 1-and 4-positions of the THQ framework. The rigid alkylated di-nitrogen species situated at the 6- and 7-positions of the coumarin core (C6- and C7-positions) were incorporated to modulate the fluorescence properties of the fluorophore such that the fluorescence response of NS715 would enhance upon interaction with serotonin. The fixed di-nitrogen species reinforce orbital alignment by restricting free rotation of the nitrogen atoms. A thiophene moiety is appended to the modified coumarin aldehyde scaffold at the C4-position and serves to provide a notable bathochromic shift in the absorption and emission profiles.

4.3.2 Synthesis

The synthesis of NS715 was accomplished in six steps from commercially available starting materials (Figure 4-4). Following literature precedent, 2-methoxy-2-nitroaniline (**22**) was reduced using hydrogen gas and palladium on carbon to achieve the diaminobenzene.[100] Treatment with glyoxal forms two imines creating compound **24** and reduction with sodium borohydride yields the tertiary amines. Friedel-Crafts acylation with 2-thiophenecarbonyl chloride acrylates the ring. Subsequent treatment with the ester-functionalized ylide gives a α,β-unsaturated ester intermediate which undergoes intramolecular transesterification to produce

the coumarin scaffold. Formylation under Vilsmeier conditions yields the final product.

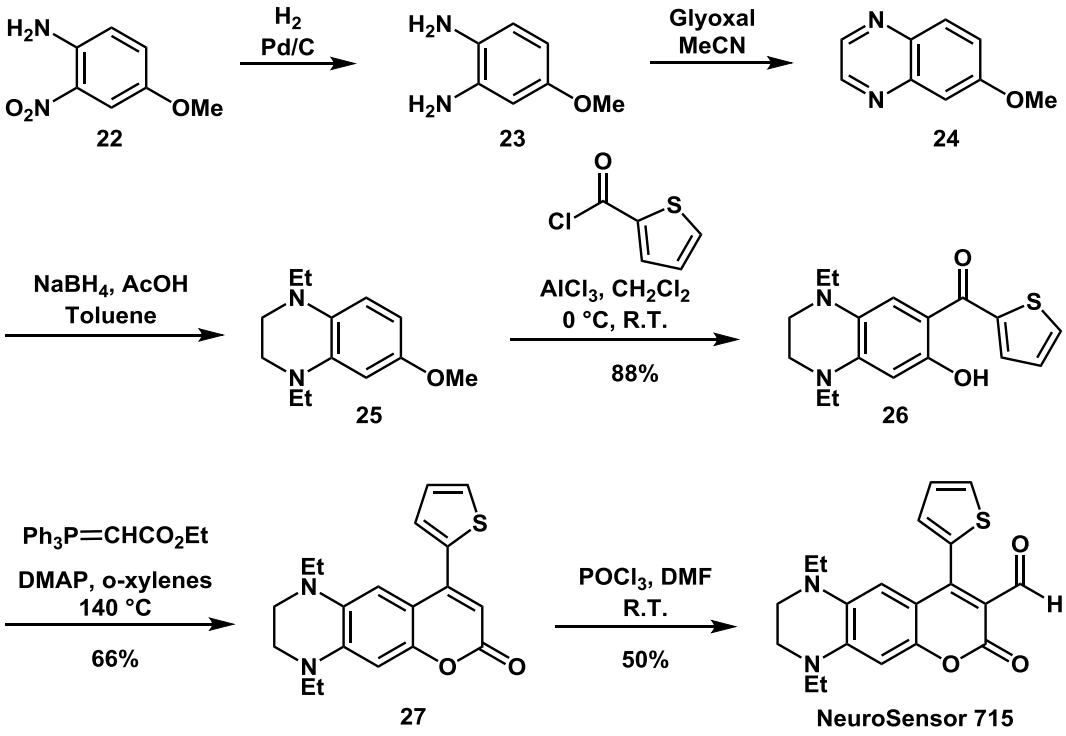

Figure 4-4. Synthesis of Neurosensor 715

4.3.3 Titrations

NeuroSensor 715 was screened with various relevant amines via absorption and fluorescence spectroscopy. As observed with other sensors in this series, NeuroSensor 715 binds to all primary amines via iminium ion formation, which produces a red shift in absorption from 500 to 546 nm (Figure 4-5A). In fluorescence mode, exciting the unbound NeuroSensor 715 at 559 nm provided fluorescence emission at 686 nm. In fluorescence mode, exciting the bound complex at 559 nm

upon adding serotonin produced a marked 3.2-fold fluorescence enhancement at 715 nm (Figure 4-5B). Table 4-1 summarizes binding and spectroscopic data for the interaction of NeuroSensor 715 with a number of relevant amines. Glutamate binds with a low binding affinity of 22.3 M^{-1} that provides a 1.7-fold fluorescence enhancement. The catecholamines norepinephrine and dopamine have on average 6.0-fold higher binding constants compared to glutamate with a binding affinity of 129 M^{-1} and 145 M^{-1} and a 2.0- and 2.6-fold fluorescence enhancement, respectively. Interestingly, serotonin has a 15-fold higher binding constant compared to glutamate with a binding affinity of 341 M^{-1} and 3.2-fold fluorescence enhancement. The bathochromic shift upon analyte binding was 46 nm, 37 nm, and 30 nm for serotonin, the catecholamines, and glutamate, respectively.

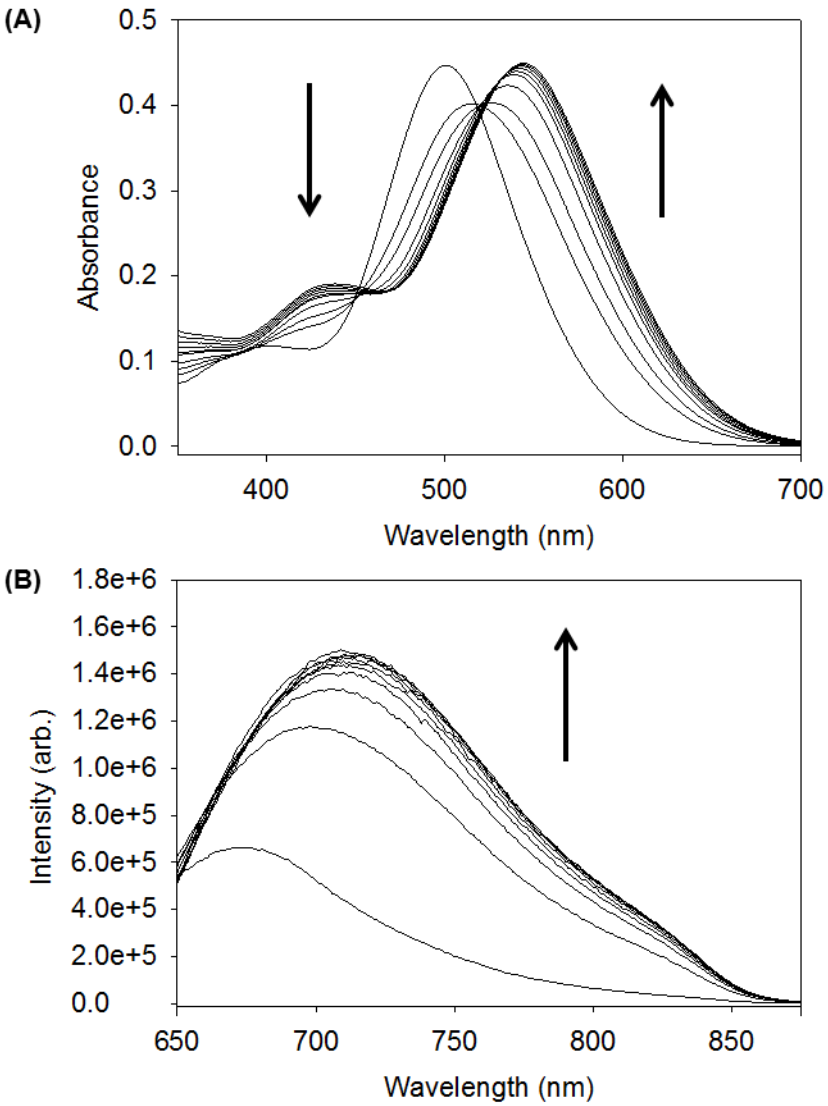

Figure 4-5. (A) UV/Vis and (B) fluorescence spectra of NS715 (20 µM) in buffer (50 mM $Na_2S_2O_3$, 120 mM NaCl, pH 5.0) adding aliquots of 200 mM serotonin. Inset is the fit to a one-site binding isotherm. λ_{ex} = 559 nm. λ_{em} = 715 nm.

Table 4-1. Association constants (K_a) and spectroscopic parameters for the binding of NS715 to various analytes

Amine Guest	K_a (M^{-1})[a]	I_{sat}/I_0[b]	$\Delta\lambda_{max,abs}$[c] (nm)
Serotonin	341	3.2	46
Dopamine	145	2.6	37
Norepinephrine	129	2.0	37
Glutamate	22.3	1.7	30

[a] K_a measured by fluorescence spectroscopy, λ_{ex} = 559 nm, λ_{em} = 715 nm. Error in K_a values are ±10% based on triplicate titrations. [b] I_{sat} = fluorescence intensity at saturation taken from the theoretical fit to the binding isotherm. [c] Bathochromic shift in absorbance upon saturating with analyte.

4.3.4 Computational Analysis

The conventional DFT calculations using the hybrid exchange-correlation function B3LYP with the 6-31* basis set as implemented in Gaussian 09W were performed on the coumarin aldehyde scaffold of NeuroSensor 521 and the modified coumarin aldehyde scaffold of NeuroSensor 715. Several starting geometries were used for the geometry optimization to ensure that the optimized structure corresponded to a global minimum.

Table 4-2 summarizes the computational calculations for the NS521 coumarin aldehyde scaffold, the NS715 THQ-derived modified coumarin aldehyde scaffold, and the indoleamine-based analyte, serotonin. The energy of the highest occupied molecular orbital (E_{HOMO}) and lowest unoccupied molecular orbital (E_{LUMO}) values of the NeuroSensor 521 coumarin aldehyde scaffold were obtained as -0.21087 and -0.08046 hartrees, respectively, that corresponds to a calculated energy band gap of

0.13041 hartrees. The E_{HOMO} and E_{LUMO} values of the modified coumarin aldehyde scaffold of NeuroSensor 715 scaffold were obtained as -0.18982 and -0.07321 hartrees, respectively, that corresponds to a calculated energy band gap of 0.11661 hartrees. The E_{HOMO} and E_{LUMO} values of serotonin were obtained as -0.00385 and -0.19282 hartrees, respectively.

Table 4-2. DFT calculations of the E_{HOMO} and E_{LUMO} values for serotonin, NS521, and NS715

Compound	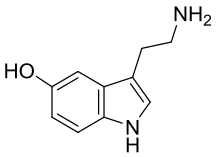	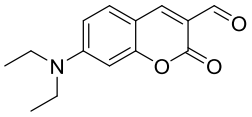	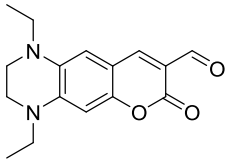
	Serotonin[a]	**NS521**[b]	**NS715**[b]
***E*HOMO (hartrees)**	-0.19282	-0.21087	-0.18982
***E*LUMO (hartrees)**	-0.00385	-0.08046	-0.07321

[a]E_{HOMO} and E_{LUMO} values of the corresponding 5-hydroxyindole moiety; [b]E_{HOMO} and E_{LUMO} values of the corresponding coumarin aldehyde scaffold (fluorophore).

4.3.5 Discussion

NeuroSensor 715

NeuroSensor 715 is a NIR fluorescence-based turn-on molecular sensor for the selective recognition and imaging of serotonin in neurosecretory vesicles. NeuroSensor 715 is envisaged to integrate with a tailored approach to comprise a method for the selective labeling and visualization of serotonin in live and fixed cells analogous to the method utilizing the NeuroSensor 521 predecessor for selective

recognition of catecholamine-based neurotransmitters norepinephrine and dopamine.[61] The method entails utilizing NeuroSensor 715 to exploit the high concentration of serotonin and acidic environment within secretory vesicles through the formation of a charged complex that prevents translocation across the vesicle membrane and accumulates within secretory vesicles.

NeuroSensor 715 features an aldehyde group that associates with the analyte amine via iminium ion formation and features a pendant thiophene moiety at the 4-position of a modified coumarin aldehyde scaffold derived from the electron-rich THQ framework. The modified coumarin aldehyde scaffold and pendant thiophene moiety are key design parameters that i) confer a fluorescence turn-on response upon binding to serotonin, and ii) impart spectroscopic properties to NeuroSensor 715 that allow for direct monitoring of the unbound and bound states using a conventional confocal microscope equipped with the standard 488 nm and 559 nm lasers, respectively. NeuroSensor 715 exhibits an unprecedented 3.2-fold fluorescence enhancement at 715 nm in the NIR spectral region with a binding affinity of 341 M^{-1} in *in vitro* analyses. NeuroSensor 715 binds to serotonin with a 15-fold and 6.0-fold higher binding constant compared and to typical primary amines and catecholamines such as glutamate and norepinephrine.

Spectral Characteristics

NeuroSensor 715 incorporates a pendant thiophene moiety and fused alkylated di-nitrogen species to that derives from the THQ framework to constitute a modified

coumarin aldehyde moiety and provides pronounced spectroscopic and photophysical properties. Table 4-3 provides a comparison of the spectral characteristics between a benzene-based NeuroSensor 521 derivative, a thiophene-based NeuroSensor 521 derivative, and NeuroSensor 715, and highlights the effect of both the incorporation of the thiophene moiety at the C4-position and the electron-rich THQ framework of the coumarin core that situates electron-donating nitrogen substituents at the C6- and C7-positions.

Replacing the pendant benzene moiety with a thiophene moiety on the coumarin aldehyde scaffold of the NeuroSensor 521 platform affords a reasonable bathochromic shift of 10 nm and 17 nm in absorbance and fluorescence emission, respectively, with a maximum absorbance and fluorescence emission at 462 nm and 522 nm, respectively. In doing so, both the unbound and bound Stokes shift increases 53 nm and 32 nm, respectively, for the benzene-based NeuroSensor 521 derivative to the unbound and bound Stokes shift of 60 nm and 37 nm, respectively for the thiophene-based NeuroSensor 521 derivative.

Modify the coumarin aldehyde scaffold by fixing electron-donating nitrogen species at the C6- and C7-positions results in a drastic bathochromic shift in the absorption and emission profiles. The pendant thiophene and THQ-derived modified coumarin aldehyde scaffold afford a noteworthy bathochromic in both the absorption and fluorescence properties with a 500 nm and 546 nm maximum absorbance and a 686 nm and 715 nm maximum fluorescence emission for the unbound and bound complex, respectively. The Stokes shift of both the unbound

and bound complex of NeuroSensor 715 increases over 125 nm compared to the thiophene-based NeuroSensor 521 derivative to 186 nm and 169 nm, respectively.

Table 4-3. Comparison of spectroscopic properties sensors based on the coumarin-3-aldehyde scaffold

	NeuroSensor 521 Derivatives		**NeuroSensor 715**
Spectral Properties	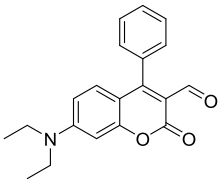	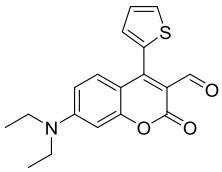	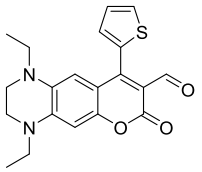
$\lambda_{abs}/\lambda_{em}$ (nm)[a]	452/505	462/522	500/686
$\lambda_{abs}/\lambda_{em}$ (nm)[b]	488/520	502/539	546/715
Stokes shift (nm)[a]	53	60	186
Stokes shift (nm)[b]	32	37	169

[a]Spectroscopic properties of the unbound sensor; [b]Spectroscopic properties of the sensor saturated with primary amine analyte.

Computational Analysis

The electron-rich nature of serotonin is known to quench the fluorescence response of fluorescent sensors upon interaction with serotonin through a photoinduced electron transfer (PET) mechanism. Until the development of NeuroSensor 715, no fluorescence-based approaches were capable of producing a turn-on fluorescence response upon interaction with serotonin. Indeed, the 5-hydroxyindoleamine moiety of serotonin strongly quenched all benzene- and thiophene-based NeuroSensor 521 derivatives. Our working hypothesis was that the E_{HOMO} value of the 5-hydroxyindoleamine moiety was significantly higher than the E_{HOMO} value of the NeuroSensor 521-based coumarin aldehyde scaffold and

quenched the fluorescence of the coumarin aldehyde scaffold (fluorophore) through an acceptor-excited PET (a-PET) process (Figure 4-6A).

Density function theory (DFT) computational analyses at the B3LYP/6-31G(d) level of theory guided the design of NeuroSensor 715 with calculations of the E_{HOMO} and E_{LUMO} values of the THQ-derived modified coumarin aldehyde scaffold that support the incorporation of a rigid alkylated di-nitrogen species by concomitantly raising the E_{HOMO} and lowering the energy band gap between the ground and excited singlet states of the fluorophore such that the fluorescence of NeuroSensor 715 enhances upon interaction with serotonin in the NIR spectral region. As depicted in Figure 4-6A, the calculated E_{HOMO} value of -0.19282 hartrees for the 5-hydroxyindoleamine moiety is considerably higher than the calculated E_{HOMO} value of -0.21087 hartrees for the NeuroSensor 521-based coumarin aldehyde scaffold and thus, permits serotonin to quench the fluorescence of the fluorophore upon excitation.

The calculations support the notion that serotonin quenches the fluorophore of the NeuroSensor 521-based derivatives through an acceptor-excited PET (a-PET) process. As depicted in Figure 4-6B, the calculated E_{HOMO} value of -0.18982 hartrees for the THQ-derived modified coumarin aldehyde scaffold elevates the ground state of the fluorophore of NeuroSensor 715 above the calculated E_{HOMO} value of the 5-hydroxyindoleamine due to situating electron-donating nitrogen species at the C6- and C7-positions of the modified coumarin aldehyde scaffold that thereby, affords an increase in fluorescence response by preventing the 5-hydroxyindoleamine

moiety from donating an electron from a lower energy lying orbital into the fluorophore of NS715 through an a-PET process.

In short, the 5-hydroxyindoleamine moiety cannot quench the fluorescence of the NS715 fluorophore due to the fluorophore exhibiting a higher ground state energy compared to the 5-hydroxyindoleamine moiety. Moreover, the pronounced photophysical properties NeuroSensor 715 demonstrates is consistent with the calculated energy band gap of 0.11661 hartrees between the E_{HOMO} and E_{LUMO} values of the THQ-derived modified coumarin aldehyde. That is, the smaller calculated energy band gap for NeuroSensor 715 compared to the calculated energy band gap of 0.13041 hartrees for NeuroSensor 521 coumarin aldehyde scaffold coincide with fluorescence emission of longer wavelength light at 715 nm in the NIR spectral region.

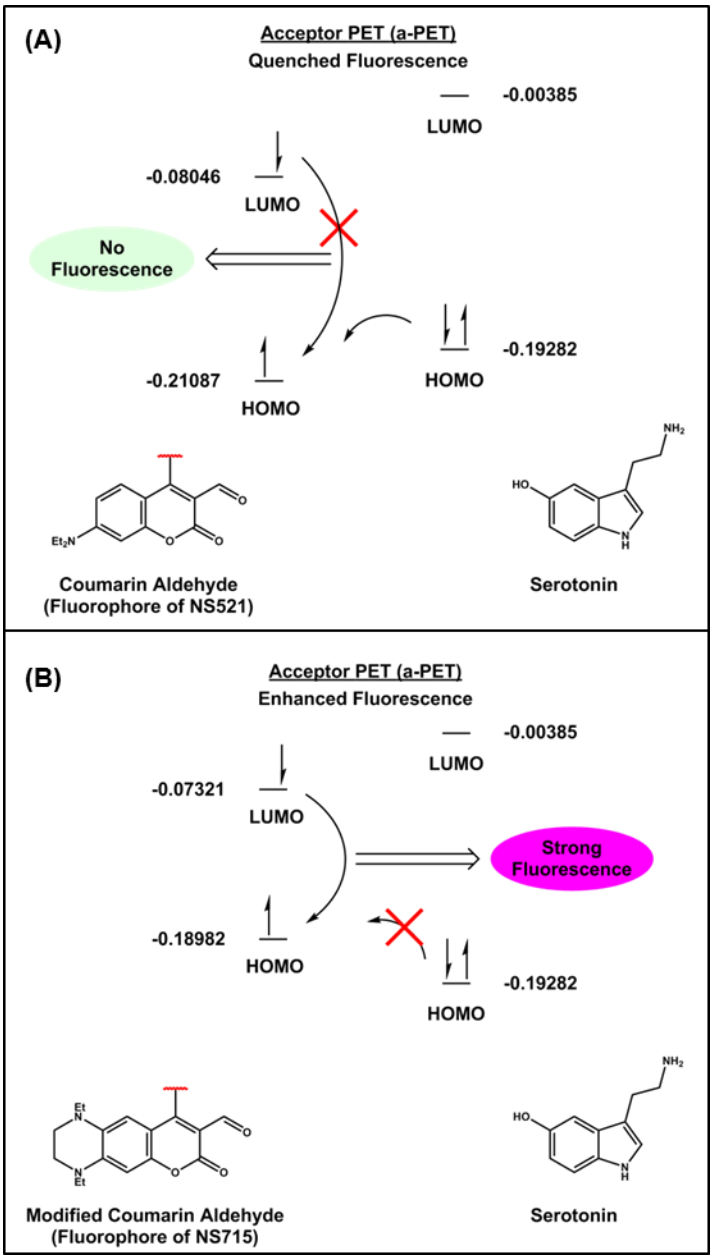

Figure 4-6. Frontier orbital energy diagram and schematic representation of acceptor-excited PET (a-PET) mechanism. Schematic representation of the (A) E_{HOMO} value of the corresponding coumarin aldehyde scaffold of derivatives of the NS521 platform, and (B) E_{HOMO} of the corresponding modified coumarin aldehyde scaffold of NS715, both in relation to the E_{HOMO} of the corresponding 5-hydroxyindole moiety of serotonin.

4.3.6 Cell Studies

Cellular studies were conducted by incubating NS715 with live chromaffin cells that were separated into norepinephrine-enriched (NE) and epinephrine-enriched (EP) subpopulations. Based on our work with NS521, we expected the NE cells to fluoresce, as norepinephrine has a primary amine and could interact with the aldehyde of NS715.[61] Epinephrine, on the other hand, has a secondary amine and therefore, should not interact with the sensor or provide a fluorescence response. A 458 nm laser was used to visualize any unbound sensors and a 633 nm laser was used to image the bound complex (Figure 4-7).

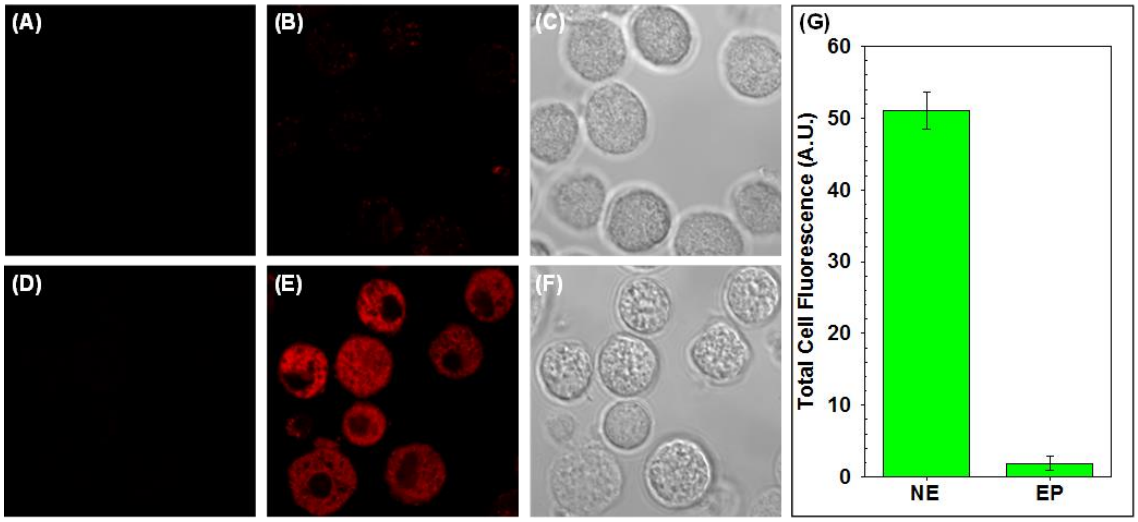

Figure 4-7. Incubation of NS715 (10 μM) with chromaffin cells. Epinephrine-enriched cells (A-C): (A) λ_{ex} = 458 nm; (B) λ_{ex} = 633 nm; (C) brightfield image. Norepinephrine-enriched cells (D-F): (D) λ_{ex} = 458 nm; (E) λ_{ex} = 633 nm; (F) brightfield image. Fluorescence was visualized using a 650-710 nm bandpass filter. (G) The mean corrected total cell fluorescence intensity for norepinephrine- and epinephrine-enriched (NE and EP, respectively) cells was 42.77 ± 0.91 and 2.52 ± 0.12 respectively. Error bars represent standard deviation (*n* = 12).

The NE cells showed strong punctate fluorescence and had a mean corrected total cell fluorescence intensity that was 17-fold greater than the EP cells which were sparsely fluorescent. These results indicate that i) NS715 can permeate the vesicular membrane of secretory vesicles, and ii) NS715 is selective for primary-amine neurotransmitters over secondary amines. Excitation of the cells at 458 nm would have visualized any unbound sensor molecules, but the lack of fluorescence signal indicates that nearly all NS715 molecules were in the bound state.

Future studies would include testing this sensor in serotonergic neurons and/or tissues to evaluate the *in vivo* response to the highly concentrated populations of intravesicular serotonin.

4.3.7 Conclusions

NeuroSensor 715 was developed as a NIR fluorescence-based turn-on molecular sensor for the selective labeling and visualization of serotonin in synaptic vesicles of neuronal cells. DFT computational analyses at the B3LYP/6-31G(d) level of theory aided in the design and inclusion of the electron-rich THQ framework into the coumarin core to provide the modified coumarin aldehyde scaffold constituting NeuroSensor 715. The rigid, electron-donating di-nitrogen species at the C6- and C7-positions of the coumarin core reinforce orbital alignment by restricting free rotation of the nitrogen atoms and impart pronounced spectroscopic and photophysical properties by simultaneously raising the calculated E_{HOMO} value above the E_{HOMO} value of the 5-hydroxyindoleamine moiety of serotonin to allow for a 3.2-

fold fluorescence enhancement at 715 nm in the NIR spectral region with a binding affinity of 341 M^{-1} in *in vitro* analyses. NeuroSensor 715 represents a convenient molecular sensor designed for integration with a tailored approached and proven method for the selective labeling and visualization of serotonin in live and fixed neuronal cells.

APPENDIX

Experimental Procedures and Characterization Data

Part I. General Information

All reagents and solvents were purchased from commercial sources (Sigma Aldrich, Acros Organic, Fisher Scientific, Alfa Aesar, TCI America, or Combi-Blocks) and used without further purification unless stated otherwise. Anhydrous dichloromethane, acetonitrile, and triethylamine were obtained by distillation from CaH_2. Anhydrous THF and toluene were obtained by distillation from sodium metal and benzophenone. All reactions were conducted using oven or flame dried glassware and under N_2 atmosphere unless stated otherwise. Flash column chromatography was carried by using 32-63 μm silica gel.

NMR spectra were obtained by a Bruker ARX-250 MHz, DRX-300 MHz, or DRX-500 MHz in $CDCl_3$ or DMSO-d6 using tetramethylsilane (TMS) as a reference. IR spectra were obtained from Nicolet FT-IR spectrometers. High resolution mass spectra (HRMS) were obtained from a Bruker Apex-Qe FTMS at Old Dominion University in Norfolk, VA.

Part II. Spectroscopic Studies

UV-Visible spectra were obtained by a Varian Cary-1E UV-Visible spectrometer. Fluorescence spectra were obtained by a Shimadzu RF-5301 PC spectrofluorometer.

Titrations were performed by using bis-tris propane or HEPES buffer with NaCl or $Na_2S_2O_3$ added unless otherwise stated. Absorbance and fluorescence spectra were processed using SigmaPlot™ 12.3 and best-fit lines fit using GraphPad Prism 6.01.

Part III. Binding Constant Determination

For all host (H) –guest (G) binding titrations, data was fit to a 1:1 binding isotherm:

$$H + G \rightleftharpoons HG$$

$$f = \frac{[HG]}{H_t} = \frac{f_{max}[G]}{K_d + [G]} \quad \text{1:1 isotherm equation} \qquad \text{(eq.1)}$$

f = fractional occupancy; H_t = concentration of total sensor; G_t = concentration of total analyte; [G] = concentration of free analyte; [HG] = concentration of bound host-guest complex; K_d = dissociation constant

There is an inverse relationship between the binding constant (K_a) and dissociation constant (K_d):

$$K_a = \frac{1}{K_d} \qquad \text{(eq. 2)}$$

Given that the concentration of total analyte is far greater than the dissociation constant, G_t is considered equal to [G]. Equation 3 can be used to estimate the K_d:

$$f = \frac{[HG]}{H_t} = \frac{f_{max} G_t}{K_d + G_t} \qquad \text{(eq. 3)}$$

For fluorescence titrations, the intensity difference upon analyte addition can be used with the concentration of free analyte and the theoretical fluorescence maximum to solve for the dissociation constant using Equation 4.

$$\left| \frac{F}{F_0} - 1 \right| = \frac{B_{max} G_t}{K_d + G_t} \qquad \text{(eq. 4)}$$

B_{max} = the theoretical fluorescence maximum when the host is saturated with guest

Part IV. Protocol for Cellular Assays

Cell Preparations:

1. **Separate cells:** Bovine chromaffin cells were obtained from Alice (Xin Liu, Gillis Group, Dalton Cardiovascular Research Center). The cells were pre-separated into epinephrine and norepinephrine-containing populations using a Percoll

gradient.[62] Each cell type was suspended in ~3 mL chromaffin medium in centrifuge tubes.

2. **Incubate cells with sensor:** Take 1 mL of each cell type from the stock and place into separate centrifuge tubes. Centrifuge the tubes for 5 min (speed "1-2" - rpm unknown). Cells form a pellet at the bottom of the tube. Remove supernatant using pipetter. Add 2 mL DMEM (Dulbecco's Modified Eagle Medium) solution to each tube. Add sensor from a DMSO stock solution so that the final concentration is 10 uL. Incubate (37 °C) and shake (250 rpm) for 30 min.
3. **Rinse & plate onto coverslips:** Centrifuge 5 min. Remove DMEM. Wash with 2 mL PBS buffer pumping up and down with a pipetter to break apart clumped cells. Centrifuge 5 min. Remove buffer and repeat. Remove supernatant using a pipetter. Add DMEM. Use pipetter and pump the cells up and down to "homogenize" the solution. Then take 3 mL of the sensor-cell mixture and plate onto each 35 mm glass-bottomed, poly-D-lysine-coated dish (Part # P35GC-1.5-14-C, MatTek Corporation). Incubate the plated cells at 37 °C for 16 hr.

<u>Confocal Fluorescence Imaging</u>:

- Bond Life Sciences Center, University of Missouri, *Columbia, MO*
    - A Zeiss LSM 510 META NLO inverted confocal microscope was utilized. Excitation was performed using the 488, 514, 543, or 633 nm laser lines. The signal was acquired viewing a 2.4 μM depth.
- Dalton Cardiovascular Research Center, University of Missouri, *Columbia, MO*

- An Olympus Optical FluoView FV1000 confocal laser scanning biological microscope was utilized. Excitation was performed using the 440 or 488 nm laser line.

Part V. Synthetic Procedures & Characterization Data

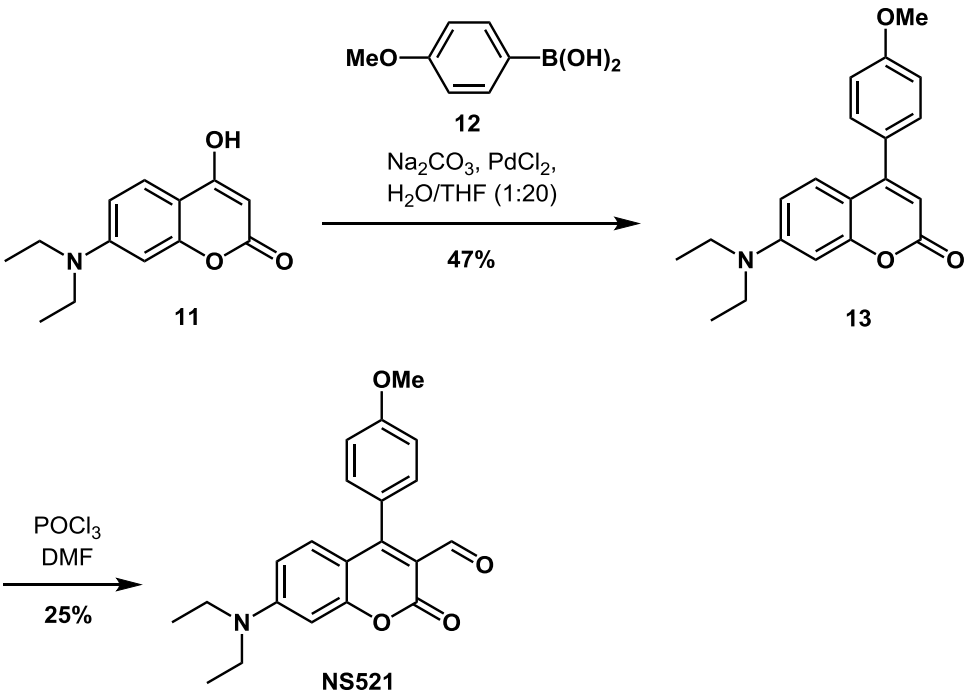

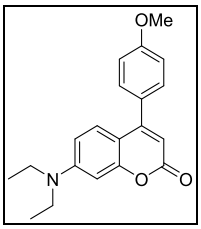

Compound 13. Compound **11** (250.0 mg, 1.072 mmol), *p*-toluenesulfonyl chloride (224.8 mg, 1.179 mmol), and Na_2CO_3 (340.8 mg, 3.215 mmol) were added to a flame-dried

round bottom flask and degassed with N_2 for 15 minutes. Degassed H_2O/THF (1:20, 15.0 mL) was added and the mixture stirred at 50 °C for 30 minutes. The mixture was allowed to cool to room temperature. 4-Methoxyphenylboronic acid (**12**) (179.2 mg, 1.179 mmol) was added and the mixture was allowed to stir at room temperature for 5 minutes. Palladium chloride (9.5 mg, 0.054 mmol) was added and the mixture stirred at 50 °C for 6 hours. The mixture was filtered and the solvent removed *in vacuo*. The remaining residue was purified by chromatography (100% CH_2Cl_2 → 95:5 CH_2Cl_2/EtOAc) to yield compound **13** (172 mg, 47%) as a pale-yellow oil: 1H NMR (500 MHz, $CDCl_3$) δ 7.40 (dd, 2H, *J* = 6.0, 1.0), 7.32 (dd, 1H, *J* = 8.8, 1.0), 7.02 (dd, 2H, *J* = 7.8, 1.5), 6.57 (d, 1H, *J* = 2.0), 6.53 (dd, 1H, *J* = 9.3, 2.0), 6.00 (d, 1H, *J* = 1.0), 3.88 (s, 3H), 3.42 (q, 4H, *J* = 7.0), 1.21 (t, 6H, *J* = 7.0); 13C NMR (125 MHz, $CDCl_3$) δ 162.3, 160.5, 156.8, 150.5, 129.8, 128.5, 127.9, 114.0, 108.4, 108.0, 107.9, 97.8, 55.4, 44.7, 12.4; IR (neat, cm-1) 2970, 1712, 1614, 1524, 1417, 1246, 1115, 829; HRMS calculated for $C_{20}H_{21}NO_3Na^+$ (M + Na^+): 346.1414. Found: 346.1415.

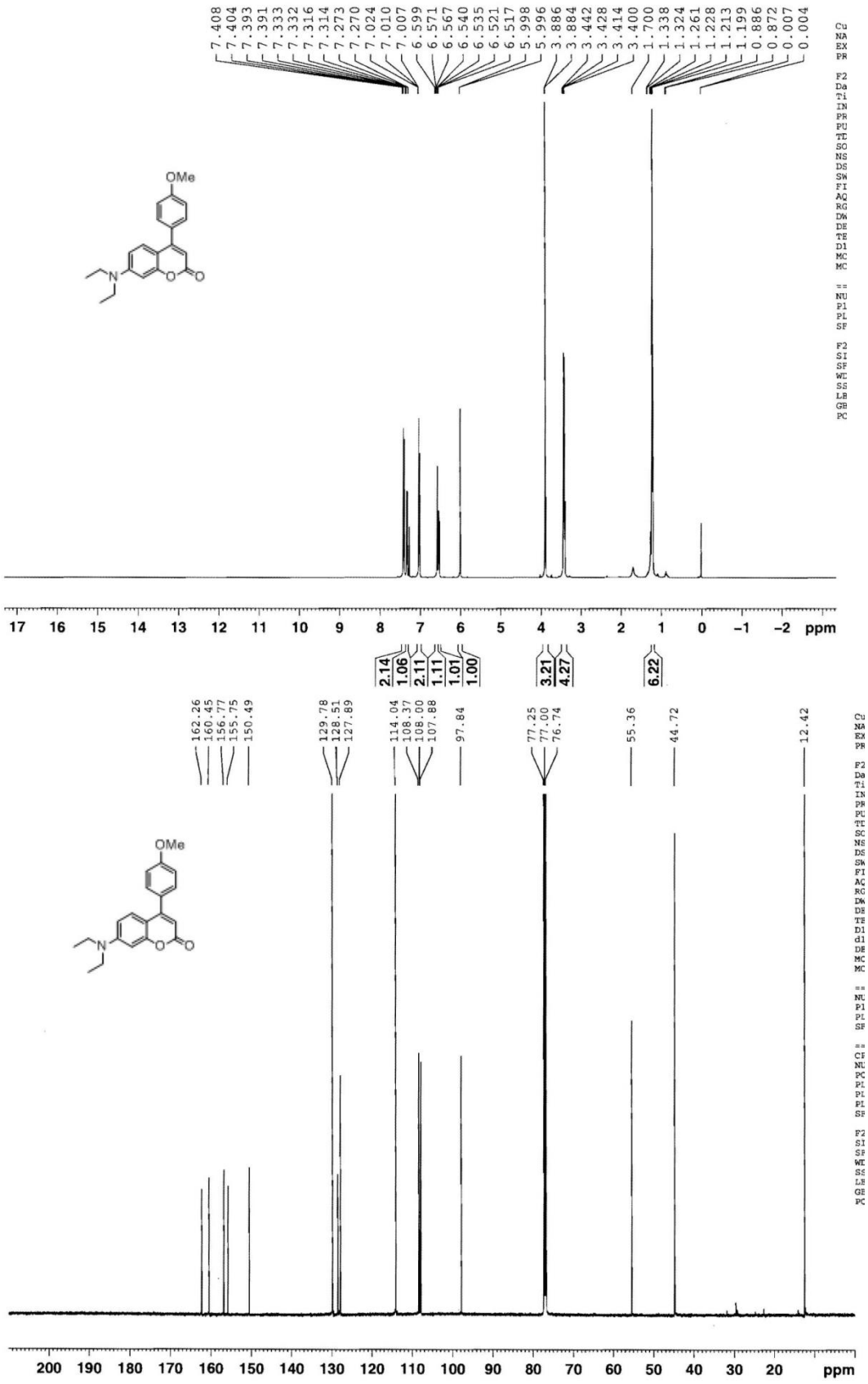
7.408
7.404
7.393
7.391
7.333
7.332
7.316
7.314
7.273
7.270
7.024
7.010
7.007
6.599
6.571
6.567
6.540
6.535
6.521
6.517
5.998
5.996
3.886
3.884
3.442
3.428
3.414
3.400
1.700
1.338
1.324
1.261
1.228
1.213
1.199
0.886
0.872
0.007
0.004
OMe
N
O
O
17 16 15 14 13 12 11 10 9 8 7 6 5 4 3 2 1 0 −1 −2 ppm
2.14
1.06
2.11
1.11
1.01
1.00
3.21
4.27
6.22
162.26
160.45
156.77
155.75
150.49
129.78
128.51
127.89
114.04
108.37
108.00
107.88
97.84
77.25
77.00
76.74
55.36
44.72
12.42
OMe
N
O
O
200 190 180 170 160 150 140 130 120 110 100 90 80 70 60 50 40 30 20 ppm

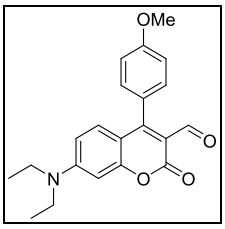

NeuroSensor 521 (Compound 1g). $POCl_3$ (5.2 mL, 56.1 mmol) was added to DMF (10.8 mL, 139.5 mmol) at 0 °C in a flame-dried round bottom flask. The Vilsmeier reagent was stirred at ambient temperature for 45 min. The Vilsmeier reagent (5 mL) was added to a solution of compound **13** (171.8 mg, 0.532 mmol) in DMF (1 mL). The solution was stirred at ambient temperature for 12 hours. The resulting red solution was poured onto cold H_2O (100 mL), basified with saturated $NaHCO_3$ (50 mL), and extracted with CH_2Cl_2 (100 mL x 3). The combined organic layers were dried over Na_2SO_4 and the solvent was removed *in vacuo*. The residue was purified by chromatography (80:20 hexanes:EtOAc → 50:50 hexanes/EtOAc) to yield NeuroSensor 521 (46.1 mg, 25%) as a yellow oil: 1H NMR (500 MHz, d-acetone) δ 9.80 (s, 1H), 7.27 (dd, 2H, *J* = 2.0, 6.5), 7.08 (dd, 2H, *J* = 2.0, 6.5), 6.99 (d, 1H, *J* = 9.5), 6.71 (dd, 1H, *J* = 2.5, 9.5), 6.55 (d, 1H, *J* = 2.5), 3.89 (s, 3H), 3.56 (q, 4H, *J* = 7.0), 1.22 (t, 6H, *J* = 7.0); 13C NMR (125 MHz, d-acetone) δ 188.0, 161.8, 161.2, 160.0, 158.7, 153.9, 131.7, 131.0, 126.2, 114.5, 113.2, 110.6, 109.8, 97.5, 55.7, 45.5, 12.7; IR (neat, cm-1) 2970, 2919, 2846, 1742, 1615, 1495, 1418, 1356, 1248, 1132; HRMS calculated for $C_{21}H_{21}NO_4Na^+$ (M + Na^+): 374.1363. Found: 374.1364.

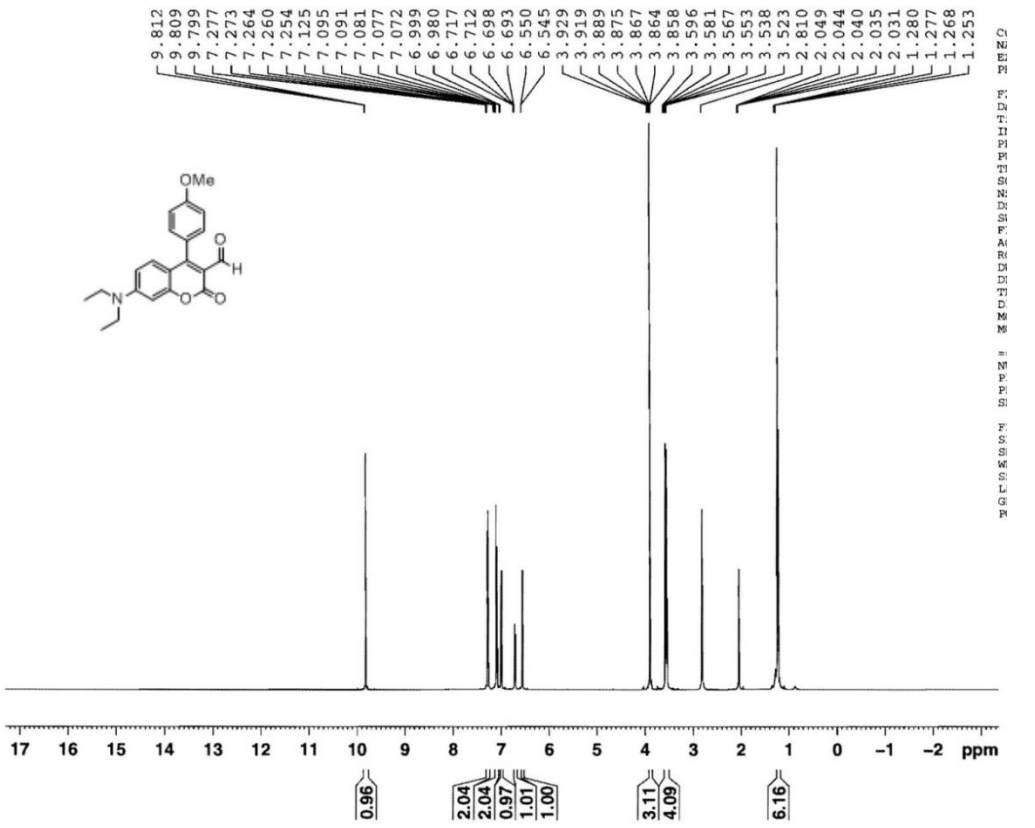
9.812
9.809
9.799
7.277
7.273
7.264
7.260
7.254
7.125
7.095
7.091
7.081
7.077
7.072
6.999
6.980
6.717
6.712
6.698
6.693
6.550
6.545
3.929
3.919
3.889
3.875
3.867
3.864
3.858
3.596
3.581
3.567
3.553
3.538
3.523
2.810
2.049
2.044
2.040
2.035
2.031
1.280
1.277
1.268
1.253
OMe
O
H
N
O
O
17 16 15 14 13 12 11 10 9 8 7 6 5 4 3 2 1 0 −1 −2 ppm
0.96
2.04
2.04
0.97
1.01
1.00
3.11
4.09
6.16

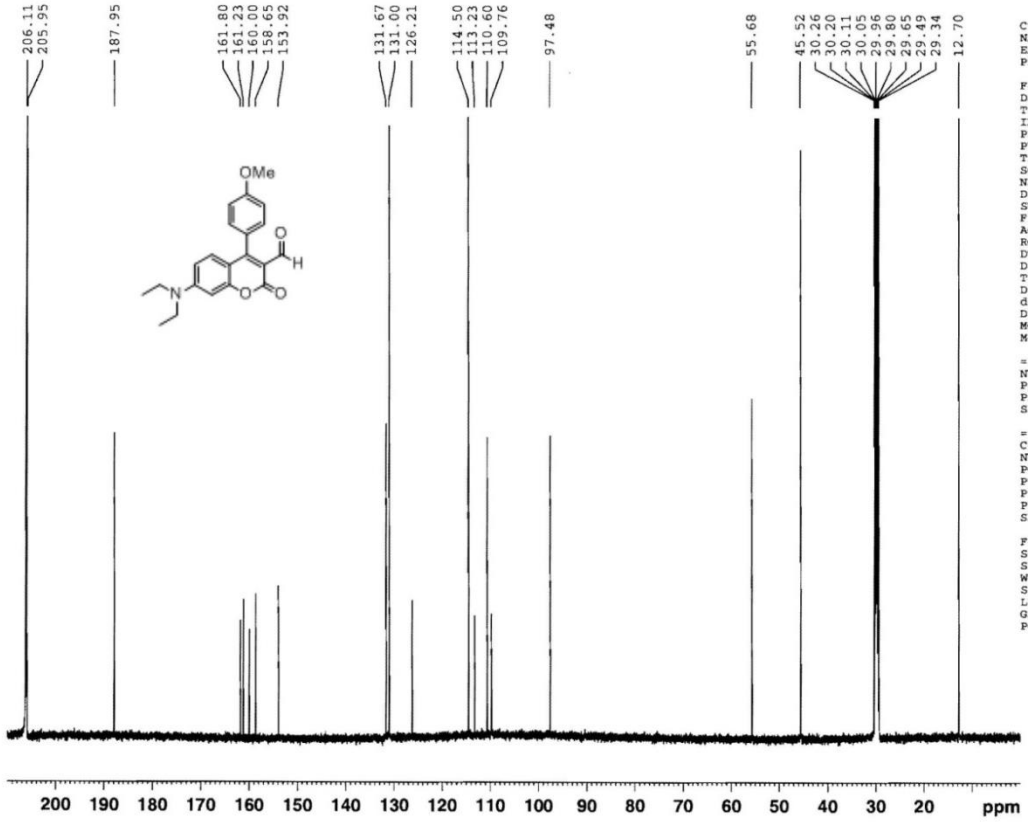
206.11
205.95
187.95
161.80
161.23
160.00
158.65
153.92
131.67
131.00
126.21
114.50
113.23
110.60
109.76
97.48
55.68
45.52
30.26
30.20
30.11
30.05
29.96
29.80
29.65
29.49
29.34
12.70
OMe
O
H
N
O
O
200 190 180 170 160 150 140 130 120 110 100 90 80 70 60 50 40 30 20 ppm

General Synthesis for Benzene-Based NS521 Derivatives

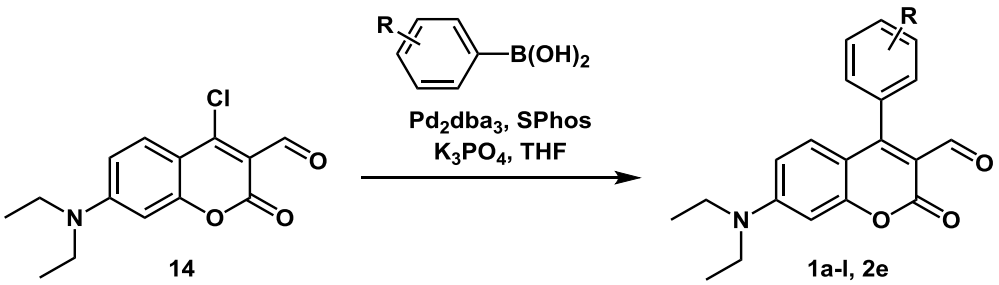

Compound **14** (0.250 g, 0.894 mmol), arylboronic acid (0.983 mmol), bis(dibenzylidene-acetone)-palladium(0) (0.041 g, 0.045 mmol), 2-dicyclohexylphosphino-2',6'-dimethoxybiphenyl (SPhos) (0.055 g, 0.134 mmol), tribasic potassium phosphate (0.381 g, 1.788 mmol) were added to a flame-dried round bottom flask and degassed with N_2 for 30 minutes. Degassed THF (distilled, 6 mL) was added and the mixture stirred at 60 °C for 12 hours under N_2. The mixture was allowed to cool to room temperature, filtered, rinsed with acetone, and the solvent removed *in vacuo*. The crude residue was purified by chromatography (100% CH_2Cl_2→80:20 CH_2Cl_2/EtOAc). The material was further purified by chromatography (90:10 hexanes/EtOAc→50:50 hexanes/EtOAc) to yield the desired compound as a yellow oil.

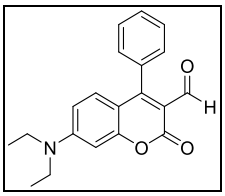

Compound 1b. Yield 64%; ^{1}H NMR (500 MHz, CD_2Cl_2) δ 9.78 (s, 1H), 7.47-7.55 (m, 3H), 7.23-7.30 (m, 2H), 6.93 (d, 1H, *J* = 10.0 Hz), 6.50-6.57 (m, 2H), 3.45 (q, 4H, *J* = 7.0 Hz), 1.23 (t, 6H, *J* = 7.0 Hz); ^{13}C NMR (125 MHz, CD_2Cl_2) δ 188.4, 162.0, 159.9, 158.1, 153.4, 133.7, 131.2, 129.3, 128.8, 128.7, 112.7, 110.2, 109.5, 97.4, 45.6, 12.5; IR (neat, cm^{-1}) 2974, 1751, 1715, 1683, 1617, 1559, 1504, 1418, 1354; HRMS calculated for $C_{20}H_{19}NO_3$ ($M + Na^+$): 344.1257. Found: 344.1254.

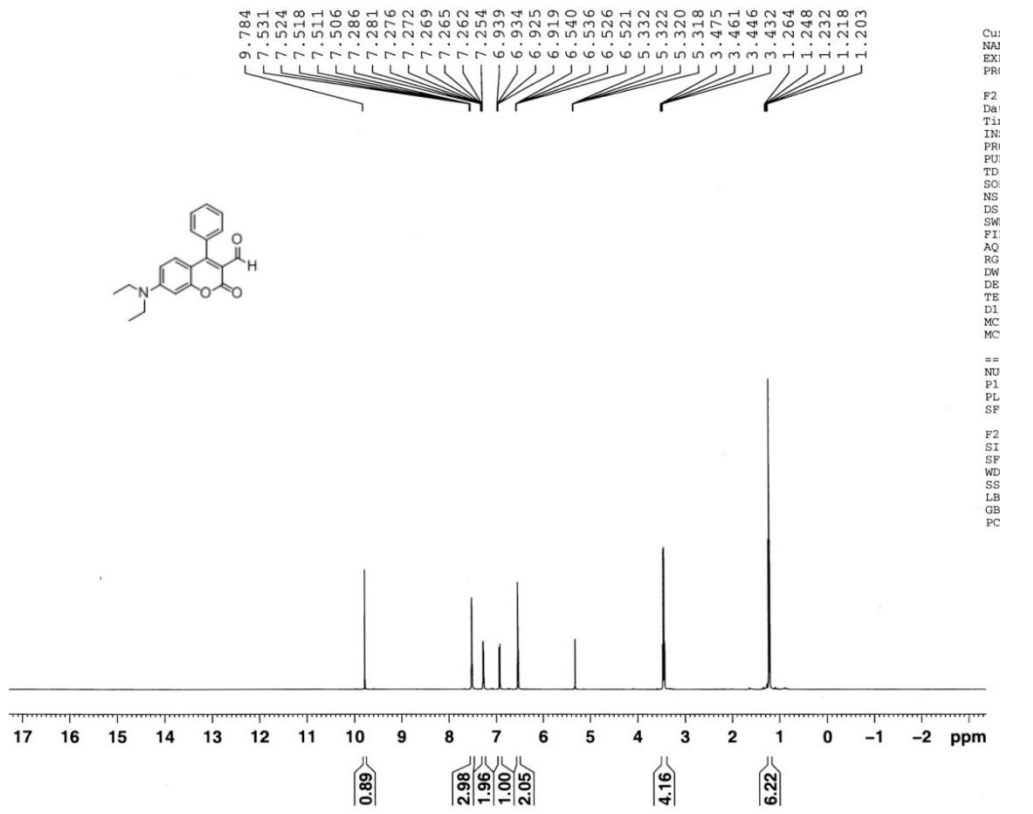
9.784
7.531
7.524
7.518
7.511
7.506
7.286
7.281
7.276
7.272
7.269
7.265
7.262
7.254
6.939
6.934
6.925
6.919
6.540
6.536
6.526
6.521
5.332
5.322
5.320
5.318
3.475
3.461
3.446
3.432
1.264
1.248
1.232
1.218
1.203
17 16 15 14 13 12 11 10 9 8 7 6 5 4 3 2 1 0 −1 −2 ppm
0.89
2.98
1.96
1.00
2.05
4.16
6.22

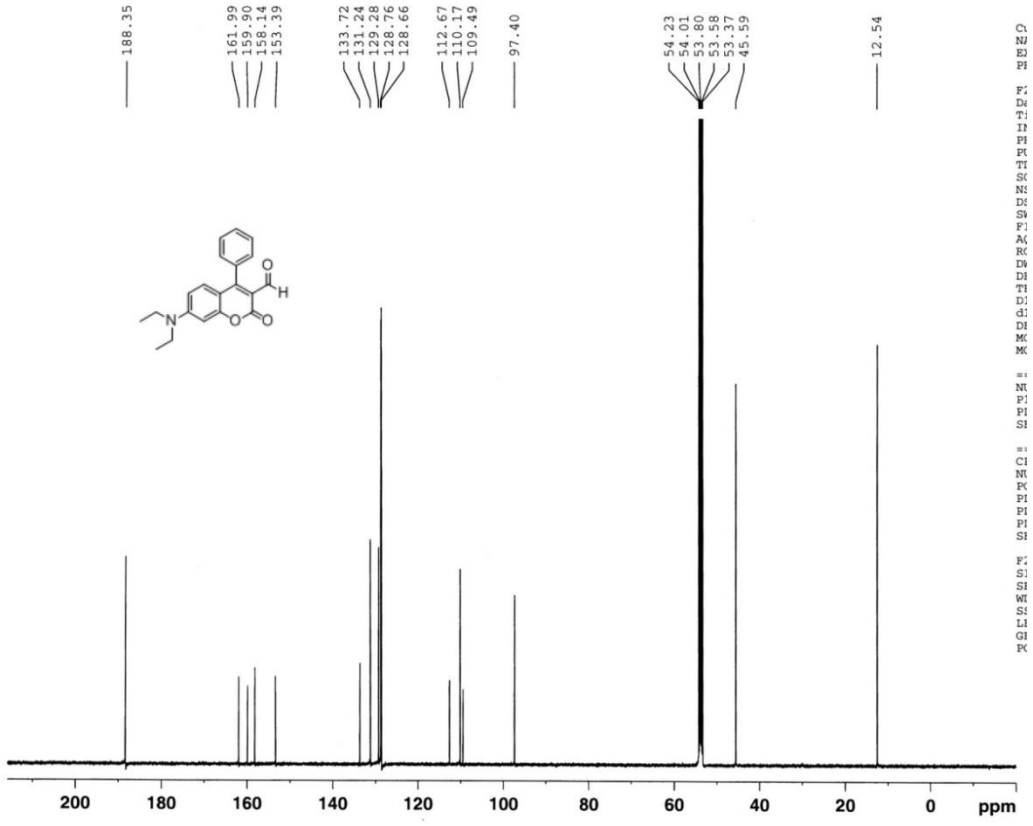
188.35
161.99
159.90
158.14
153.39
133.72
131.24
129.28
128.76
128.66
112.67
110.17
109.49
97.40
54.23
54.01
53.80
53.58
53.37
45.59
12.54
200 180 160 140 120 100 80 60 40 20 0 ppm

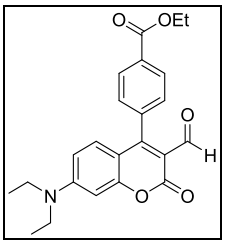

Compound 1a. Yield 83%; ^{1}H NMR (500 MHz, $CDCl_3$) δ 9.95 (s, 1H), 8.18 (d, 2H, *J* = 8.0 Hz), 7.32 (d, 2H, *J* = 8.5 Hz), 6.84 (d, 1H, *J* = 9.0 Hz), 6.52 (d, 1H, *J* = 2.5 Hz), 6.49 (dd, 1H, *J* = 9.0, 2.5 Hz), 4.43 (q, 2H, *J* = 7.0 Hz), 3.45 (q, 4H, *J* = 7.5 Hz), 1.43 (t, 3H, *J* = 7.0 Hz), 1.23 (t, 6H, *J* = 7.0 Hz); ^{13}C NMR (125 MHz, $CDCl_3$) δ 188.0, 166.0, 160.5, 159.7, 157.8, 153.1, 138.3, 130.9, 130.8, 129.6, 128.1, 111.7, 109.9, 108.8, 97.1, 61.2, 45.2, 14.3, 12.4; IR (neat, cm^{-1}) 2978, 1716, 1614, 1556, 1499, 1356, 1270, 1127, 1103, 727; HRMS calculated for $C_{23}H_{23}NO_5$ ($M + Na^+$): 416.1468. Found: 416.1464.

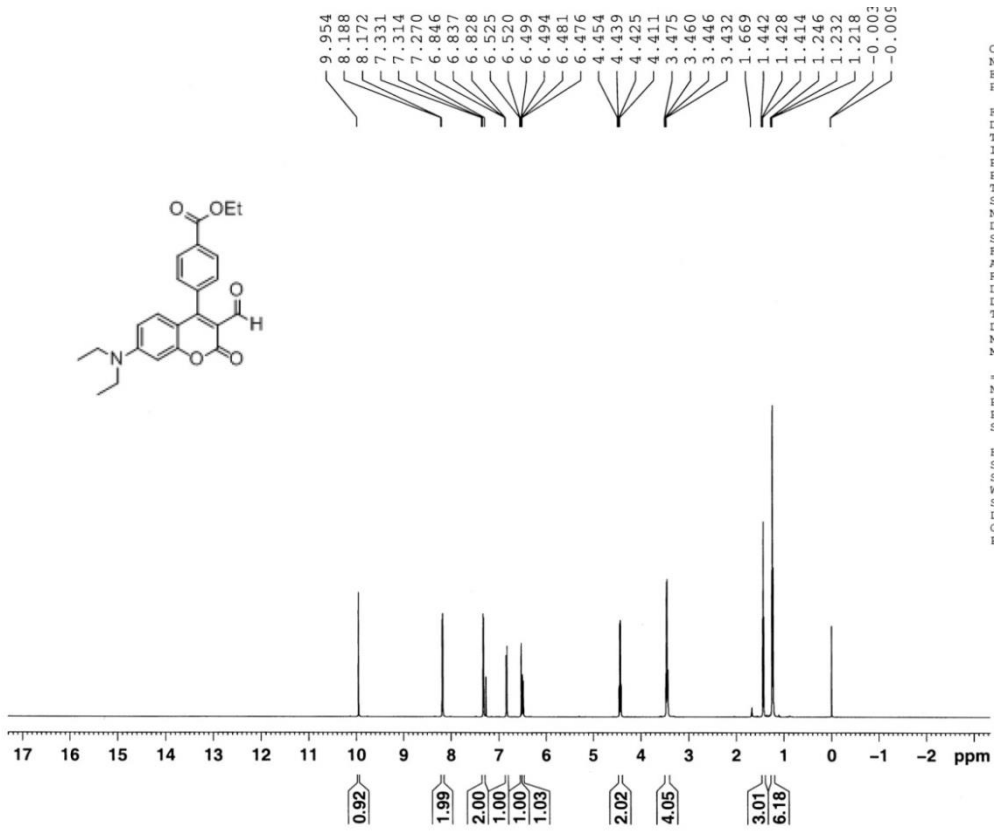
9.954
8.188
8.172
7.331
7.314
7.270
6.846
6.837
6.828
6.525
6.520
6.499
6.494
6.481
6.476
4.454
4.439
4.425
4.411
3.475
3.460
3.446
3.432
1.669
1.442
1.428
1.414
1.246
1.232
1.218
-0.003
-0.005
O
OEt
O
H
N
O
O
17 16 15 14 13 12 11 10 9 8 7 6 5 4 3 2 1 0 −1 −2 ppm
0.92
1.99
2.00
1.00
1.00
1.03
2.02
4.05
3.01
6.18

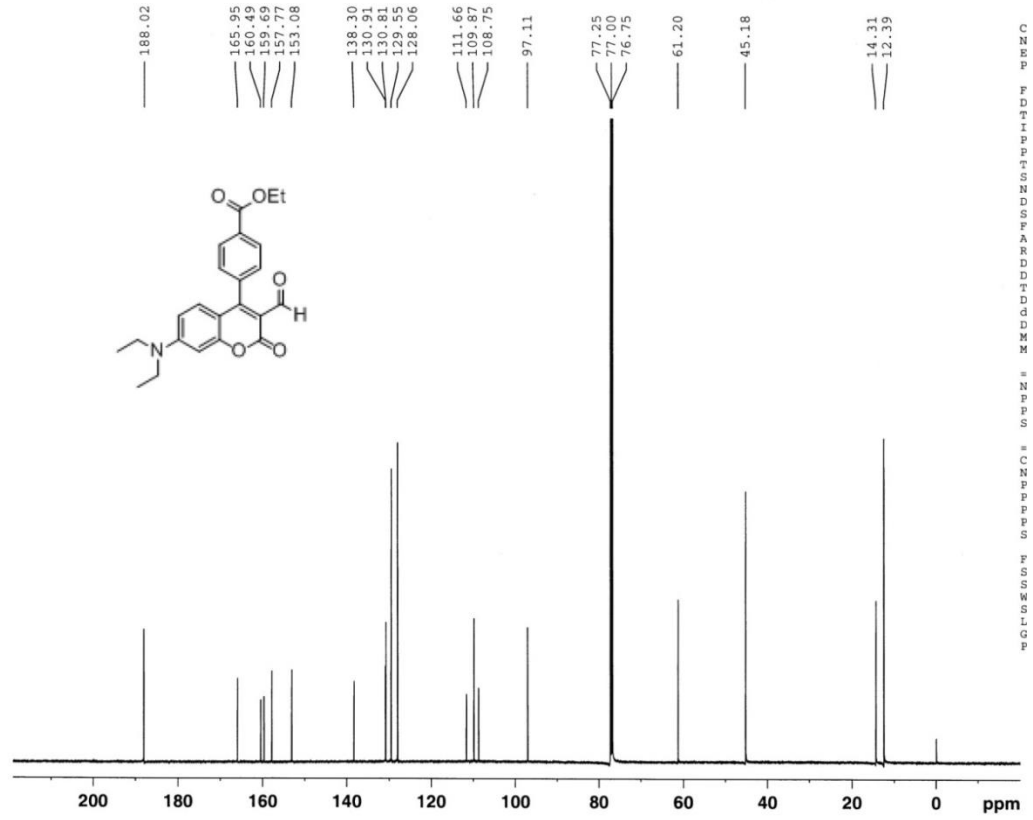
188.02
165.95
160.49
159.69
157.77
153.08
138.30
130.91
130.81
129.55
128.06
111.66
109.87
108.75
97.11
77.25
77.00
76.75
61.20
45.18
14.31
12.39
O
OEt
O
H
N
O
O
200 180 160 140 120 100 80 60 40 20 0 ppm

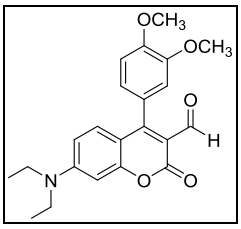

Compound 1i. Yield 77%; ^{1}H NMR (500 MHz, $CDCl_3$) δ 9.82 (s, 1H), 7.08 (d, 1H, *J* = 9.0 Hz), 7.00 (d, 1H, *J* = 8.0 Hz), 6.87 (dd, 1H, *J* = 8.0, 2.0 Hz), 6.80 (d, 1H, *J* = 1.5 Hz), 6.50-6.55 (m, 2H), 3.97 (s, 3H), 3.88 (s, 3H), 3.46 (q, 4H, *J* = 7.0 Hz), 1.25 (t, 6H, *J* = 7.0 Hz); ^{13}C NMR (125 MHz, $CDCl_3$) δ 188.5, 162.2, 159.4, 157.7, 153.0, 149.8, 148.9, 130.9, 125.0, 121.6, 112.6, 111.9, 110.9, 109.6, 109.1, 97.1, 56.1, 56.0, 45.2, 12.4; IR (neat, cm^{-1}) 2974, 1736, 1650, 1615, 1506, 1455, 1377, 1168; HRMS calculated for $C_{22}H_{23}NO_5$ ($M + Na^+$): 404.1468. Found: 404.1465.

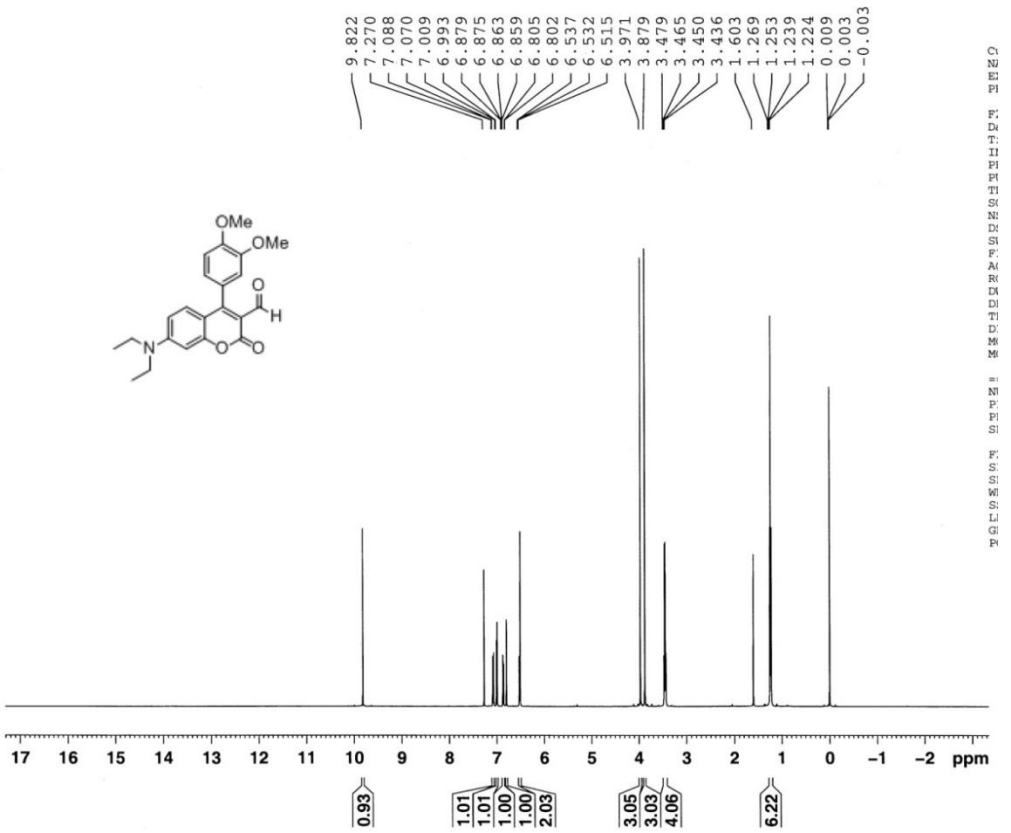
9.822
7.270
7.088
7.070
7.009
6.993
6.879
6.875
6.863
6.859
6.805
6.802
6.537
6.532
6.515
3.971
3.879
3.479
3.465
3.450
3.436
1.603
1.269
1.253
1.239
1.224
0.009
0.003
-0.003
OMe
OMe
O
H
N
O
O
17 16 15 14 13 12 11 10 9 8 7 6 5 4 3 2 1 0 −1 −2 ppm
0.93
1.01
1.01
1.00
2.03
3.05
3.03
4.06
6.22

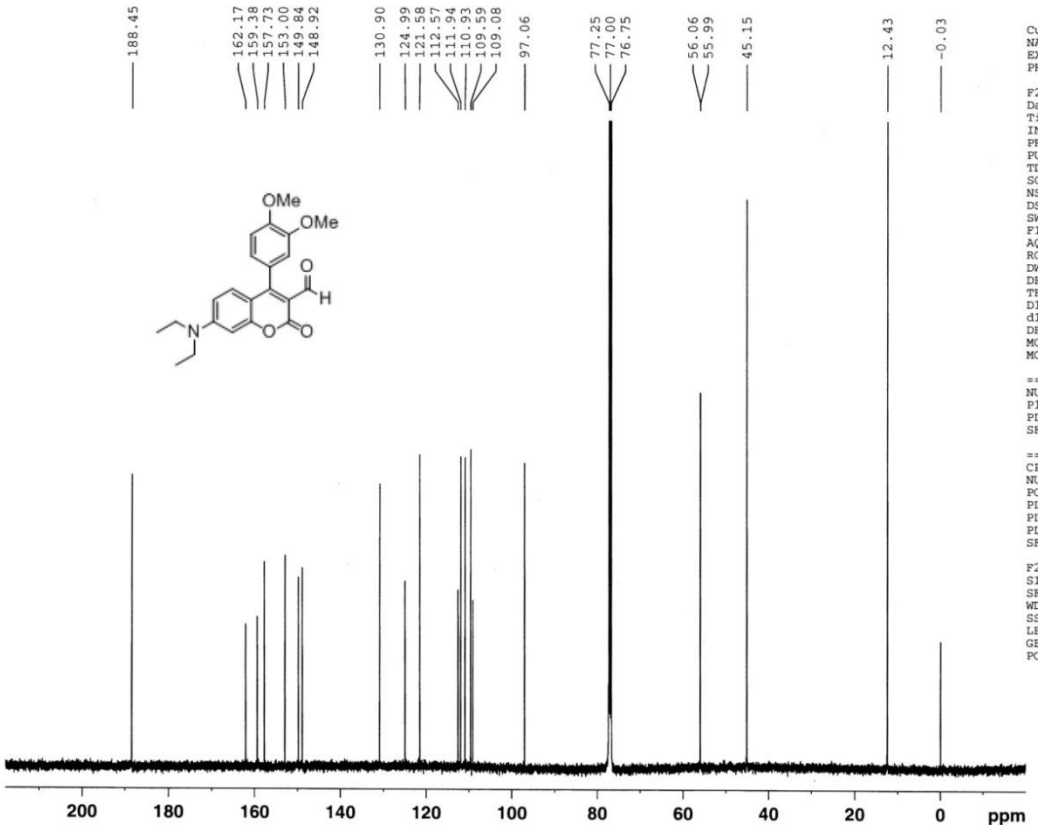
188.45
162.17
159.38
157.73
153.00
149.84
148.92
130.90
124.99
121.58
112.57
111.94
110.93
109.59
109.08
97.06
77.25
77.00
76.75
56.06
55.99
45.15
12.43
-0.03
OMe
OMe
O
H
N
O
O
200 180 160 140 120 100 80 60 40 20 0 ppm

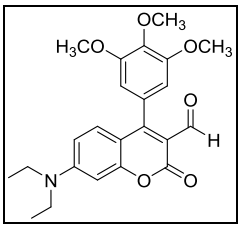

Compound 1k. Yield 37%; ^{1}H NMR (500 MHz, $CDCl_3$) δ 9.81 (s, 1H), 7.08 (d, 1H, *J* = 9.0 Hz), 6.55 (dd, 1H, *J* = 9.0, 2.5 Hz), 6.52 (d, 1H, *J* = 2.5 Hz), 6.51 (s, 2H), 3.94 (s, 3H), 3.86 (s, 6H), 3.46 (q, 4H, *J* = 7.0 Hz), 1.24 (t, 6H, *J* = 7.0 Hz); ^{13}C NMR (125 MHz, $CDCl_3$) δ 188.3, 162.3, 159.1, 157.7, 153.4, 138.5, 130.8, 128.2, 112.4, 109.7, 108.8, 105.9, 97.0, 61.1, 56.3, 45.2, 12.4; IR (neat, cm^{-1}) 1748, 1618, 1495, 1417, 1352, 1123; HRMS calculated for $C_{23}H_{25}NO_6$ ($M + Na^+$): 434.1574. Found: 434.1570.

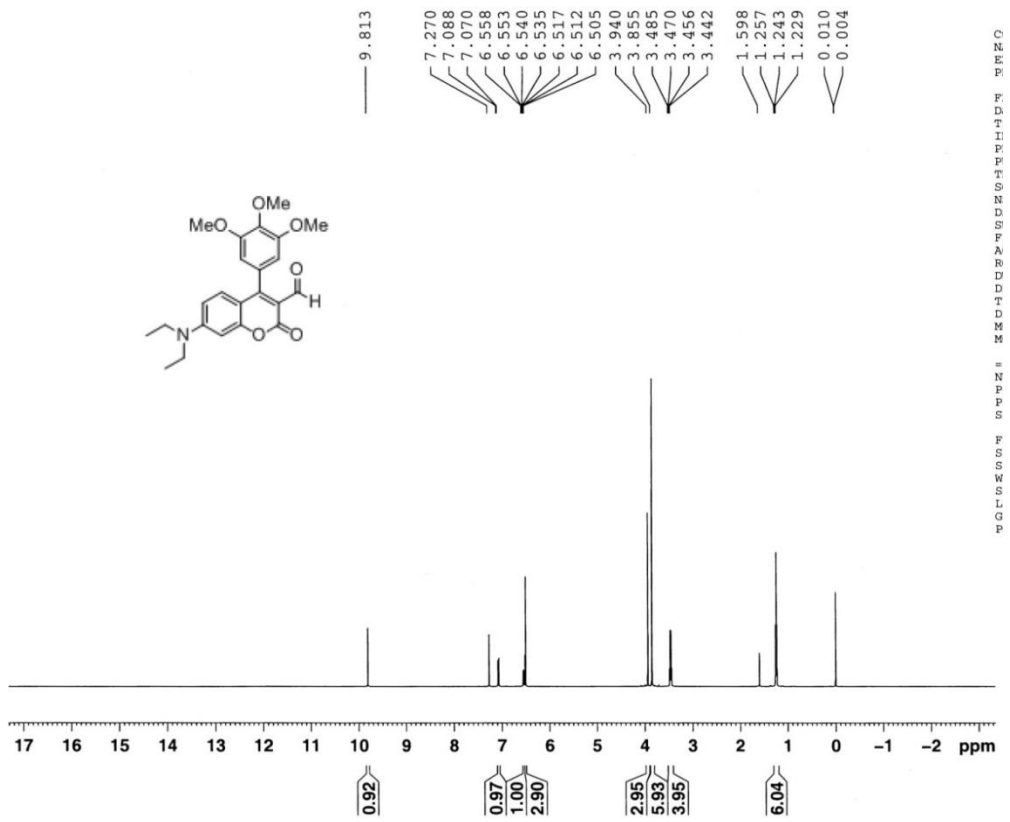
9.813
7.270
7.088
7.070
6.558
6.553
6.540
6.535
6.517
6.512
6.505
3.940
3.855
3.485
3.470
3.456
3.442
1.598
1.257
1.243
1.229
0.010
0.004
OMe
MeO
OMe
O
H
N
O
O
17 16 15 14 13 12 11 10 9 8 7 6 5 4 3 2 1 0 −1 −2 ppm
0.92
0.97
1.00
2.90
2.95
5.93
3.95
6.04

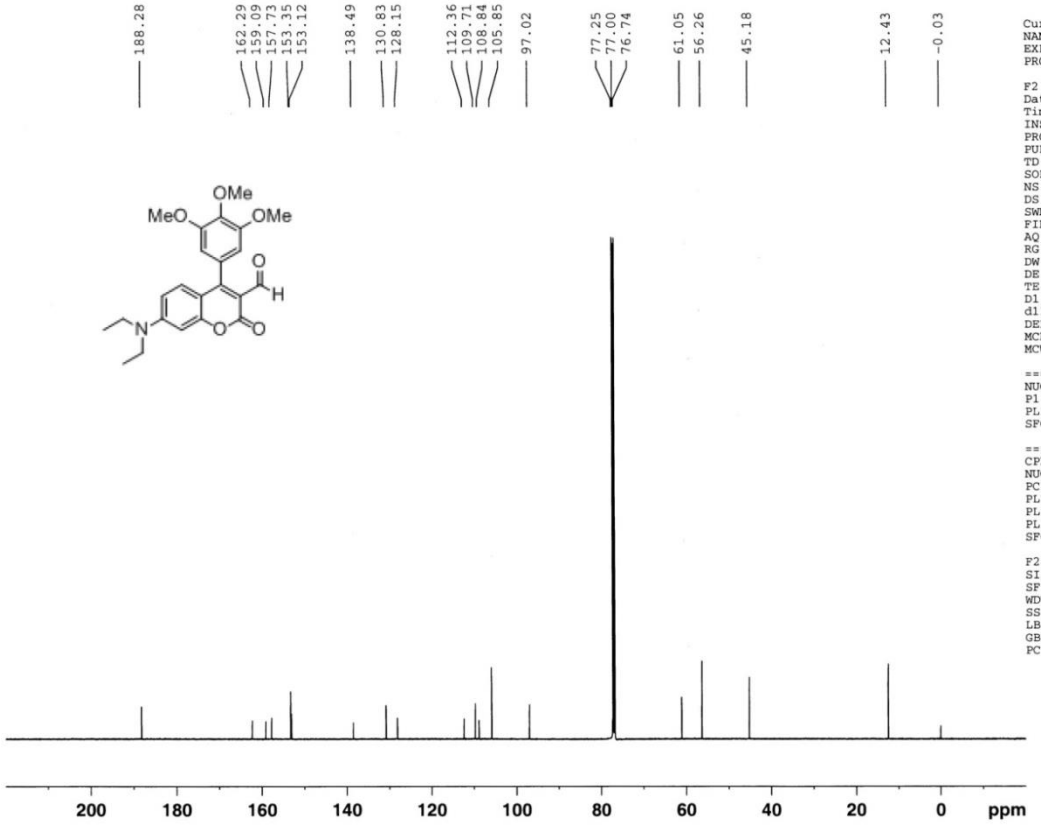
188.28
162.29
159.09
157.73
153.35
153.12
138.49
130.83
128.15
112.36
109.71
108.84
105.85
97.02
77.25
77.00
76.74
61.05
56.26
45.18
12.43
-0.03
OMe
MeO
OMe
O
H
N
O
O
200 180 160 140 120 100 80 60 40 20 0 ppm

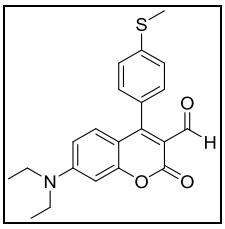

Compound 1d. Yield 36%; ^{1}H NMR (500 MHz, $CDCl_3$) δ 9.88 (s, 1H), 7.36 (d, 2H, *J* = 8.5 Hz), 7.20 (d, 2H, *J* = 8.5 Hz), 7.01 (d, 1H, *J* = 8.0 Hz), 6.48-6.52 (m, 2H), 3.45 (q, 4H, *J* = 7.0 Hz), 2.56 (s, 3H), 1.24 (t, 6H, *J* = 7.0); ^{13}C NMR (125 MHz, $CDCl_3$) δ 188.3, 161.3, 159.9, 157.8, 153.0, 140.5, 130.9, 129.3, 129.0, 125.7, 112.3, 109.6, 109.0, 97.1, 45.2, 15.3, 12.4; IR (neat, cm^{-1}) 1746, 1714, 1612, 1558, 1507, 1487, 1420, 1353, 1132; HRMS calculated for $C_{21}H_{21}NO_3S$ ($M + Na^+$): 390.113435. Found: 390.113229.

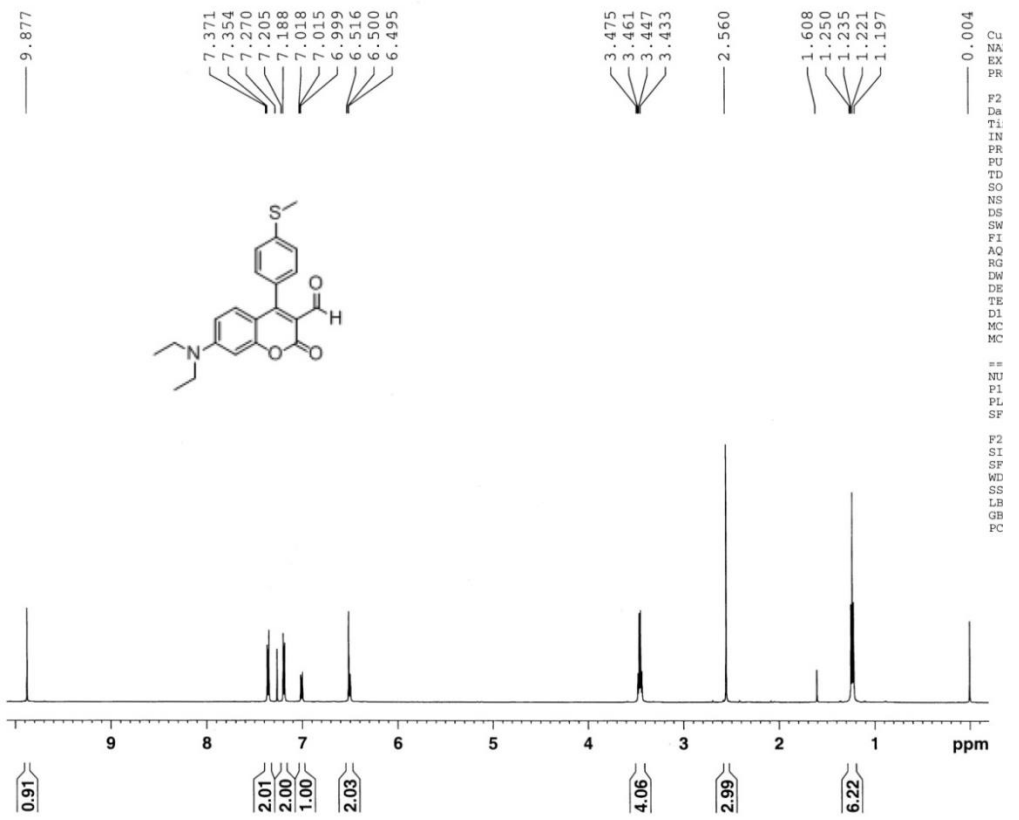
9.877
7.371
7.354
7.270
7.205
7.188
7.018
7.015
6.999
6.516
6.500
6.495
3.475
3.461
3.447
3.433
2.560
1.608
1.250
1.235
1.221
1.197
0.004
S
O
H
N
O
O
9
8
7
6
5
4
3
2
1
ppm
0.91
2.01
2.00
1.00
2.03
4.06
2.99
6.22

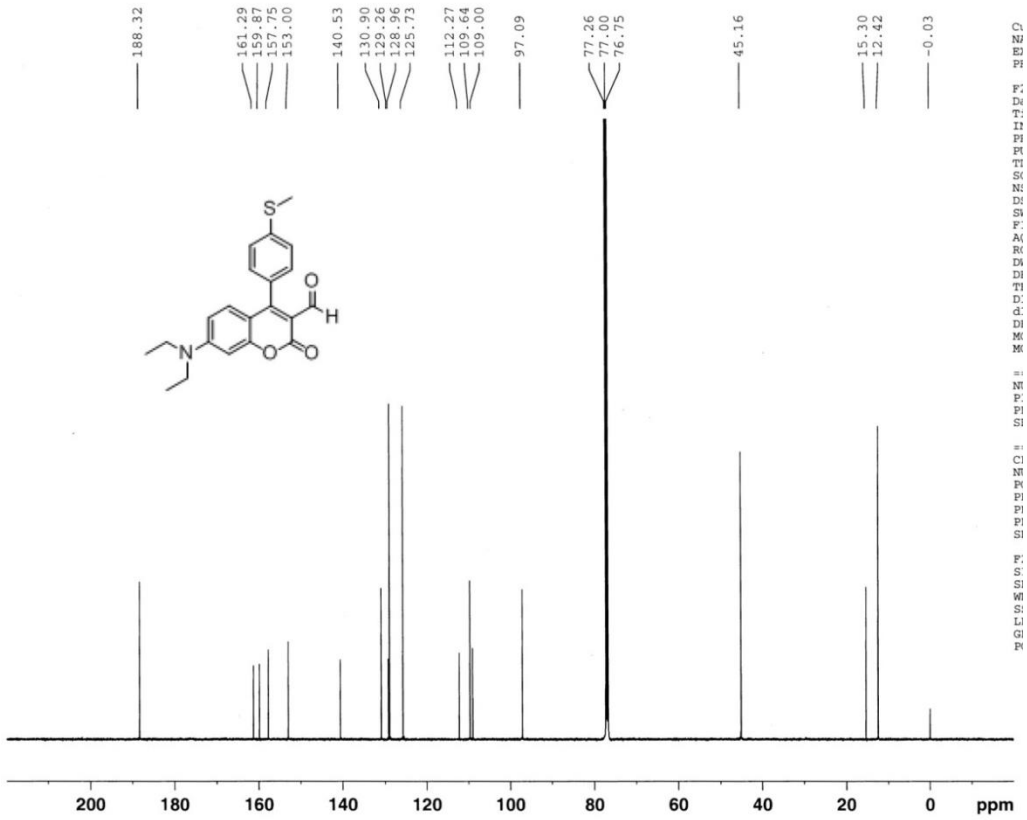
188.32
161.29
159.87
157.75
153.00
140.53
130.90
129.26
128.96
125.73
112.27
109.64
109.00
97.09
77.26
77.00
76.75
45.16
15.30
12.42
-0.03
S
O
H
N
O
O
200
180
160
140
120
100
80
60
40
20
0
ppm

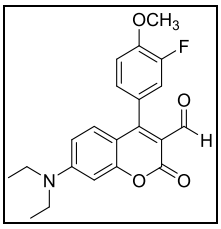

Compound 1f. Yield 69%; ^{1}H NMR (500 MHz, $CDCl_3$) δ 9.91 (s, 1H), 7.09 (t, 1H, *J* = 8.5 Hz), 6.98-7.03 (m, 3H), 6.49-6.55 (m, 2H), 3.98 (s, 3H), 3.46 (q, 4H, *J* = 7.0 Hz), 1.22 (t, 6H, *J* = 7.0 Hz) ; ^{13}C NMR (125 MHz, $CDCl_3$) δ 188.2, 160.1, 159.8, 157.8, 153.0, 152.9, 151.0, 148.4, 148.3, 130.8, 125.5, 125.4, 124.8, 116.6 (C-F, d, *J* = 20.0 Hz), 113.2, 113.1, 112.2, 109.8, 109.0, 97.1, 56.3, 45.2, 12.4 ; IR (neat, cm^{-1}) 1747, 1614, 1556, 1520, 1499, 1429, 1417, 1354, 1270, 1136; HRMS calculated for $C_{21}H_{20}FNO_4$ ($M + Na^+$): 392.126857. Found: 392.126718.

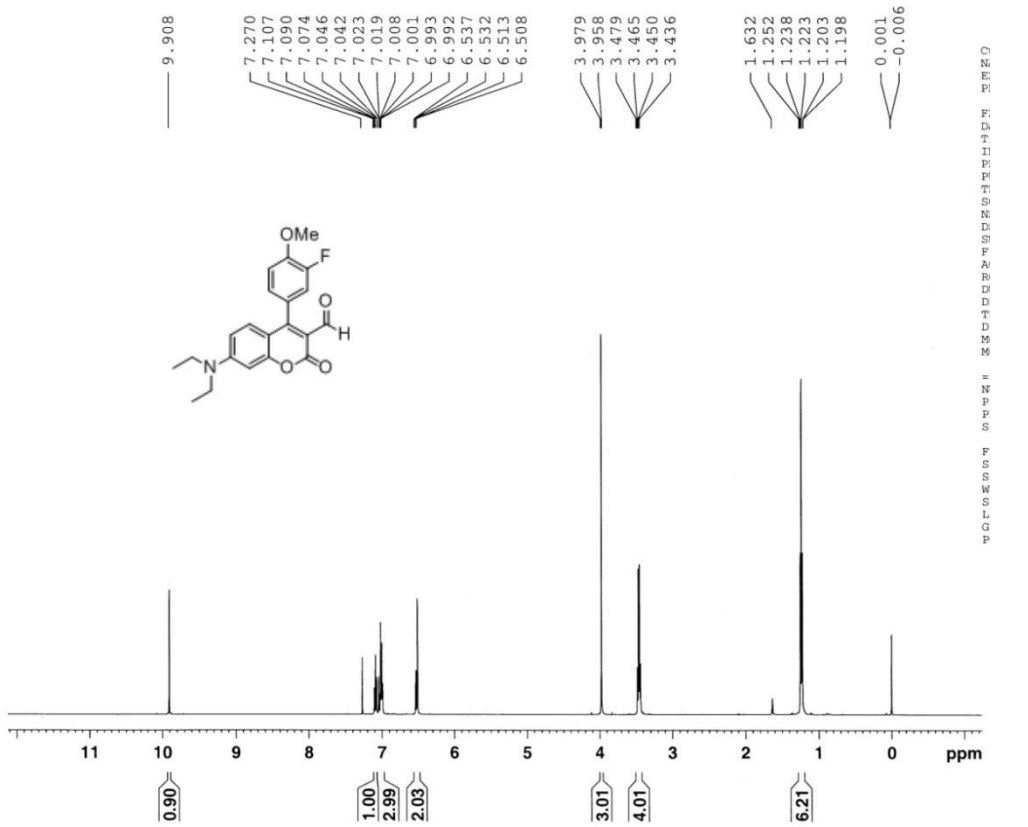
9.908
7.270
7.107
7.090
7.074
7.046
7.042
7.023
7.019
7.008
7.001
6.993
6.992
6.537
6.532
6.513
6.508
3.979
3.958
3.479
3.465
3.450
3.436
1.632
1.252
1.238
1.223
1.203
1.198
0.001
-0.006
OMe
F
O
H
N
O
O
11
10
9
8
7
6
5
4
3
2
1
0
ppm
0.90
1.00
2.99
2.03
3.01
4.01
6.21

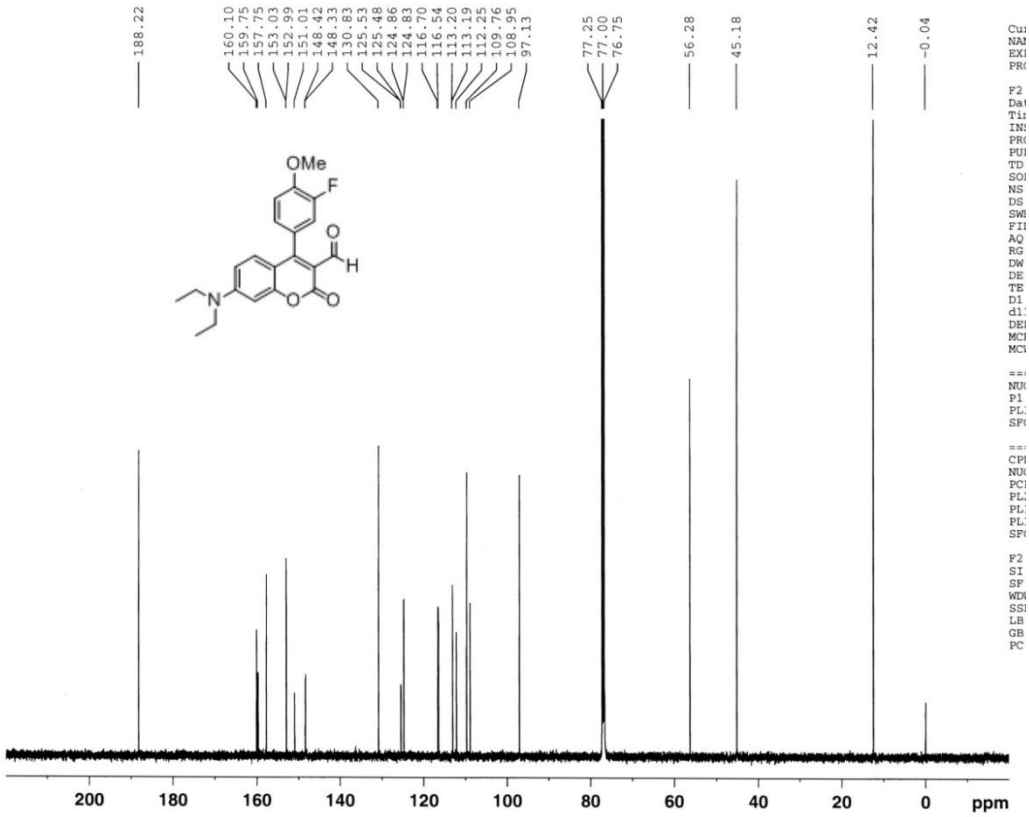
188.22
160.10
159.75
157.75
157.03
153.03
152.99
151.01
148.42
148.33
130.83
125.53
125.48
124.86
124.83
116.70
116.54
113.20
113.19
112.25
109.76
109.26
108.95
97.13
77.25
77.00
76.75
56.28
45.18
12.42
-0.04
OMe
F
O
H
N
O
O
200
180
160
140
120
100
80
60
40
20
0
ppm

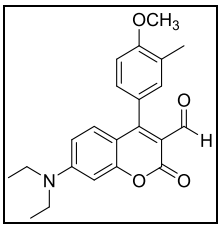

Compound 1j. Yield 54%; ^{1}H NMR (500 MHz, $CDCl_3$) δ 9.75 (s, 1H), 7.03-7.10 (m, 3H), 6.91 (d, 1H, *J* = 8.5 Hz), 6.50 (dd, 1H, *J* = 8.5, 2.0 Hz), 6.48 (d, 1H, *J* = 2.0 Hz), 3.89 (s, 3H), 3.43 (q, 4H, *J* = 7.0 Hz), 2.25 (s, 3H), 1.21 (t, 6H, *J* = 7.0 Hz); ^{13}C NMR (125 MHz, $CDCl_3$) δ 188.6, 162.8, 159.2, 158.6, 157.6, 152.9, 131.1, 130.9, 127.8, 126.8, 124.0, 112.5, 109.5, 109.4, 109.0, 96.9, 55.4, 45.1, 16.2, 12.4; IR (neat, cm^{-1}) 1746, 1611, 1511, 1495, 1419, 1353, 1251, 1137; HRMS calculated for $C_{22}H_{23}NO_4$ (M + Na^+): 388.151929. Found: 388.151777.

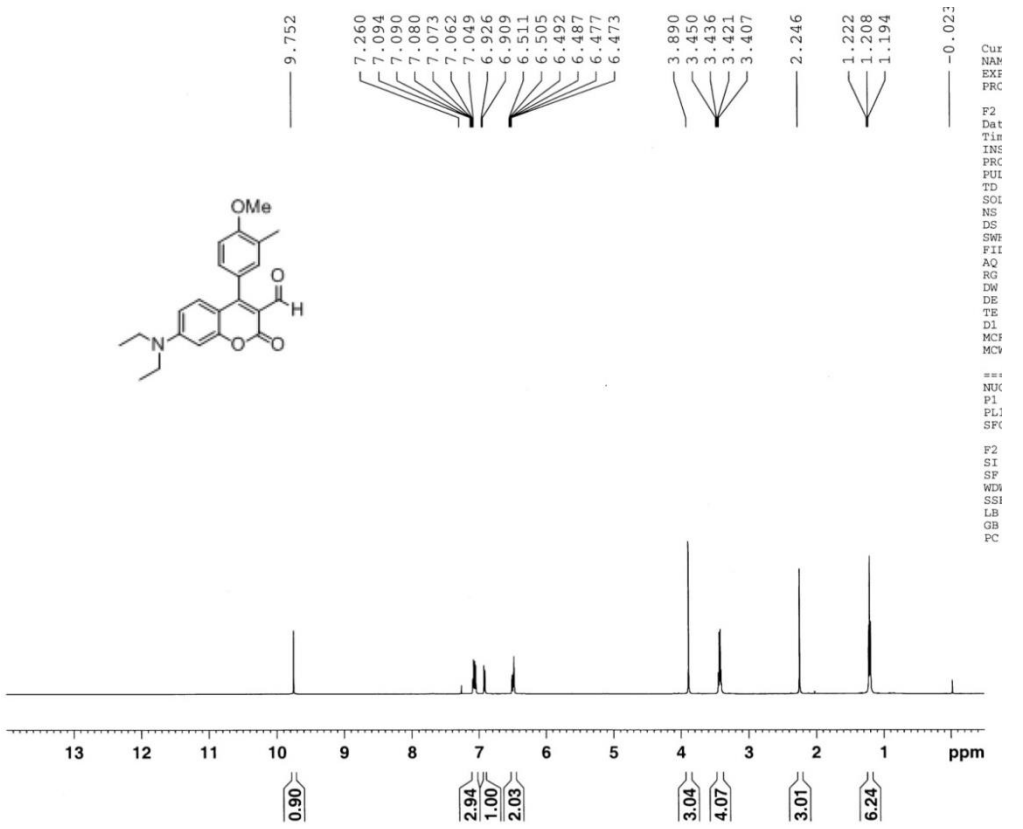
9.752
7.260
7.094
7.090
7.080
7.073
7.062
7.049
6.926
6.909
6.511
6.505
6.492
6.487
6.477
6.473
3.890
3.450
3.436
3.421
3.407
2.246
1.222
1.208
1.194
-0.023
OMe
O
H
N
O
O
13
12
11
10
9
8
7
6
5
4
3
2
1
ppm
0.90
2.94
1.00
2.03
3.04
4.07
3.01
6.24

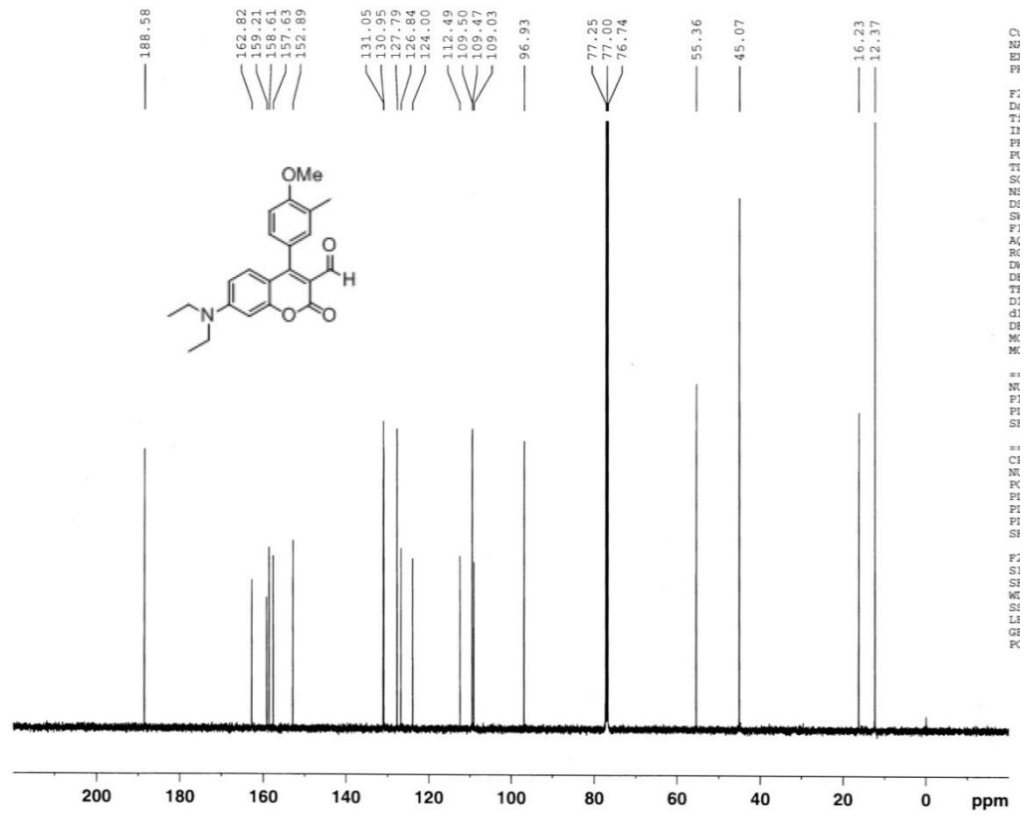
188.58
162.82
159.21
158.61
157.63
152.89
131.05
130.95
127.79
126.84
124.00
112.49
109.50
109.47
109.03
96.93
77.25
77.00
76.74
55.36
45.07
16.23
12.37
OMe
O
H
N
O
O
200
180
160
140
120
100
80
60
40
20
0
ppm

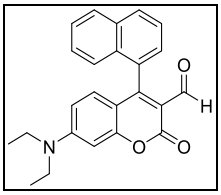

Compound 1h. Yield 67%; ^{1}H NMR (500 MHz, $CDCl_3$) δ 9.72 (s, 1H), 7.98 (d, 1H, *J* = 8.5 Hz), 7.94 (dd, 1H, *J* = 8.5, 1.5 Hz), 7.58 (t, 1H, *J* = 7.5 Hz), 7.48-7.54 (m, 2H), 7.41 (td, 1H, *J* = 8.0, 1.0 Hz), 7.34 (dd, 1H, *J* = 7.0, 1.0 Hz), 6.70 (d, 1H, *J* = 9.0), 6.55 (d, 1H, *J* = 2.5 Hz), 6.37 (dd, 1H, *J* = 9.5, 2.5 Hz), 3.42 (q, 4H, *J* = 7.0 Hz), 1.21 (t, 6H, *J* = 7.0 Hz); ^{13}C NMR (125 MHz, $CDCl_3$) δ 188.0, 161.1, 159.7, 153.2, 133.2, 131.1, 131.0, 130.9, 129.3, 128.5, 127.1, 126.5, 126.0, 125.1, 125.0, 113.3, 109.8, 109.5, 96.9, 45.2, 12.4; IR (neat, cm^{-1}) 1744, 1716, 1679, 1614, 1552, 1499, 1417, 1352, 1136; HRMS calculated for $C_{24}H_{21}NO_3$ ($M + Na^+$): 394.141365. Found: 394.141303.

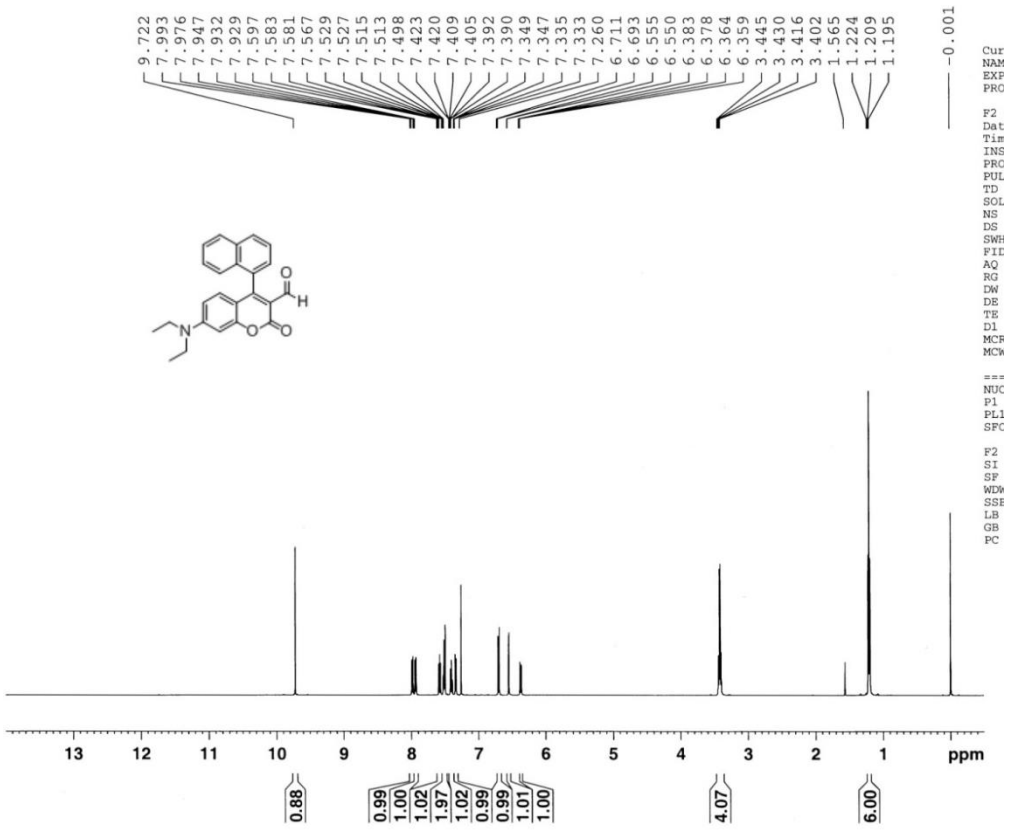
9.722
7.993
7.976
7.947
7.932
7.929
7.597
7.583
7.581
7.567
7.529
7.527
7.515
7.513
7.498
7.423
7.420
7.409
7.405
7.392
7.390
7.349
7.347
7.335
7.333
7.260
6.711
6.693
6.555
6.550
6.383
6.378
6.364
6.359
3.445
3.430
3.416
3.402
1.565
1.224
1.209
1.195
0.001
O
H
N
O
O
13
12
11
10
9
8
7
6
5
4
3
2
1
ppm
0.88
0.99
1.00
1.02
1.97
1.02
0.99
0.99
1.01
1.00
4.07
6.00

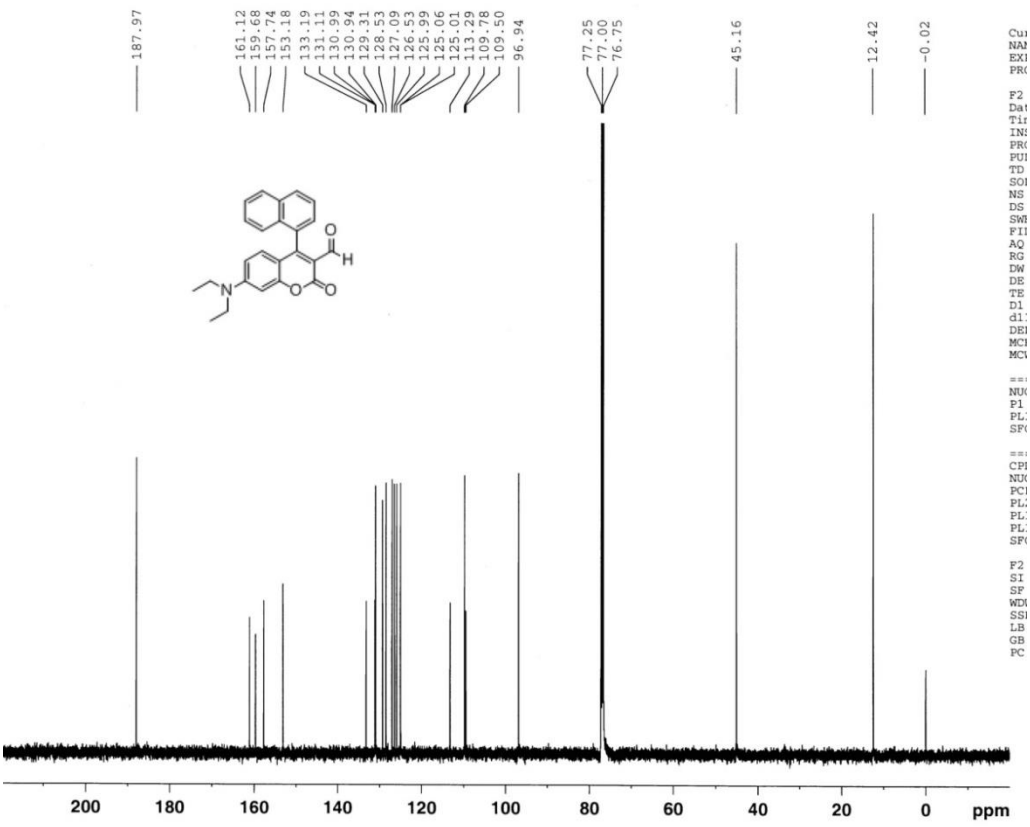
187.97
161.12
159.68
157.74
153.18
133.19
131.11
130.99
130.94
129.31
128.53
127.09
126.53
125.99
125.06
125.01
113.29
109.78
109.50
96.94
77.25
77.00
76.75
45.16
12.42
-0.02
O
H
N
O
O
200
180
160
140
120
100
80
60
40
20
0
ppm

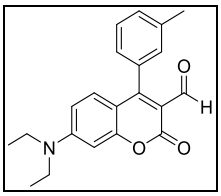

Compound 1c. Yield 82%; ^{1}H NMR (500 MHz, $CDCl_3$) δ 9.79 (s, 1H), 7.39 (t, 1H, *J* = 8.0 Hz), 7.31 (d, 1H, *J* = 8.0 Hz), 7.06-7.09 (m, 2H), 6.98 (d, 1H, *J* = 10.0 Hz), 6.48-6.53 (m, 2H), 3.43 (q, 4H, *J* = 7.0 Hz), 2.42 (s, 3H), 1.22 (t, 6H, *J* = 7.0 Hz); ^{13}C NMR (125 MHz, $CDCl_3$) δ 188.4, 162.6, 159.4, 157.7, 153.0, 138.2, 132.8, 131.0, 129.9, 129.0, 128.3, 125.6, 112.3, 109.6, 109.0, 97.0, 45.1, 21.4, 12.4; IR (neat, cm^{-1}) 1744, 1712, 1614, 1556, 1503, 1417, 1352, 1127, 730; HRMS calculated for $C_{21}H_{21}NO_3$ ($M + Na^+$): 358.141365. Found: 358.141274.

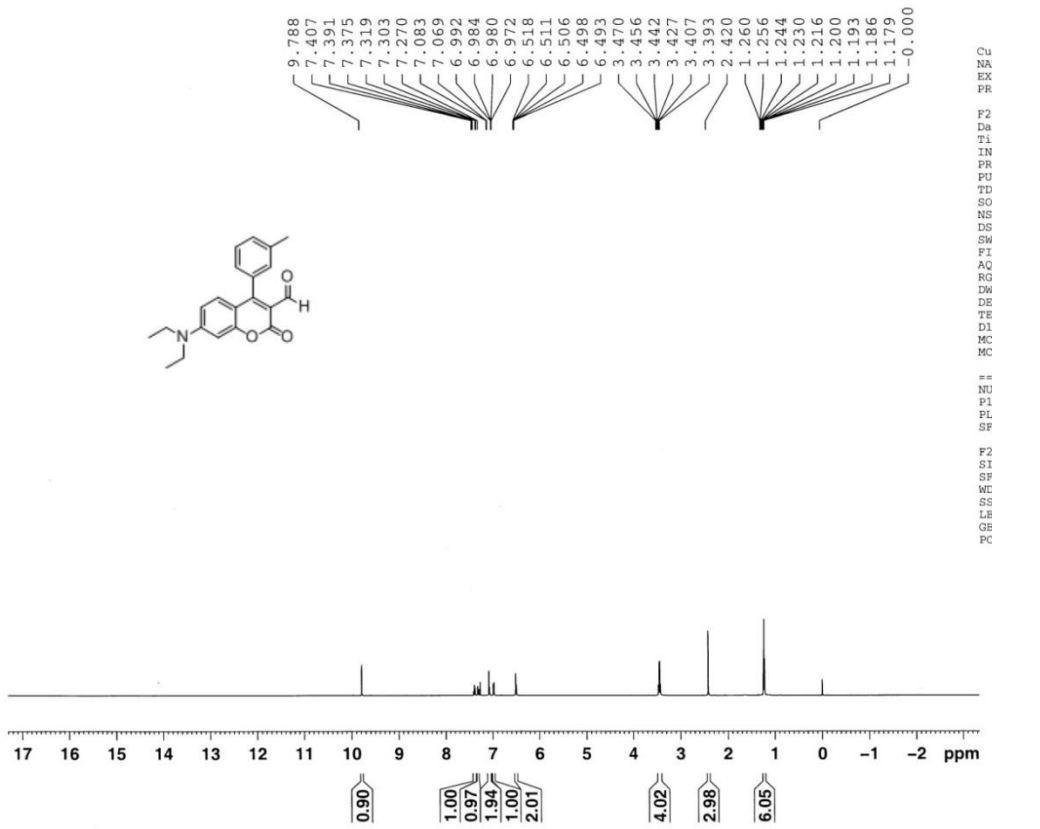
9.788
7.407
7.391
7.375
7.319
7.303
7.270
7.083
7.069
6.992
6.984
6.980
6.972
6.518
6.511
6.506
6.498
6.493
3.470
3.456
3.442
3.427
3.407
3.393
2.420
1.260
1.256
1.244
1.230
1.216
1.200
1.193
1.186
1.179
-0.000
17 16 15 14 13 12 11 10 9 8 7 6 5 4 3 2 1 0 −1 −2 ppm
0.90
1.00
0.97
1.94
1.00
2.01
4.02
2.98
6.05

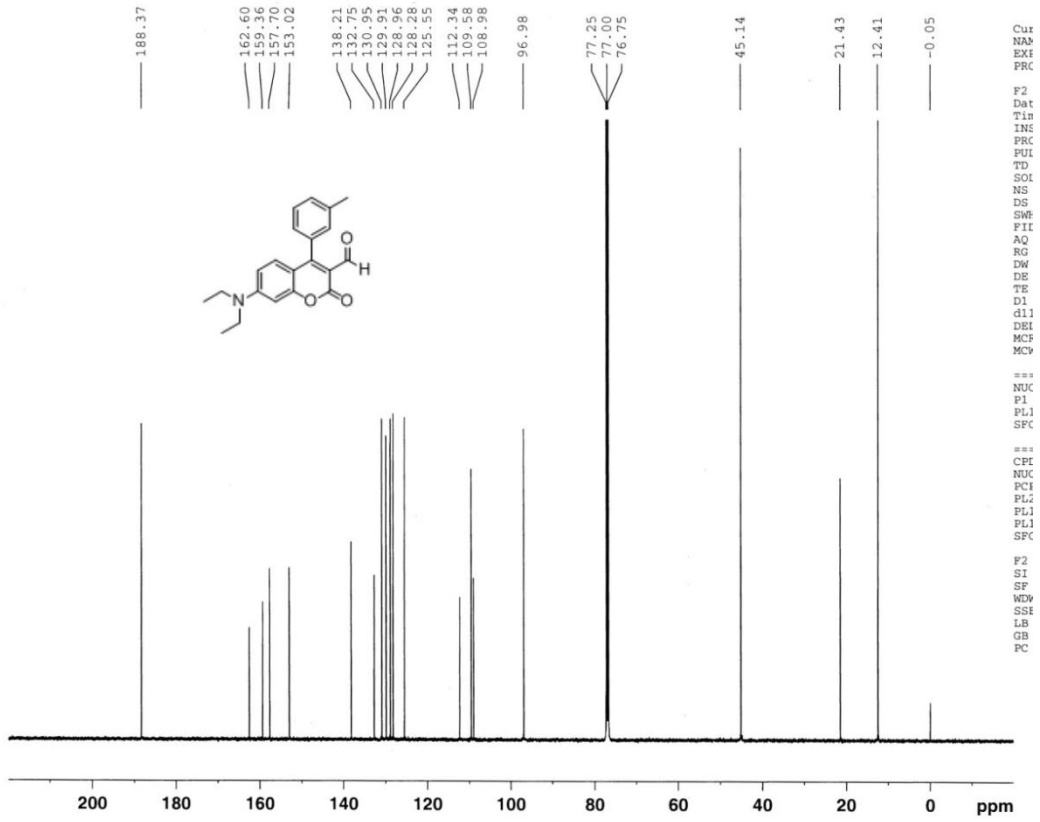
188.37
162.60
159.36
157.70
153.02
138.21
132.75
130.95
129.91
128.96
128.28
125.55
112.34
109.58
108.98
96.98
77.25
77.00
76.75
45.14
21.43
12.41
-0.05
200 180 160 140 120 100 80 60 40 20 0 ppm

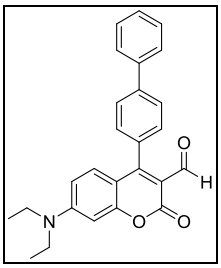

Compound 1e. Yield 25%; ^{1}H NMR (500 MHz, $CDCl_3$) δ 9.92 (s, 1H), 7.74 (d, 2H, *J* = 8.5 Hz), 7.68 (d, 2H, *J* = 8.0 Hz), 7.50 (t, 2H, *J* = 7.5 Hz), 7.42 (t, 1H, *J* = 7.5 Hz), 7.36 (d, 2H, *J* = 8.0 Hz), 7.06 (d, 1H, *J* = 9.5 Hz), 6.51-6.56 (m, 2H), 3.45 (q, 4H, *J* = 7.5 Hz), 1.26 (t, 6H, *J* = 7.5 Hz); ^{13}C NMR (125 MHz, $CDCl_3$) δ 188.4, 161.7, 159.8, 157.8, 153.1, 142.0, 140.1, 131.9, 131.0, 129.0, 128.9, 127.8, 127.2, 127.1, 112.4, 109.7, 109.1, 97.1, 45.2, 12.4; IR (neat, cm^{-1}) 1745, 1711, 1610, 1558, 1498, 1419, 1352, 1131; HRMS calculated for $C_{26}H_{23}NO_3$ ($M + Na^+$): 420.157015. Found: 420.156830.

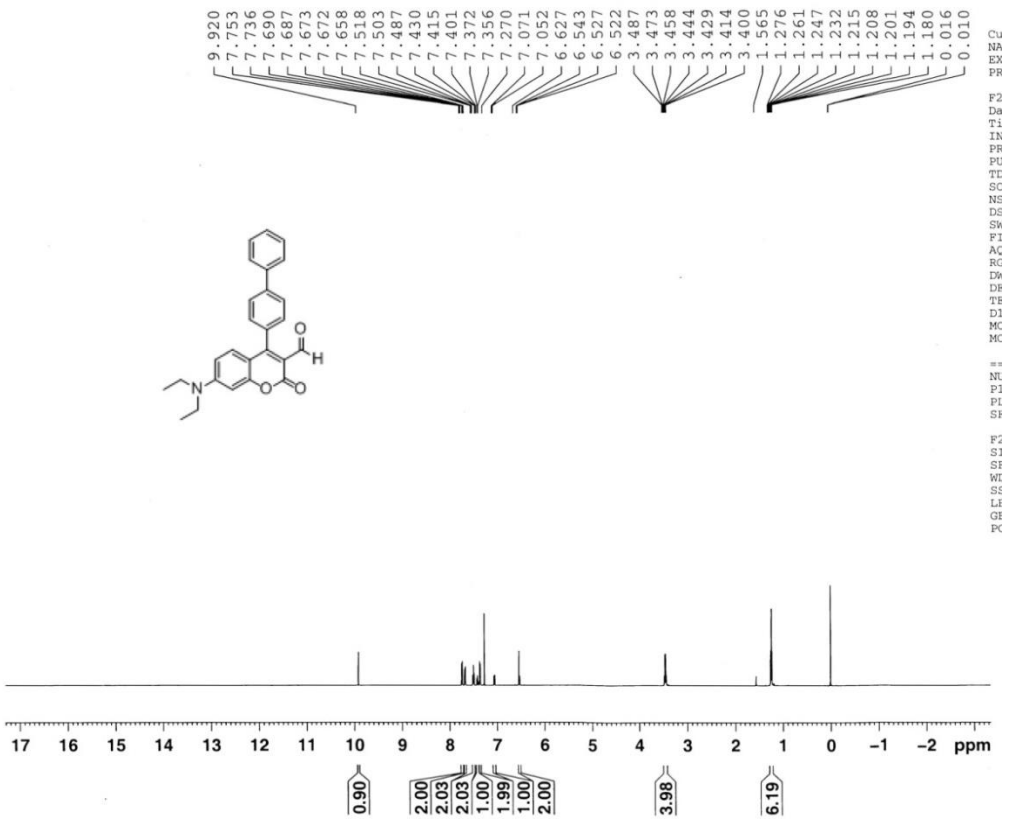
9.920
7.753
7.736
7.690
7.687
7.673
7.672
7.658
7.518
7.503
7.487
7.430
7.415
7.401
7.372
7.356
7.270
7.071
7.052
6.627
6.543
6.527
6.522
3.487
3.473
3.458
3.444
3.429
3.414
3.400
1.565
1.276
1.261
1.247
1.232
1.215
1.208
1.201
1.194
1.180
0.016
0.010
17 16 15 14 13 12 11 10 9 8 7 6 5 4 3 2 1 0 −1 −2 ppm
0.90
2.00
2.03
2.03
1.00
1.99
1.00
2.00
3.98
6.19

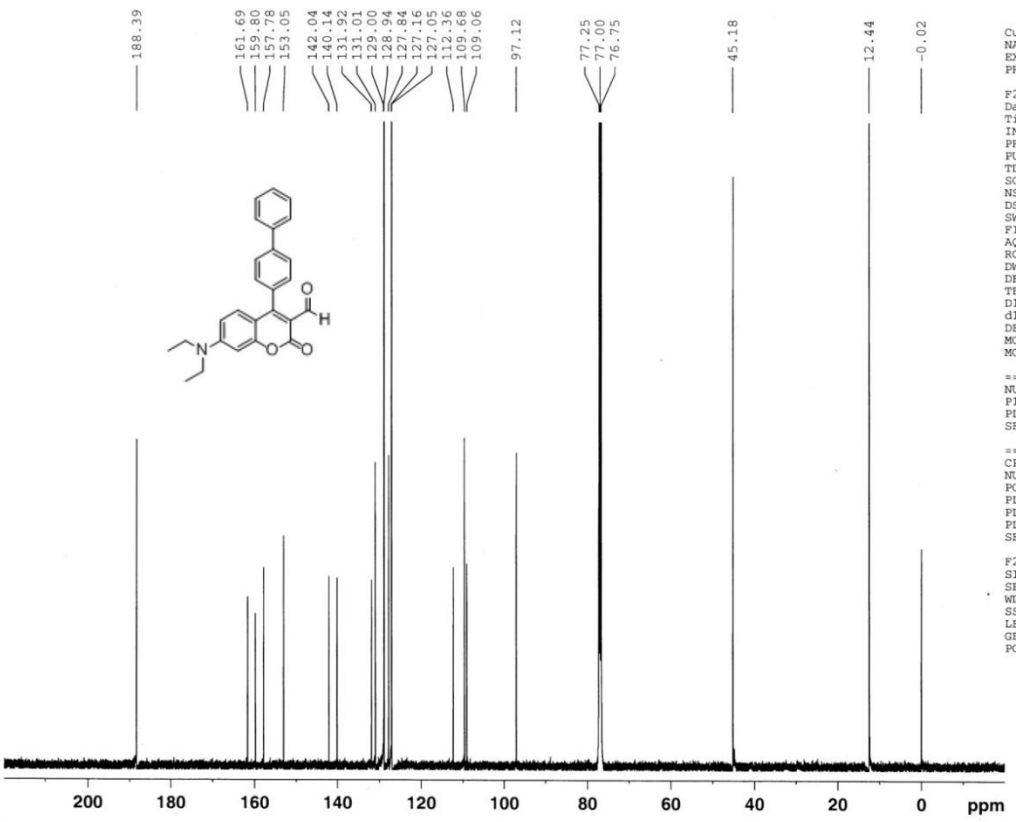
188.39
161.69
159.80
157.78
153.05
142.04
140.14
131.92
131.01
129.00
128.94
127.84
127.16
127.05
112.36
109.68
109.06
97.12
77.25
77.00
76.75
45.18
12.44
-0.02
200 180 160 140 120 100 80 60 40 20 0 ppm

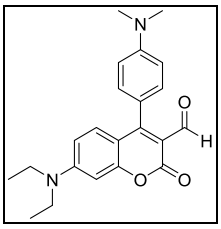

Compound 1l. Yield 10%. ^{1}H NMR (500 MHz, $CDCl_3$) δ 9.77 (s, 1H), 7.24 (d, 1H, *J* = 8.0 Hz), 7.21 (d, 2H, *J* = 7.0 Hz), 6.79 (d, 2H, *J* = 9.0 Hz), 6.49-6.54 (m, 2H), 3.45 (q, 4H, *J* = 7.0 Hz), 3.07 (s, 6H), 1.23 (t, 6H, *J* = 7.0 Hz); ^{13}C NMR (125 MHz, $CDCl_3$) δ 199.9, 163.4, 159.3, 157.7, 152.7, 151.2, 131.0, 130.9, 119.1, 112.5, 111.3, 109.3, 109.1, 97.1, 45.1, 40.2, 12.5; IR (neat, cm^{-1}) 1743, 1610, 1558, 1496, 1418, 1355, 1132; HRMS calculated for $C_{22}H_{24}N_2O_3Na$ ($M + Na^+$): 365.1860. Found: 365.1860.

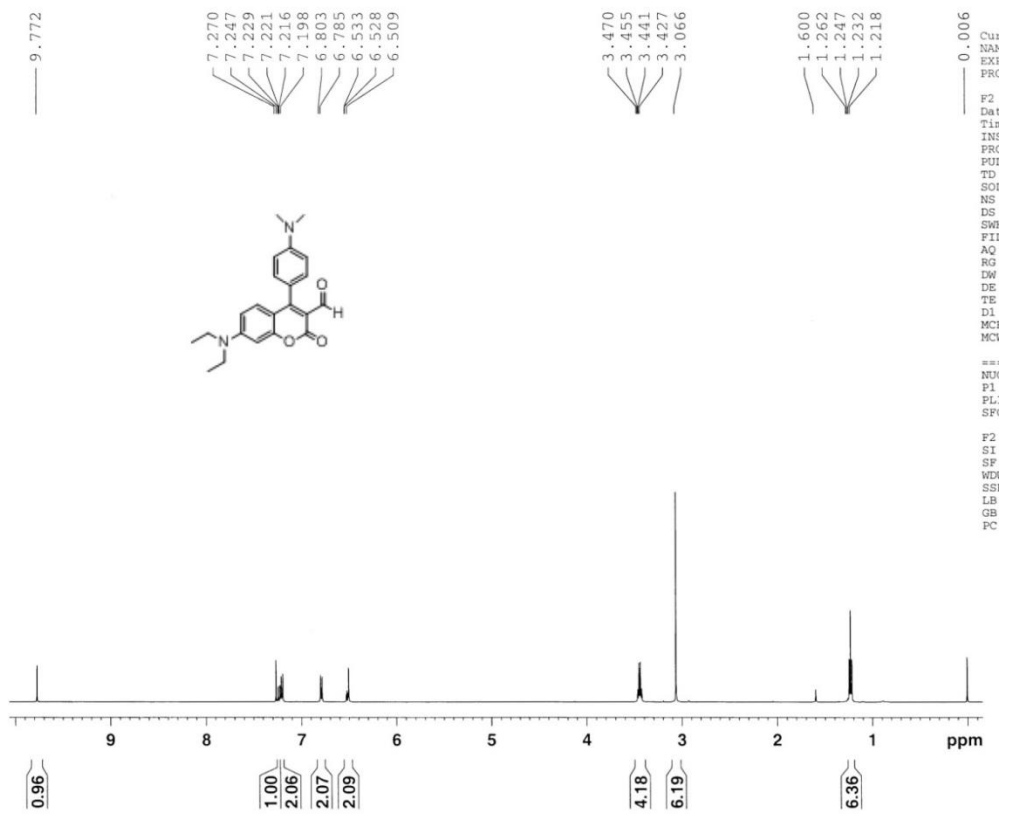
9.772
7.270
7.247
7.229
7.221
7.216
7.198
6.803
6.785
6.533
6.528
6.509
3.470
3.455
3.441
3.427
3.066
1.600
1.262
1.247
1.232
1.218
0.006
ppm
0.96
1.00
2.06
2.07
2.09
4.18
6.19
6.36

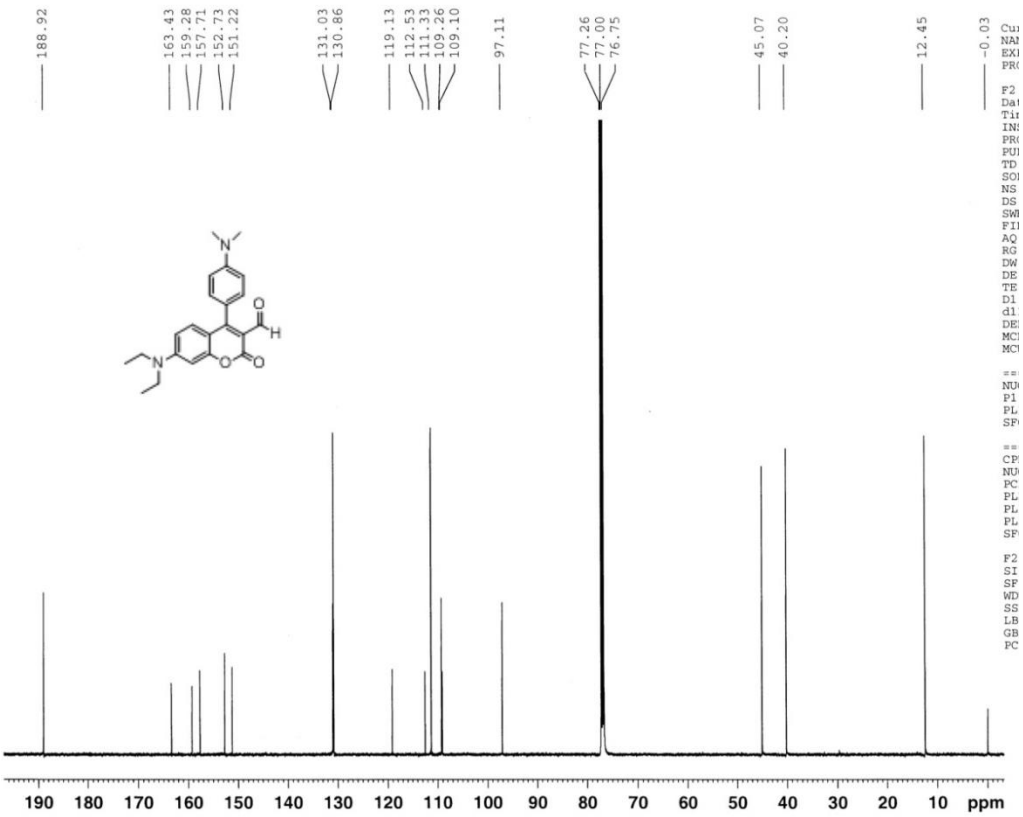
188.92
163.43
159.28
157.71
152.73
151.22
131.03
130.86
119.13
112.53
111.33
109.26
109.10
97.11
77.26
77.00
76.75
45.07
40.20
12.45
-0.03
ppm

General Synthesis for Suzuki Coupling of Thiophene-Substituted NS521 Derivatives

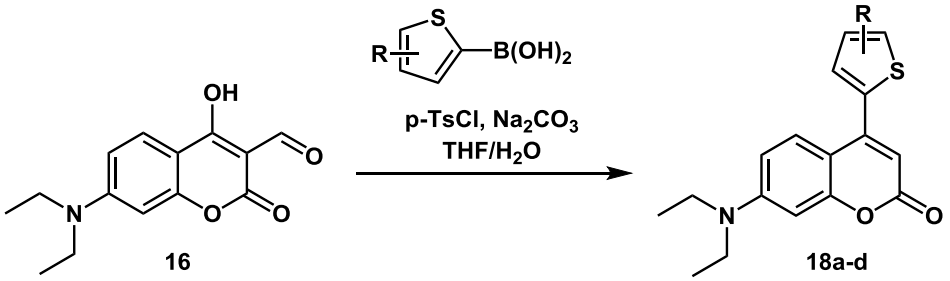

Compound **16** (250.0 mg, 1.072 mmol), *p*-toluenesulfonyl chloride (224.8 mg, 1.179 mmol), and Na_2CO_3 (340.8 mg, 3.215 mmol) were added to a flame-dried round bottom flask and degassed with N_2 for 15 minutes. Degassed H_2O/THF (1:20, 15.0 mL) was added and the mixture stirred at 50 °C for 30 minutes. The mixture was allowed to cool to room temperature. Thiophene or substituted thiopheneboronic acid (1.179 mmol) was added to the mixture and was allowed to stir at room temperature for 5 minutes. Palladium chloride (9.5 mg, 0.054 mmol) was added and the mixture stirred at 50 °C for 6 hours. The mixture was filtered and the solvent removed *in vacuo*. The remaining residue was purified by chromatography (100% CH_2Cl_2→95:5 CH_2Cl_2/EtOAc). The material was further purified by chromatography (90:10 hexanes/EtOAc→50:50 hexanes/EtOAc) to yield the desired compound as a pale yellow oil.

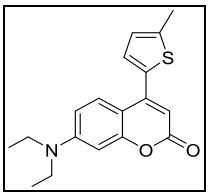

Compound 18d. Yield 22%; ^{1}H NMR (500 MHz, $CDCl_3$) δ 7.75 (d, 1H, *J* = 9.0 Hz), 7.21 (d, 1H, *J* = 3.5 Hz), 6.85 (dd, 1H, *J* = 2.5, 1.0 Hz), 6.58 (dd, 1H, *J* = 9.0, 2.5 Hz) 6.56 (d, 1H, *J* = 2.5 Hz), 6.11 (s, 1H), 3.43 (q, 4H, *J* = 7.0 Hz), 2.57 (s, 3H), 1.22 (t, 6H, *J* = 7.0 Hz); ^{13}C NMR (125 MHz, $CDCl_3$) δ 162.0, 156.8, 150.6, 148.3, 143.0, 134.8, 128.9, 127.6, 126.2, 108.5, 107.5, 107.1, 98.0, 44.8, 15.4, 12.5; IR (neat, cm^{-1}) 2970, 1712, 1610, 1585, 1409, 1352, 1107; HRMS calculated for $C_{18}H_{19}NO_2S$ ($M + Na^+$): 336.1029. Found: 336.1026.

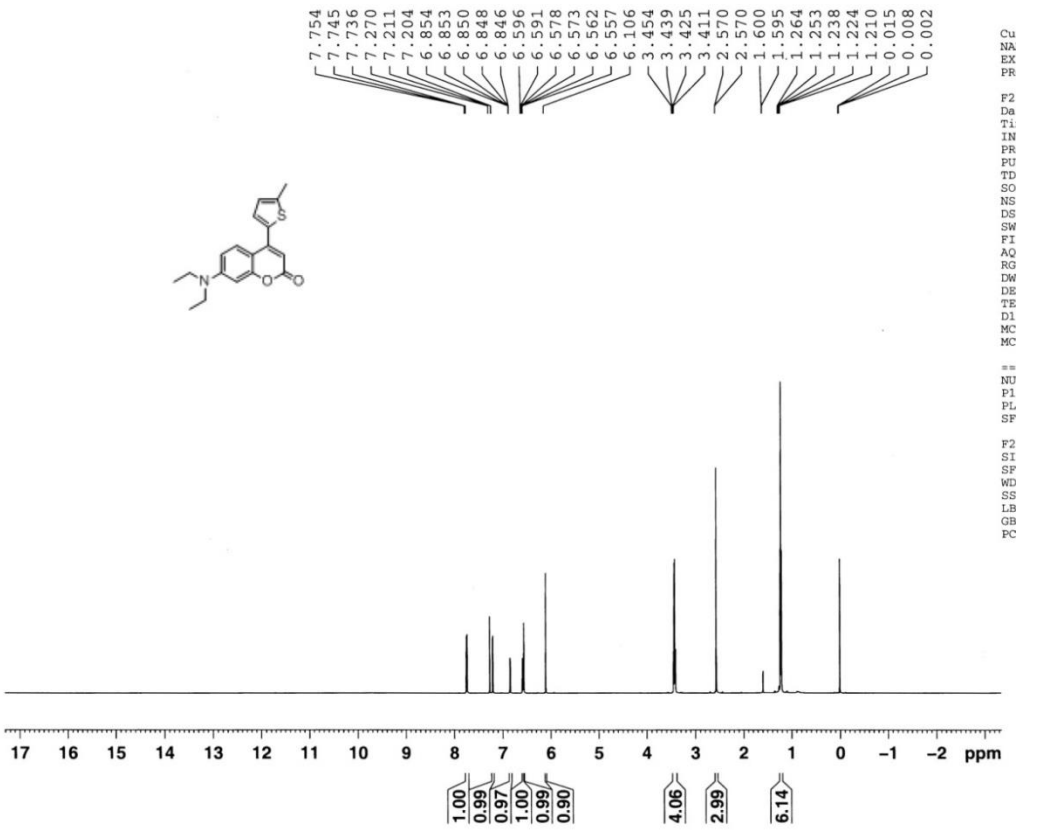
7.754
7.745
7.736
7.270
7.211
7.204
6.854
6.853
6.850
6.848
6.846
6.596
6.591
6.578
6.573
6.562
6.557
6.106
3.454
3.439
3.425
3.411
2.570
2.570
1.600
1.595
1.264
1.253
1.238
1.224
1.210
0.015
0.008
0.002
17 16 15 14 13 12 11 10 9 8 7 6 5 4 3 2 1 0 −1 −2 ppm
1.00
0.99
0.97
1.00
0.99
0.90
4.06
2.99
6.14

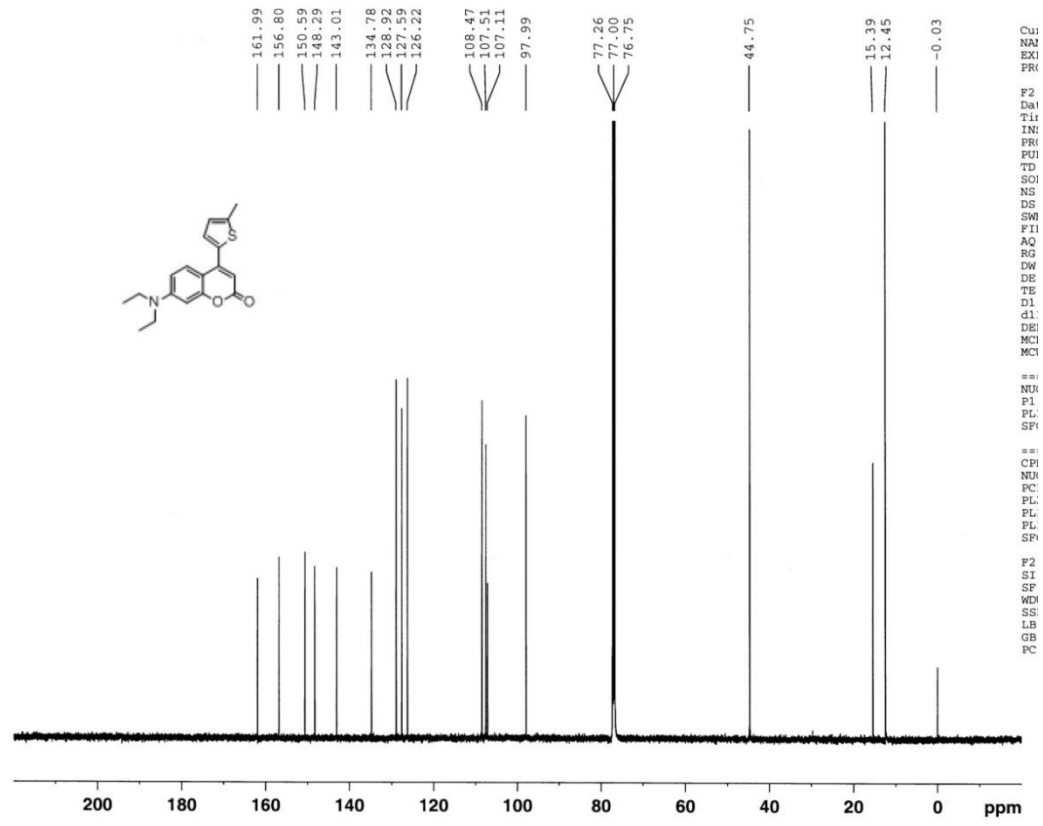
161.99
156.80
150.59
148.29
143.01
134.78
128.92
127.59
126.22
108.47
107.51
107.11
97.99
77.26
77.00
76.75
44.75
15.39
12.45
-0.03
200 180 160 140 120 100 80 60 40 20 0 ppm

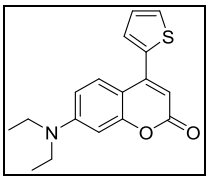

Compound 18b. Yield 23%; ^{1}H NMR (500 MHz, $CDCl_3$) δ 7.69 (d, 1H, *J* = 8.5 Hz), 7.51 (dd, 1H, *J* = 5.5, 0.5 Hz), 7.39 (dd, 1H, *J* = 3.5, 0.5 Hz), 7.18-7.21 (m, 1H), 6.55-6.61 (m, 2H), 6.15 (s, 1H), 3.44 (q, 4H, *J* = 7.0 Hz), 1.23 (t, 6H, *J* = 7.0 Hz); ^{13}C NMR (125 MHz, $CDCl_3$) δ 161.8, 156.8, 15.7, 148.2, 137.2, 128.6, 127.8, 127.7, 127.6, 108.6, 108.2, 107.1, 98.0, 44.8, 12.4; IR (neat, cm^{-1}) 3101, 2974, 1704, 1614, 1430, 1405, 1352, 1274, 1107; HRMS calculated for $C_{17}H_{17}NO_2S$ ($M + Na^+$): 322.0872. Found: 322.0871.

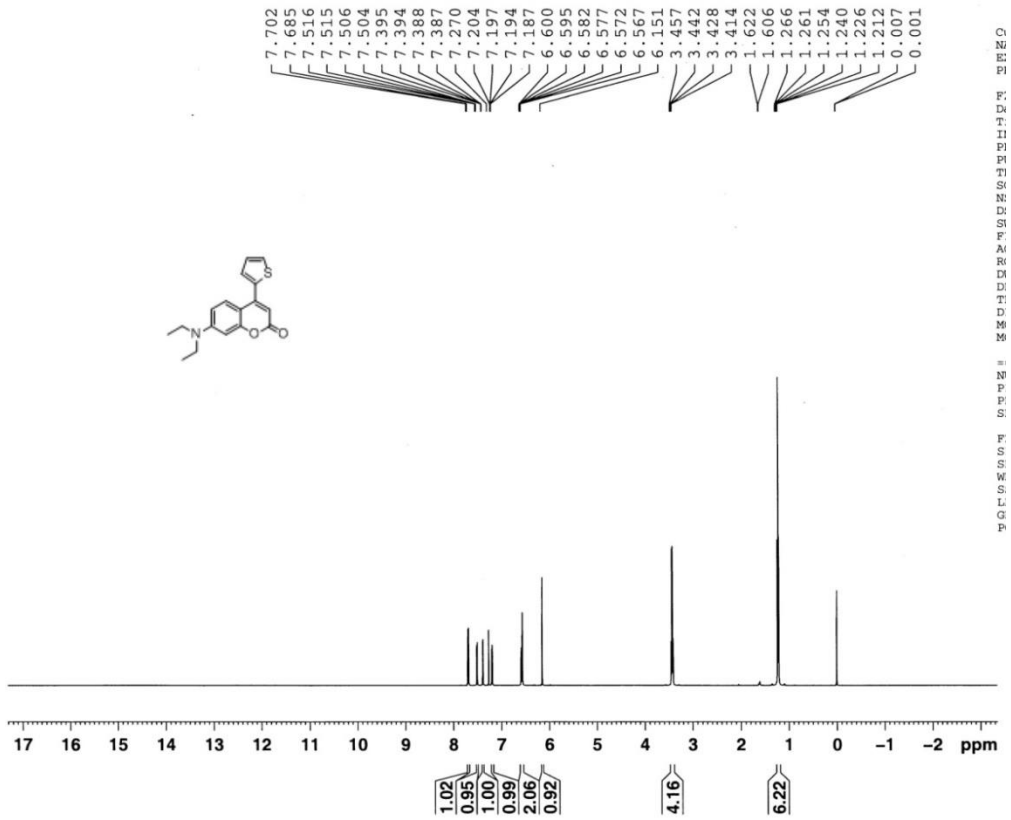
7.702
7.685
7.516
7.515
7.506
7.504
7.395
7.394
7.388
7.387
7.270
7.204
7.197
7.194
7.187
6.600
6.595
6.582
6.577
6.572
6.567
6.151
3.457
3.442
3.428
3.414
1.622
1.606
1.266
1.261
1.254
1.240
1.226
1.212
0.007
0.001
17 16 15 14 13 12 11 10 9 8 7 6 5 4 3 2 1 0 −1 −2 ppm
1.02
0.95
1.00
0.99
2.06
0.92
4.16
6.22

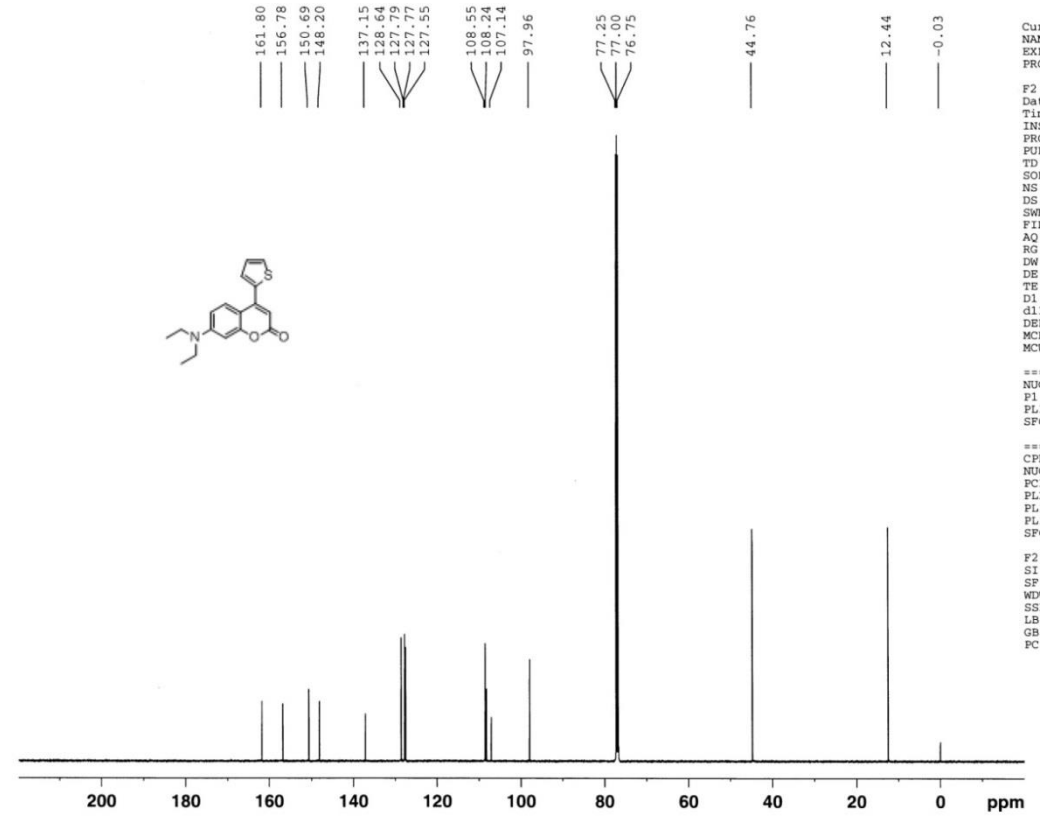
161.80
156.78
150.69
148.20
137.15
128.64
127.79
127.77
127.55
108.55
108.24
107.14
97.96
77.25
77.00
76.75
44.76
12.44
-0.03
200 180 160 140 120 100 80 60 40 20 0 ppm

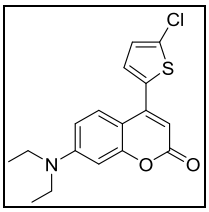

Compound 18a. Yield 26%; ^{1}H NMR (500 MHz, $CDCl_3$) δ 7.64 (d, 1H, *J* = 9.0 Hz), 7.16 (d, 1H, *J* = 4.0 Hz), 7.01 (d, 1H, *J* = 4.0 Hz), 6.58 (dd, 1H, *J* = 9.0, 2.5 Hz), 6.55 (d, 1H, *J* = 2.5 Hz), 6.07 (s, 1H), 3.43 (q, 4H, *J* = 7.0 Hz), 1.22 (t, 6H, *J* = 7.0 Hz); ^{13}C NMR (125 MHz, $CDCl_3$) δ 161.6, 156.8, 150.8, 147.1, 135.6, 132.6, 128.0, 127.2, 126.9, 108.7, 108.1, 106.7, 98.0, 44.8, 12.4; IR (neat, cm^{-1}) 2974, 1712, 1614, 1585, 1516, 1434, 1352, 1266, 1103; HRMS calculated for $C_{17}H_{16}ClNO_2S$ ($M + Na^+$): 356.0482. Found: 356.0481.

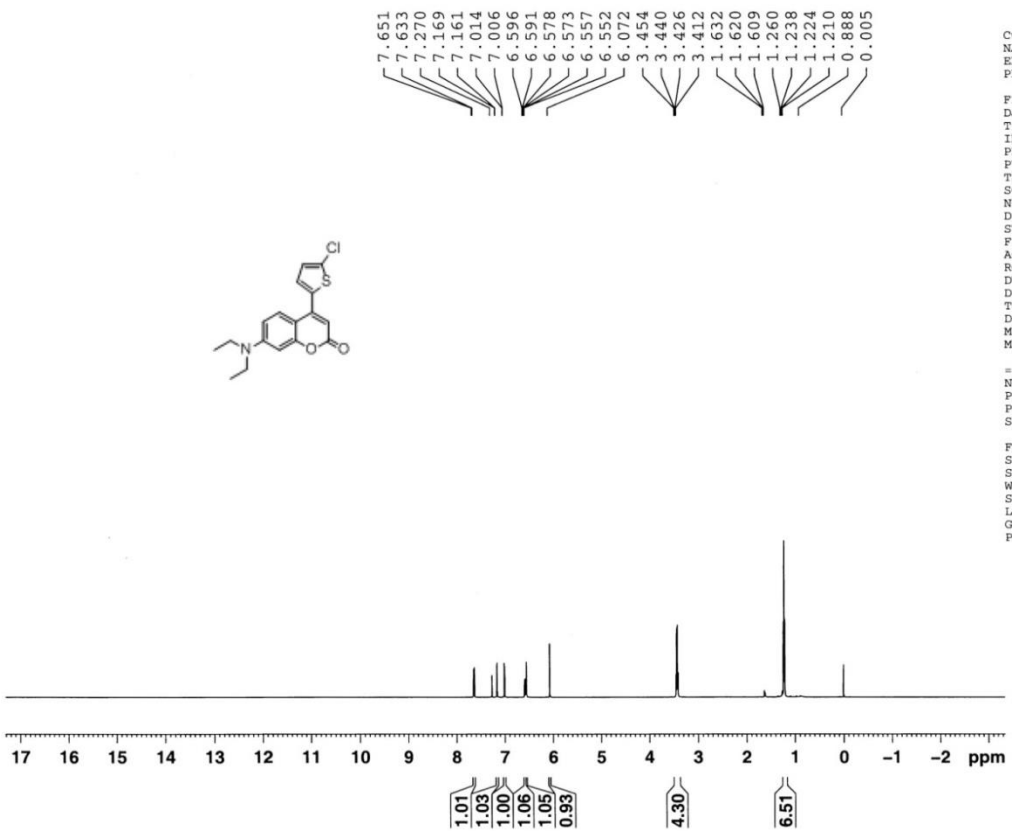
7.651
7.633
7.270
7.169
7.161
7.014
7.006
6.596
6.591
6.578
6.573
6.557
6.552
6.072
3.454
3.440
3.426
3.412
1.632
1.620
1.609
1.260
1.238
1.224
1.210
0.888
0.005
Cl
S
N
O
O
17 16 15 14 13 12 11 10 9 8 7 6 5 4 3 2 1 0 −1 −2 ppm
1.01
1.03
1.00
1.06
1.05
0.93
4.30
6.51

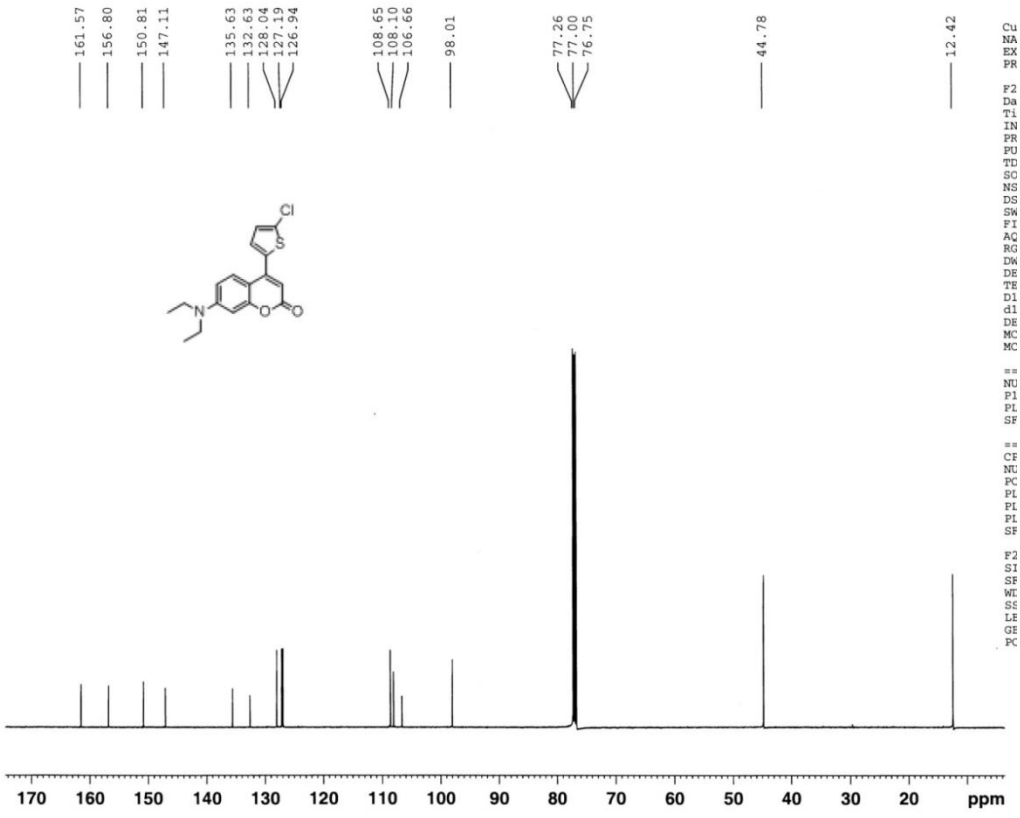
161.57
156.80
150.81
147.11
135.63
132.63
128.04
127.19
126.94
108.65
108.10
106.66
98.01
77.26
77.00
76.75
44.78
12.42
Cl
S
N
O
O
170 160 150 140 130 120 110 100 90 80 70 60 50 40 30 20 ppm

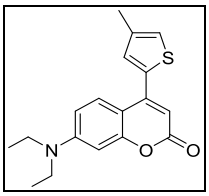

Compound 18c. Yield 42%; ^{1}H NMR (500 MHz, $CDCl_3$) δ 7.73 (d, 1H, *J* = 9.0 Hz), 7.20 (s, 1H), 7.09 (s, 1H), 6.60 (dd, 1H, *J* = 9.0, 3.0 Hz), 6.57 (d, 1H, *J* = 2.5 Hz), 6.13 (s, 1H), 3.44 (q, 4H, *J* = 7.0 Hz), 2.35 (s, 3H), 1.23 (t, 6H, *J* = 7.0 Hz); ^{13}C NMR (125 MHz, $CDCl_3$) δ 161.9, 156.8, 150.7, 148.4, 138.5, 137.0, 130.9, 127.6, 123.3, 108.5, 107.9, 107.2, 98.0, 44.8, 15.8, 12.5; IR (neat, cm^{-1}) 2921, 1708, 1610, 1584, 1516, 1409, 1352, 1099; HRMS calculated for $C_{18}H_{19}NO_2S$ ($M + Na^+$): 336.102871. Found: 336.102867.

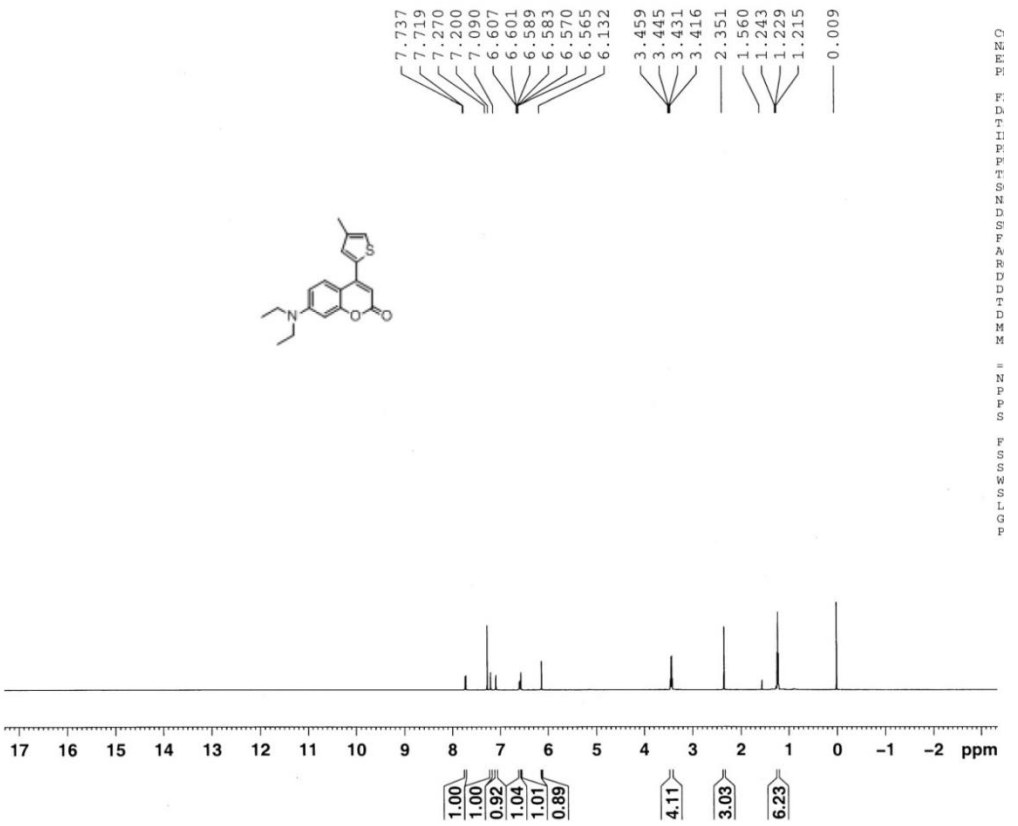
7.737
7.719
7.270
7.200
7.090
6.607
6.601
6.589
6.583
6.570
6.565
6.132
3.459
3.445
3.431
3.416
2.351
1.560
1.243
1.229
1.215
0.009
17 16 15 14 13 12 11 10 9 8 7 6 5 4 3 2 1 0 −1 −2 ppm
1.00
1.00
0.92
1.04
1.01
0.89
4.11
3.03
6.23

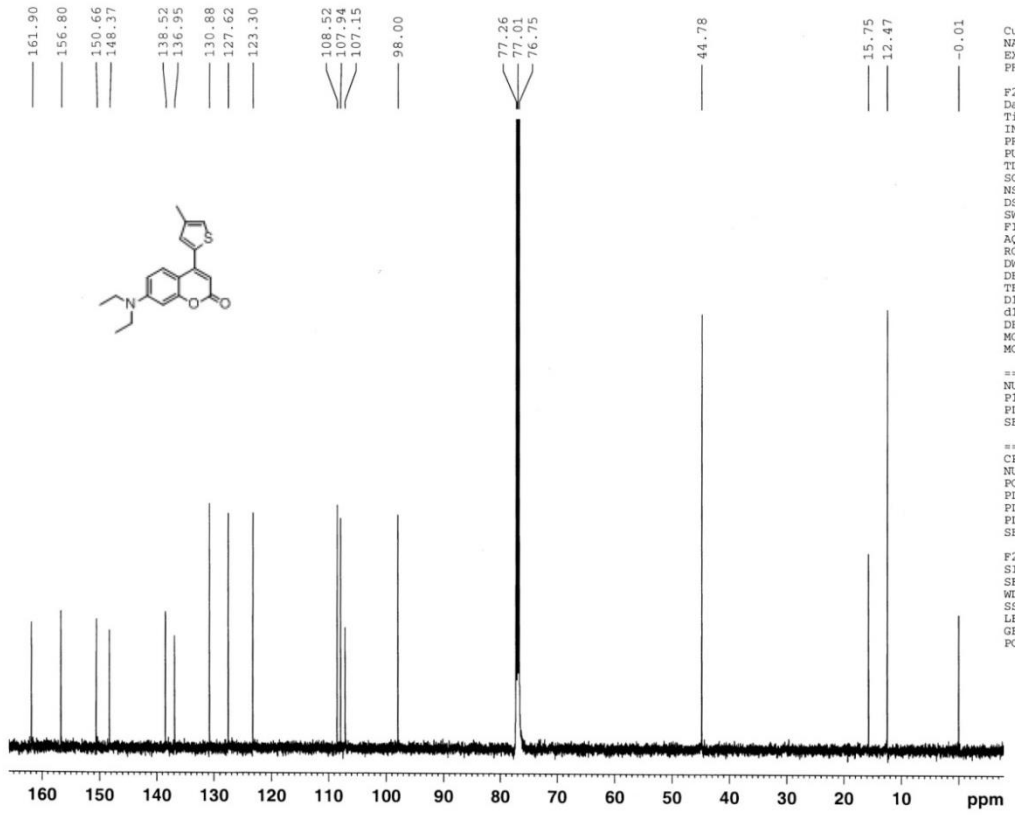
161.90
156.80
150.66
148.37
138.52
136.95
130.88
127.62
123.30
108.52
107.94
107.15
98.00
77.26
77.01
76.75
44.78
15.75
12.47
-0.01
160 150 140 130 120 110 100 90 80 70 60 50 40 30 20 10 ppm

General Synthesis for Formylation of Thiophene-Substituted NS521 Derivatives

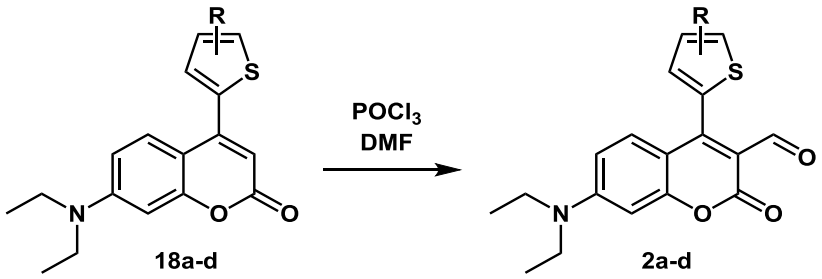

$POCl_3$ (5.2 mL, 56.1 mmol) was added to DMF (10.8 mL, 139.5 mmol) at 0 °C in a flame-dried round bottom flask. The Vilsmeier reagent was stirred at ambient temperature for 45 min. The Vilsmeier reagent (5 mL) was added to a solution of 4-thiophene-substituted-7-diethylaminocoumarin (**18a-d**) in DMF (1 mL). The solution was stirred at ambient temperature for 12 hours. The resulting red solution was poured onto cold H_2O (100 mL), basified with saturated $NaHCO_3$ (50 mL), and extracted with CH_2Cl_2 (100 mL x 3). The combined organic layers were dried over Na_2SO_4 and the solvent was removed *in vacuo*. The residue was purified by chromatography (90:10 hexanes:EtOAc → 50:50 hexanes/EtOAc) to yield the desired formylated compound as a yellow oil.

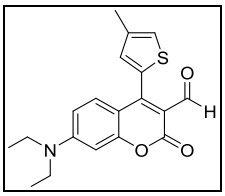

Compound 2c. Yield 72%; ^{1}H NMR (500 MHz, $CDCl_3$) δ 9.89 (s, 1H), 7.34 (d, 1H, *J* = 8.5 Hz), 7.19 (s, 1H), 6.97 (s, 1H), 6.57 (dd, 1H, *J* = 9.0, 2.5 Hz), 6.50 (d, 1H, *J* = 2.5 Hz), 3.46 (q, 4H, *J* = 7.0 Hz), 2.36 (s, 3H), 1.25 (t, 6H, *J* = 7.0 Hz); ^{13}C NMR (125 MHz, $CDCl_3$) δ 188.0, 158.8, 157.5, 155.3, 153.1, 138.1, 132.3, 131.8, 130.6, 124.0, 113.5, 109.7, 109.1, 97.1, 45.2, 15.6, 12.5; IR (neat, cm^{-1}) 2966, 1748, 1712, 1610, 1438, 1373, 1270, 1070, 731; HRMS calculated for $C_{19}H_{19}NO_3S$ ($M + Na^+$): 364.097785. Found: 364.097734.

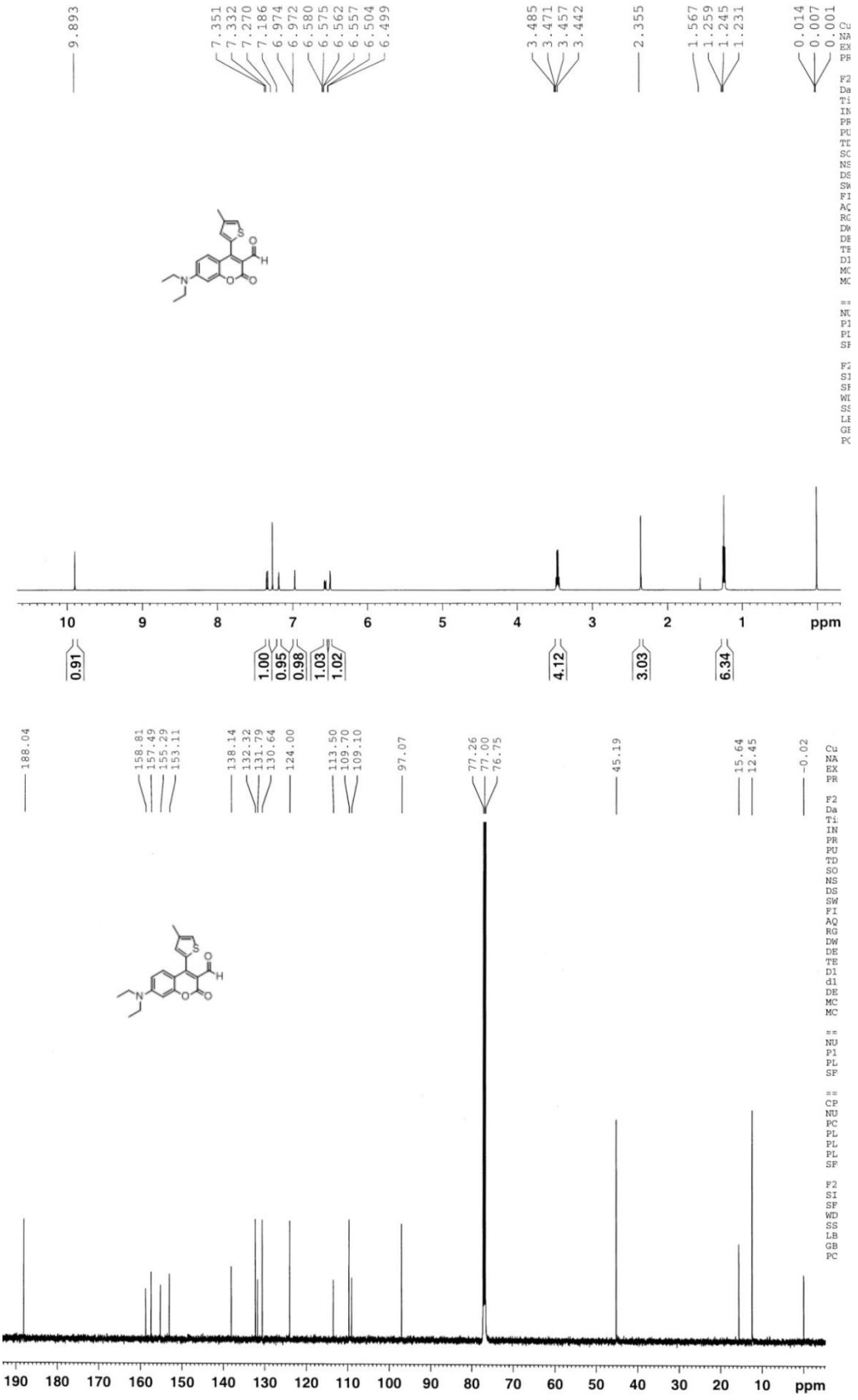
9.893
7.351
7.332
7.270
7.186
6.974
6.972
6.580
6.575
6.562
6.557
6.504
6.499
3.485
3.471
3.457
3.442
2.355
1.567
1.259
1.245
1.231
0.014
0.007
0.001
10
9
8
7
6
5
4
3
2
1
ppm
0.91
1.00
0.95
0.98
1.03
1.02
4.12
3.03
6.34
188.04
158.81
157.49
155.29
153.11
138.14
132.32
131.79
130.64
124.00
113.50
109.70
109.10
97.07
77.26
77.00
76.75
45.19
15.64
12.45
-0.02
190
180
170
160
150
140
130
120
110
100
90
80
70
60
50
40
30
20
10
ppm

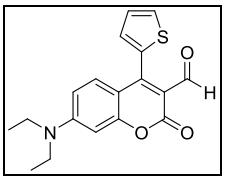

NeuroSensor 539 (Compound 2b). Yield 54%; ^{1}H NMR (500 MHz, CD_2Cl_2) δ 9.84 (s, 1H), 7.64 (dd, 1H, *J* = 5.0, 1.0 Hz), 7.20-7.25 (m, 2H), 7.16 (dd, 1H, *J* = 4.0, 1.0 Hz), 6.60 (dd, 1H, *J* = 9.0, 2.5 Hz), 6.53 (d, 1H, *J* = 2.5 Hz), 3.46 (q, 4H, *J* = 7.5 Hz), 1.23 (t, 6H, *J* = 7.5 Hz); ^{13}C NMR (125 MHz, CD_2Cl_2) δ 188.0, 159.2, 157.9, 155.0, 153.5, 132.7, 130.9, 130.2, 128.7, 127.7, 114.0, 110.4, 109.8, 97.5, 45.7, 12.6; IR (neat, cm^{-1}) 2921, 1740, 1614, 1495, 1442, 1417, 1356; HRMS calculated for $C_{18}H_{17}NO_3S$ ($M + Na^+$): 350.0821. Found: 350.0818.

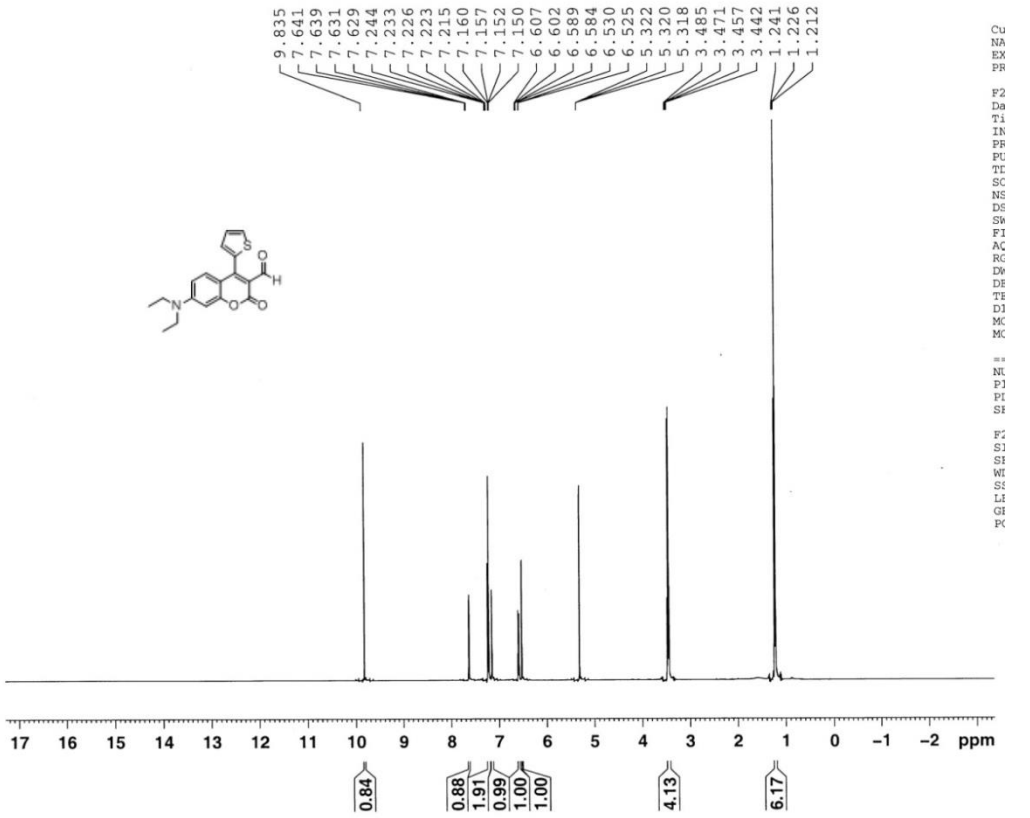
9.835
7.641
7.639
7.631
7.629
7.244
7.233
7.226
7.223
7.215
7.160
7.157
7.152
7.150
6.607
6.602
6.589
6.584
6.530
6.525
5.322
5.320
5.318
3.485
3.471
3.457
3.442
1.241
1.226
1.212
17 16 15 14 13 12 11 10 9 8 7 6 5 4 3 2 1 0 −1 −2 ppm
0.84
0.88
1.91
0.99
1.00
1.00
4.13
6.17

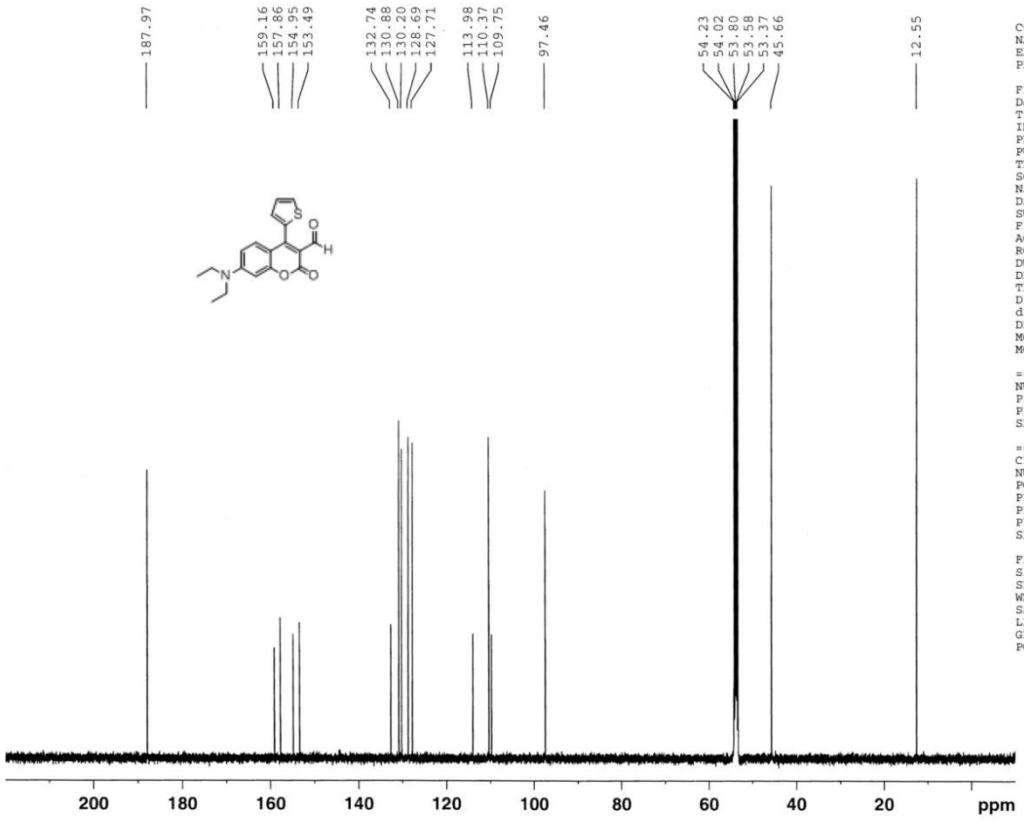
187.97
159.16
157.86
154.95
153.49
132.74
130.88
130.20
128.69
127.71
113.98
110.37
109.75
97.46
54.23
54.02
53.80
53.58
53.37
45.66
12.55
200 180 160 140 120 100 80 60 40 20 ppm

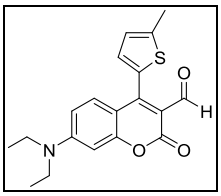

Compound 2d. Yield 83%; ^{1}H NMR (500 MHz, $CDCl_3$) δ 9.92 (s, 1H), 7.41 (d, 1H, *J* = 9.5 Hz), 6.99 (d, 1H, *J* = 3.5 Hz), 6.88 (dd, 1H, *J* = 3.5, 1.0 Hz), 6.58 (dd, 1H, *J* = 9.0, 2.5 Hz), 6.52 (d, 1H, *J* = 2.5 Hz), 3.48 (q, 4H, *J* = 7.0 Hz), 2.61 (s, 3H), 1.26 (t, 6H, *J* = 7.0 Hz); ^{13}C NMR (125 MHz, $CDCl_3$) δ 188.1, 158.9, 157.5, 155.2, 153.0, 144.0, 130.7, 130.5, 129.5, 125.8, 113.5, 109.6, 109.1, 97.1, 45.2, 15.3, 12.5; IR (neat, cm^{-1}) 1744, 1610, 1561, 1499, 1422, 1266, 1123; HRMS calculated for $C_{19}H_{19}NO_3S$ (M + Na^+): 364.0978. Found: 364.0975.

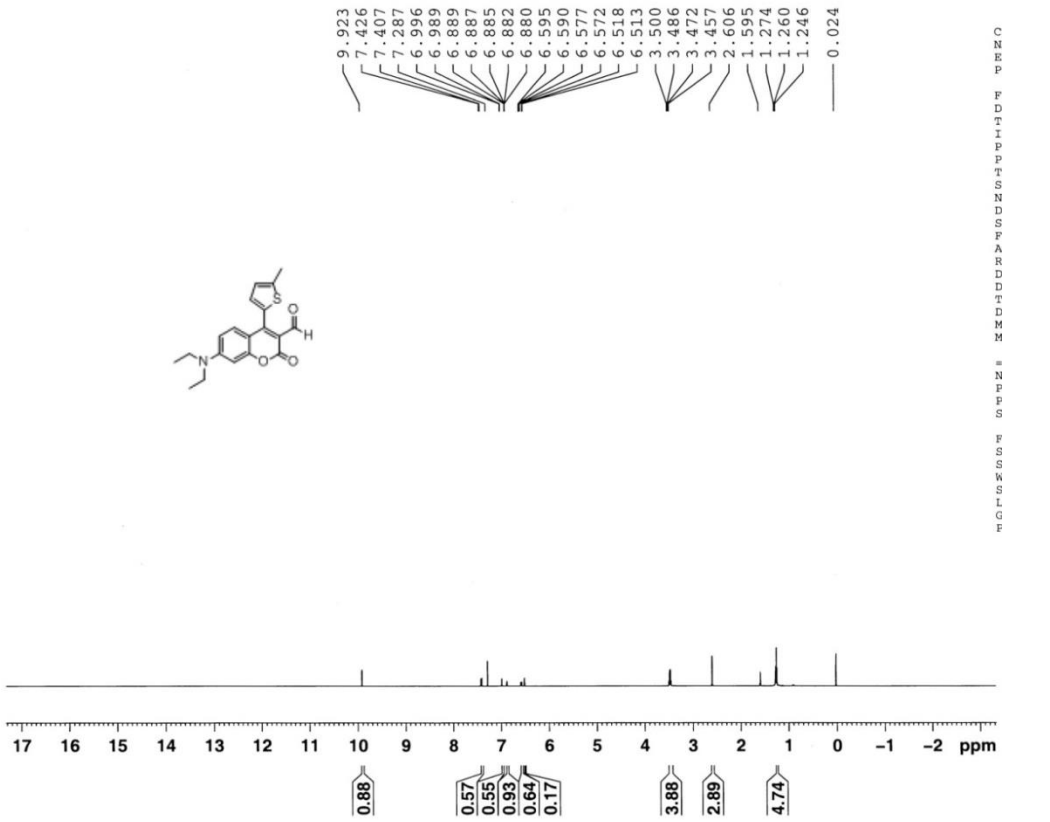
9.923
7.426
7.407
7.287
6.996
6.989
6.889
6.887
6.885
6.882
6.880
6.595
6.590
6.577
6.572
6.518
6.513
3.500
3.486
3.472
3.457
2.606
1.595
1.274
1.260
1.246
0.024
17 16 15 14 13 12 11 10 9 8 7 6 5 4 3 2 1 0 −1 −2 ppm
0.88
0.57
0.55
0.93
0.64
0.17
3.88
2.89
4.74

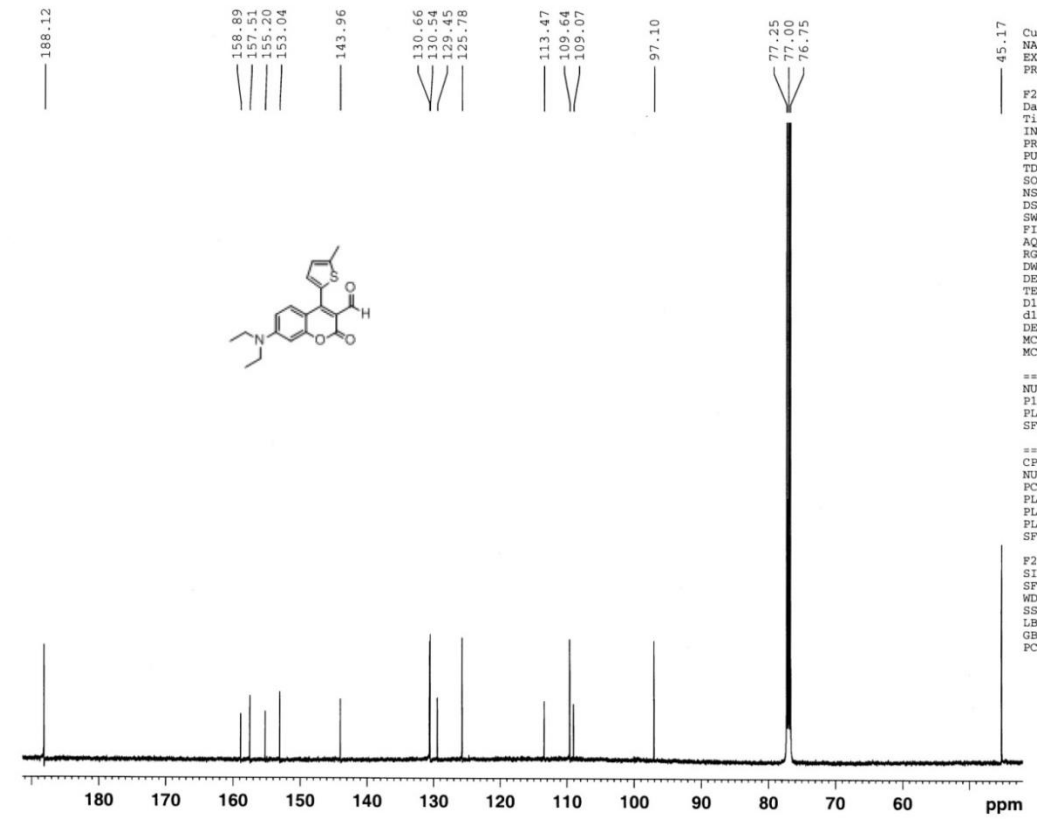
188.12
158.89
157.51
155.20
153.04
143.96
130.66
130.54
129.45
125.78
113.47
109.64
109.07
97.10
77.25
77.00
76.75
45.17
180 170 160 150 140 130 120 110 100 90 80 70 60 ppm

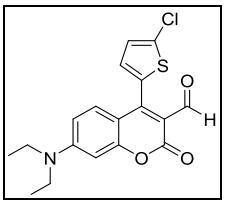

Compound 2a. Yield 78%; ^{1}H NMR (500 MHz, $CDCl_3$) δ 10.00 (s, 1H), 7.30 (d, 1H, *J* = 9.5 Hz), 7.02 (d, 1H, *J* = 4.0 Hz), 6.89 (d, 1H, *J* = 4.0 Hz), 6.57 (dd, 1H, *J* = 9.0, 2.5), 6.49 (d, 1H, *J* = 2.5 Hz), 3.47 (q, 4H, *J* = 7.0 Hz), 1.24 (t, 6H, *J* = 7.0 Hz); ^{13}C NMR (125 MHz, $CDCl_3$) δ 187.7, 159.6, 157.5, 153.2, 152.4, 133.1, 131.1, 130.5, 128.8, 126.4, 113.2, 110.0, 109.1, 97.1, 45.2, 12.4; IR (neat, cm^{-1}) 2970, 1748, 1717, 1611, 1559, 1499, 1439, 1412; HRMS calculated for $C_{18}H_{16}ClNO_3S$ ($M + Na^+$): 384.0432. Found: 384.0432.

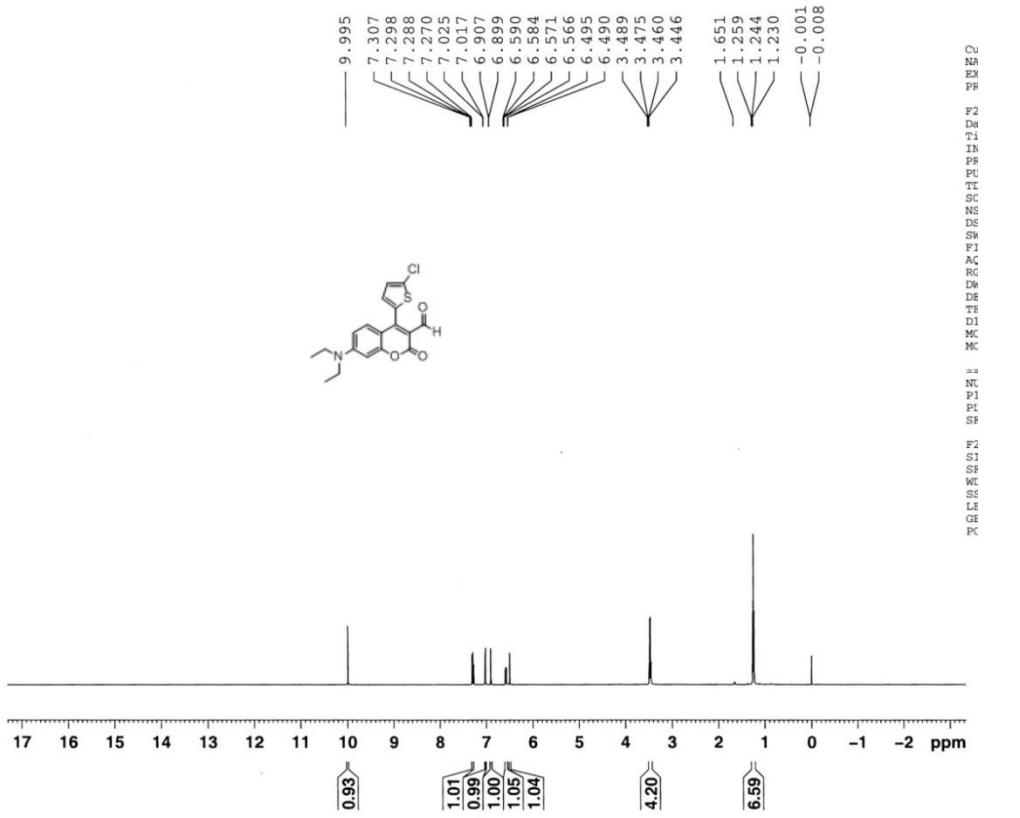
9.995
7.307
7.298
7.288
7.270
7.025
7.017
6.907
6.899
6.590
6.584
6.571
6.566
6.495
6.490
3.489
3.475
3.460
3.446
1.651
1.259
1.244
1.230
-0.001
-0.008
Cl
S
O
H
N
O
O
17 16 15 14 13 12 11 10 9 8 7 6 5 4 3 2 1 0 −1 −2 ppm
0.93
1.01
0.99
1.00
1.05
1.04
4.20
6.59

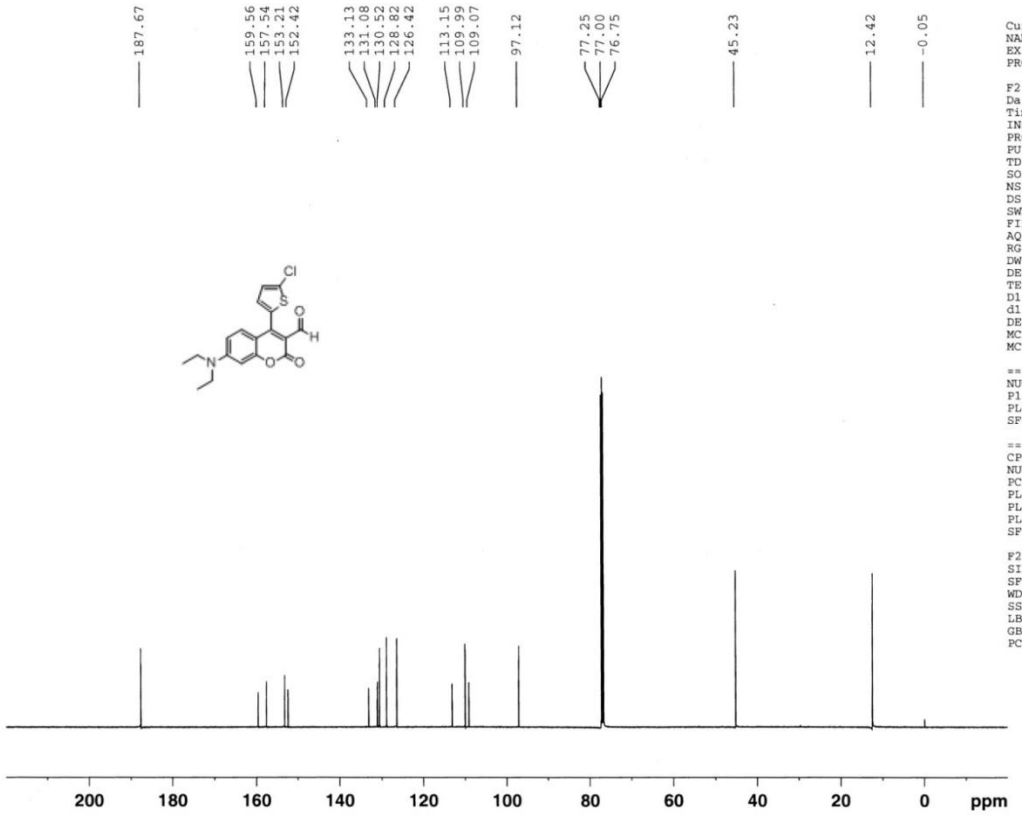
187.67
159.56
157.54
153.21
152.42
133.13
131.08
130.52
128.82
126.42
113.15
109.99
109.07
97.12
77.25
77.00
76.75
45.23
12.42
-0.05
Cl
S
O
H
N
O
O
200 180 160 140 120 100 80 60 40 20 0 ppm

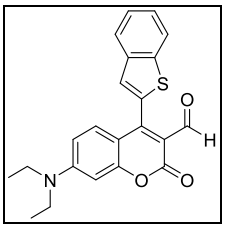

Compound 2e. Yield 89%; ^{1}H NMR (500 MHz, $CDCl_3$) δ 9.99 (s, 1H), 7.88 (dd, 1H, *J* = 8.5, 1.5 Hz), 7.85 (dd, 1H, *J* = 7.0, 2.0 Hz), 7.40-7.48 (m, 2H), 7.35 (s, 1H), 7.29 (d, 1H, *J* = 9.0 Hz), 6.50-6.56 (2H), 3.46 (q, 4H, *J* = 7.0 Hz), 1.24 (t, 6H, *J* = 7.0 Hz); ^{13}C NMR (125 MHz, $CDCl_3$) δ 187.7, 159.2, 157.5, 154.3, 153.2, 140.7, 139.2, 132.9, 130.7, 126.1, 125.3, 125.0, 124.2, 122.2, 113.2, 109.9, 109.0, 97.0, 45.2, 12.4; IR (neat, cm^{-1}) 1742, 1615, 1491, 1418, 1356, 1268, 1148, 723; HRMS calculated for $C_{22}H_{19}NO_3S$ ($M + Na^+$): 400.097785. Found: 400.097669.

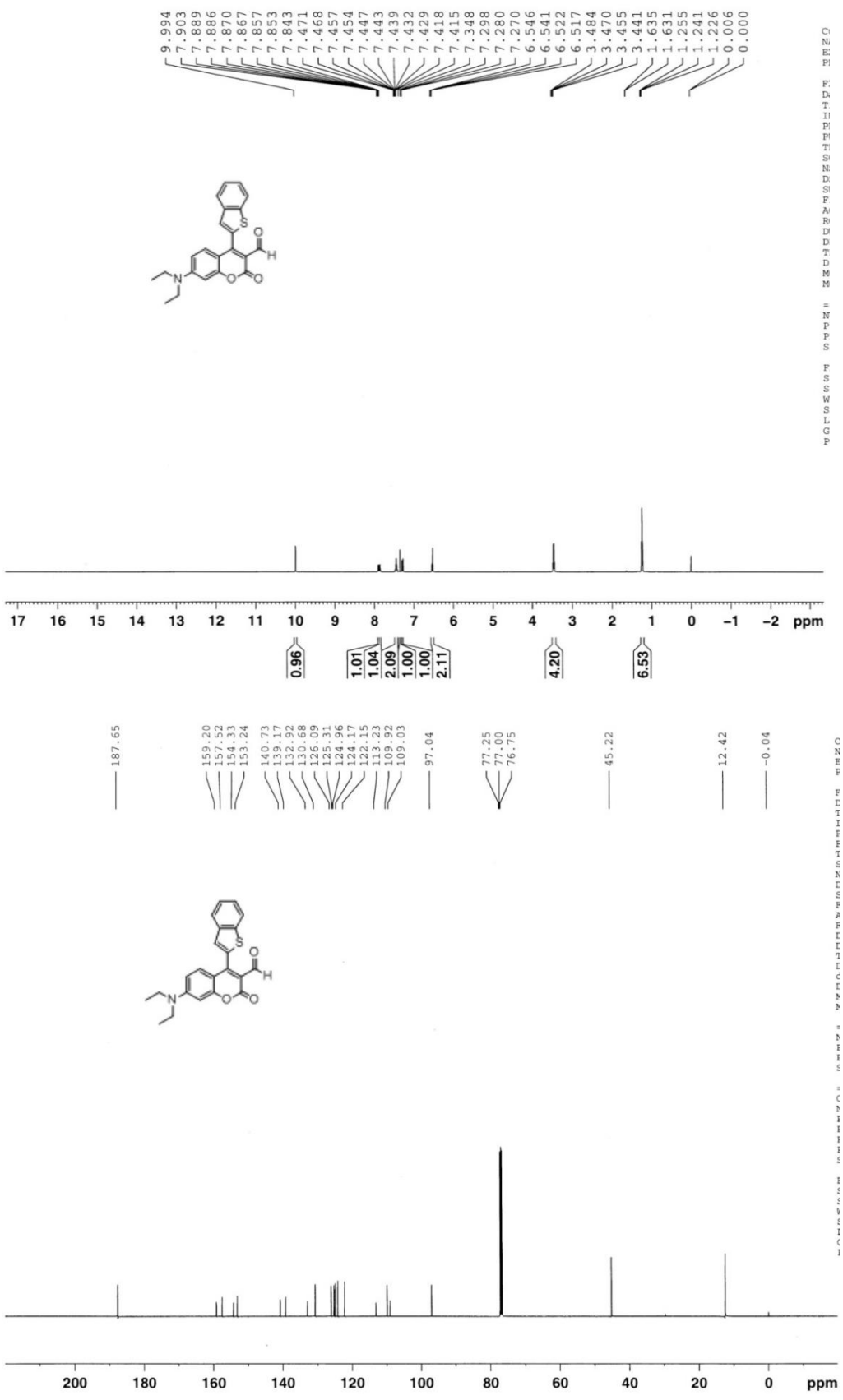
9.994
7.903
7.889
7.886
7.870
7.867
7.857
7.853
7.843
7.471
7.468
7.457
7.454
7.447
7.443
7.439
7.432
7.429
7.418
7.415
7.348
7.298
7.280
7.270
6.546
6.541
6.522
6.517
3.484
3.470
3.455
3.441
1.635
1.631
1.255
1.241
1.226
0.006
0.000
17 16 15 14 13 12 11 10 9 8 7 6 5 4 3 2 1 0 −1 −2 ppm
0.96
1.01
1.04
2.09
1.00
1.00
2.11
4.20
6.53
187.65
159.20
157.52
154.33
153.24
140.73
139.17
132.92
130.68
126.09
125.31
124.96
124.17
122.15
113.23
109.92
109.03
97.04
77.25
77.00
76.75
45.22
12.42
-0.04
200 180 160 140 120 100 80 60 40 20 0 ppm

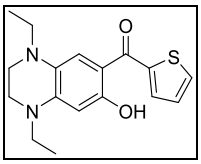

Compound 26. Compound **25** (250.0 mg, 1.136 mmol) was dissolved in 11.3 mL CH_2Cl_2 and cooled to 0 °C. Aluminium chloride (605.2 mg, 4.542 mmol) was added and the solution stirred for 10 min. 2-Thiophene carbonyl chloride (166.5 mg, 1.136 mmol) was then added. The mixture stirred for 5 min at 0 °C then warmed to room temperature and stirred for 4 hours while sonicating intermittently. Then 6 M HCl was slowly added to the mixture which stirred another 10 min. The crude product was extracted with CH_2Cl_2 (50 mL x 3), the organic layers combined and dried over Na_2SO_4, and the solvent removed *in vacuo*. After purifying twice by column chromatography (9:1 CH_2Cl_2/EtOAc then 8:2 hexanes/EtOAc), compound **26** was isolated as a red oil (316.2 mg, 1.000 mmol, 88%): ^{1}H NMR (500 MHz, $CDCl_3$) δ 12.83 (s, 1H), 7.69 (dd, 1H, *J* = 4.0, 1.0 Hz), 7.61 (dd, 1H, *J* = 5.0, 1.0 Hz), 7.14-7.18 (m, 1H), 7.07 (s, 1H), 6.13 (s, 1H), 3.53 (t, 2H, *J* = 5.0 Hz), 3.41 (q, 2H, *J* = 7.0 Hz), 3.24 (q, 2H, *J* = 7.5 Hz), 3.17 (t, 2H, *J* = 5.0 Hz), 1.17-1.25 (m, 6H); ^{13}C NMR (125 MHz, $CDCl_3$) δ 186.8, 161.1, 144.5, 143.2, 131.6, 131.1, 127.6, 127.3, 112.1, 108.1, 96.6, 47.8, 45.7, 45.5, 44.9, 10.7, 10.3; IR (neat, cm^{-1}) 3101, 2970, 1618, 1524, 1409, 1324, 1217, 1119; HRMS calculated for $C_{17}H_{20}N_2O_2SNa^+$ (M + Na^+): 339.1138. Found: 339.1135.

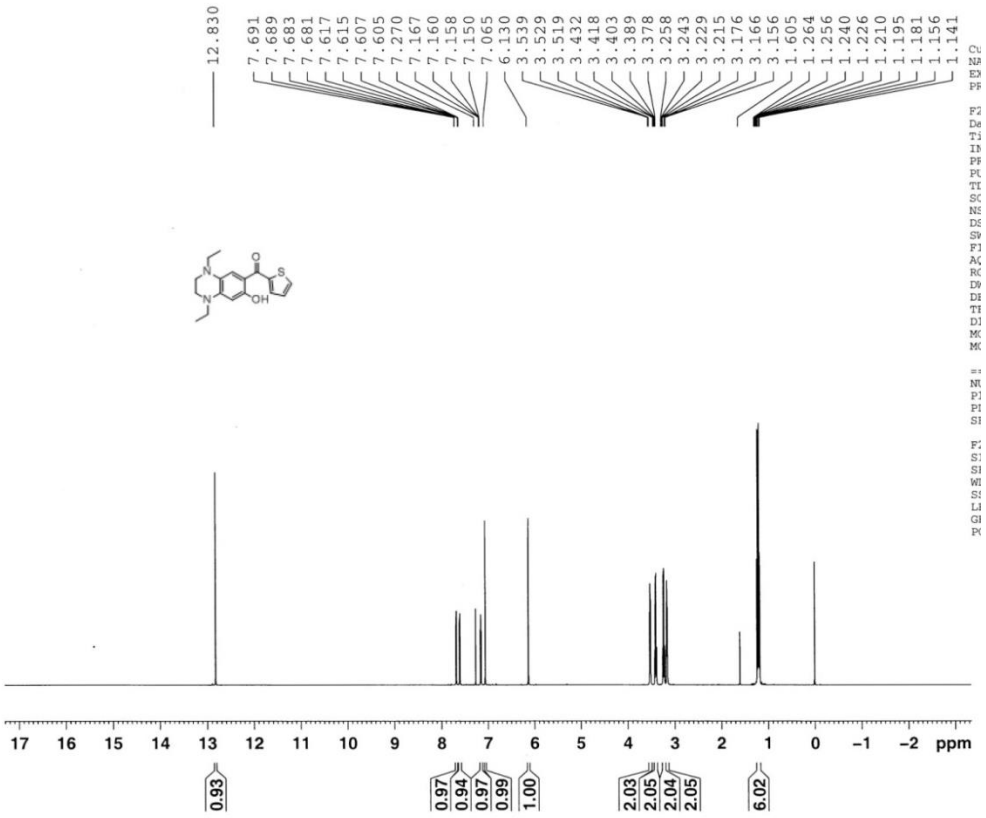
12.830
7.691
7.689
7.683
7.681
7.617
7.615
7.607
7.605
7.270
7.167
7.160
7.158
7.150
7.065
6.130
3.539
3.529
3.519
3.432
3.418
3.403
3.389
3.378
3.258
3.243
3.229
3.215
3.176
3.166
3.156
1.605
1.264
1.256
1.240
1.226
1.210
1.195
1.181
1.156
1.141
17 16 15 14 13 12 11 10 9 8 7 6 5 4 3 2 1 0 −1 −2 ppm
0.93
0.97
0.94
0.97
0.99
1.00
2.03
2.05
2.04
2.05
6.02

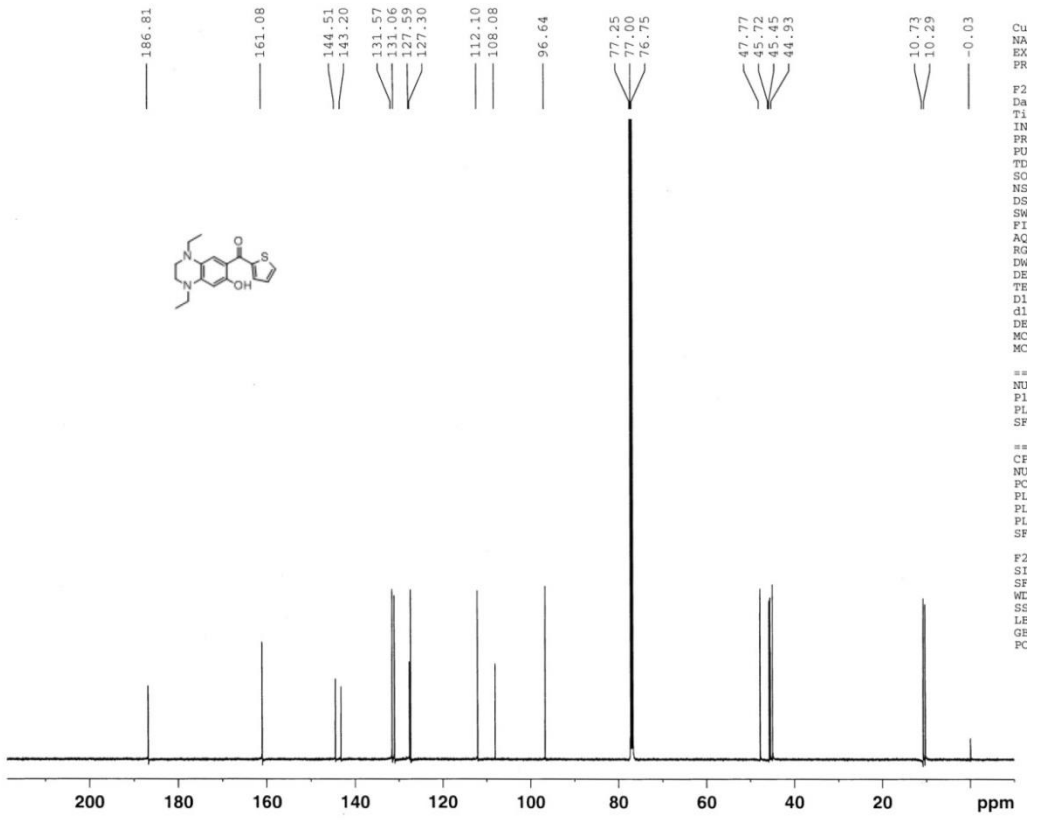
186.81
161.08
144.51
143.20
131.57
131.06
127.59
127.30
112.10
108.08
96.64
77.25
77.00
76.75
47.77
45.72
45.45
44.93
10.73
10.29
-0.03
200 180 160 140 120 100 80 60 40 20 ppm

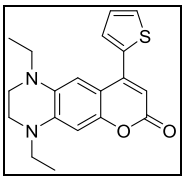

Compound 27. Compound **26** (72.5 mg, 0.229 mmol), (carbethoxymethylene)triphenylphosphorane (87.9 mg, 0.252 mmol), DMAP (2.8 mg, 0.023 mmol), and 2 mL *o*-xylene were combined in a round bottom flask and heated at 140 °C for 4 h. The solvent was boiled off and the remaining crude product was purified via column chromatography (8:2 hexanes/EtOAc) to yield compound **27** as an orange oil (51.7 mg, 0.176 mmol, 66%): ^{1}H NMR (500 MHz, $CDCl_3$) δ 7.52 (dd, 1H, *J* = 5.0, 1.0 Hz), 7.40 (dd, 1H, *J* = 3.5, 1.0 Hz), 7.18-7.21 (m, 1H), 6.93 (s, 1H), 6.51 (s, 1H), 6.17 (s, 1H), 3.51 (t, 2H, *J* = 5.0 Hz), 3.41 (q, 2 H, *J* = 7.5 Hz), 3.24-3.30 (m, 4H), 1.22 (t, 3H, *J* = 7.5 Hz), 1.17 (t, 3H, *J* = 7.0 Hz); ^{13}C NMR (125 MHz, $CDCl_3$) δ 162.2, 150.2, 147.9, 140.1, 137.8, 131.9, 128.3, 127.8, 127.7, 108.3, 107.5, 105.6, 97.0, 47.2, 45.7, 45.5, 45.2, 10.3, 10.0; IR (neat, cm^{-1}) 2966, 1716, 1699, 1608, 1538, 1418, 1373, 1334; HRMS calculated for $C_{19}H_{20}N_2O_2SNa^+$ (M + Na^+): 363.1138. Found: 363.1133.

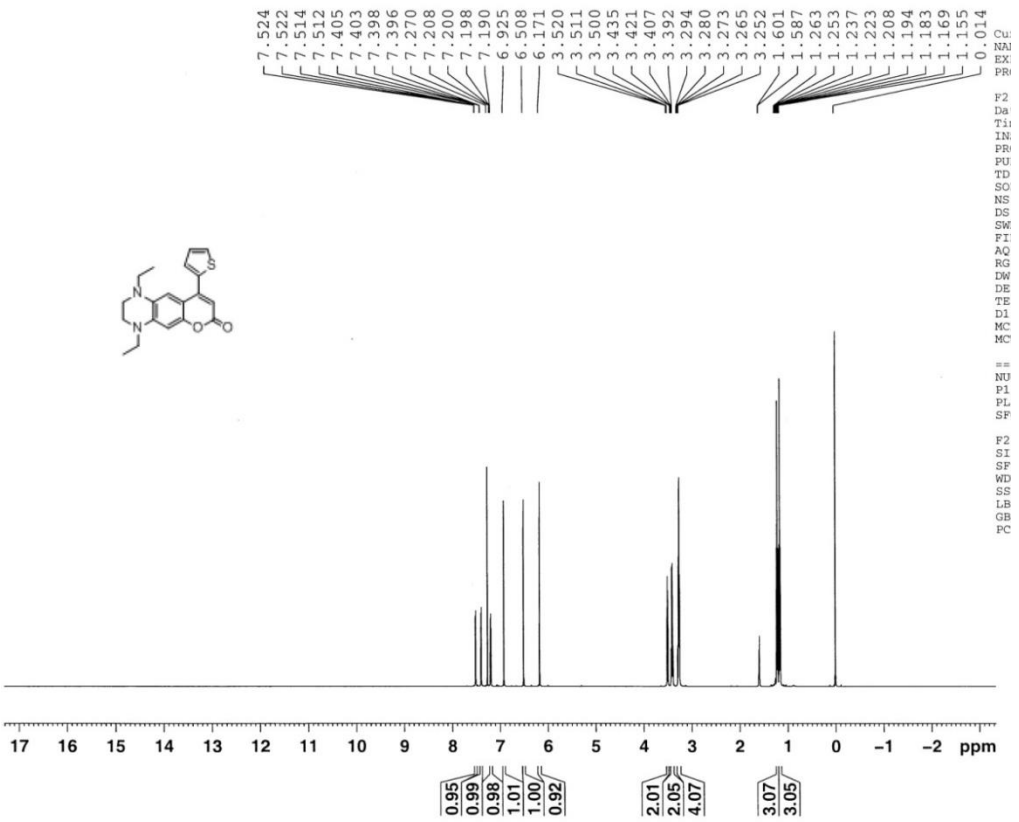
7.524
7.522
7.514
7.512
7.405
7.403
7.398
7.396
7.270
7.208
7.200
7.198
7.190
6.925
6.508
6.171
3.520
3.511
3.500
3.435
3.421
3.407
3.392
3.294
3.280
3.273
3.265
3.252
1.601
1.587
1.263
1.253
1.237
1.223
1.208
1.194
1.183
1.169
1.155
0.014
17 16 15 14 13 12 11 10 9 8 7 6 5 4 3 2 1 0 −1 −2 ppm
0.95
0.99
0.98
1.01
1.00
0.92
2.01
2.05
4.07
3.07
3.05

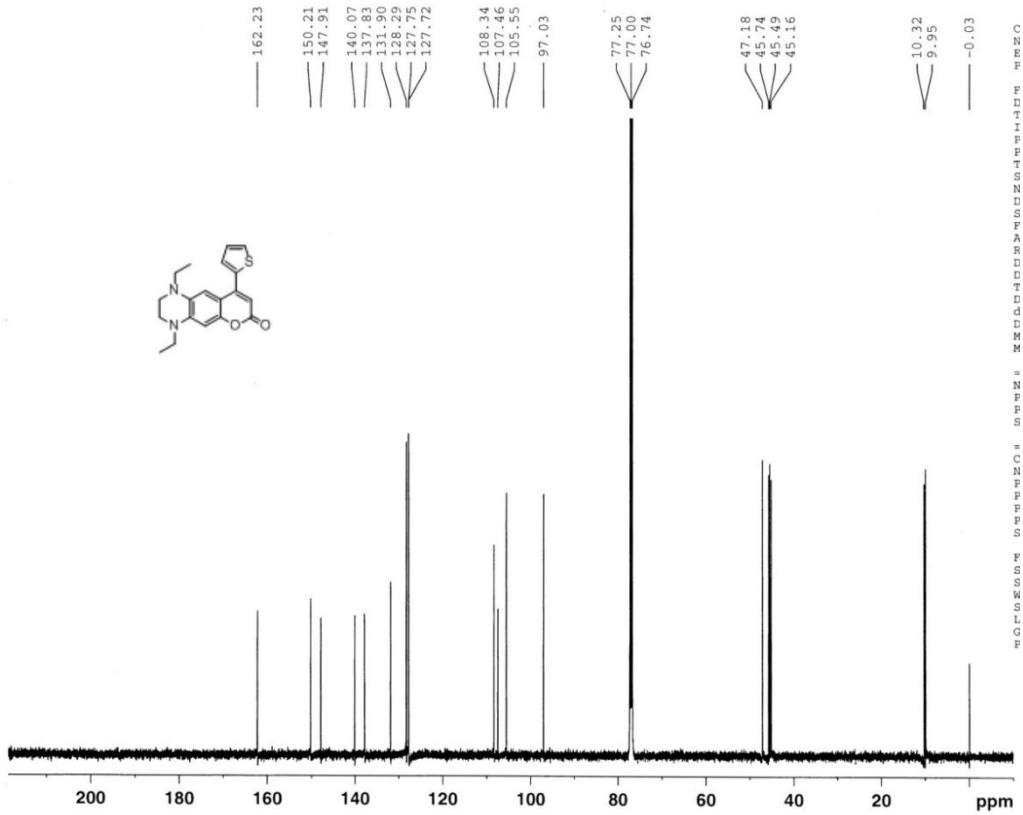
162.23
150.21
147.91
140.07
137.83
131.90
128.29
127.75
127.72
108.34
107.46
105.55
97.03
77.25
77.00
76.74
47.18
45.74
45.49
45.16
10.32
9.95
-0.03
200 180 160 140 120 100 80 60 40 20 ppm

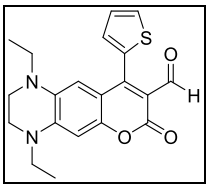

NeuroSensor 715. The Vilsmeier reagent was made by combining 10.8 mL DMF and 5.23 mL $POCl_3$ at 0 °C in a flame-dried round bottom flask. The solution was stirred for 1 h. In a separate dry flask, compound **27** (66.0 mg, 0.194 mmol) was dissolved in 2 mL DMF and purged with N_2. To the starting material was added 0.5 mL of the Vilsmeier reagent and the mixture stirred at ambient temperature for 2.5 h. The mixture was poured over ice chips (100 g), basified to pH 7 with $NaHCO_3$, and extracted with CH_2Cl_2 (25 mL x 5). The solvent was removed *in vacuo* without heating and the crude product purified via column chromatography (1:1 hexanes/EtOAc → 100% EtOAc → 100% acetone) to yield NeuroSensor 715 as a red oil (35.4 mg, 0.096 mmol, 50%) : ^{1}H NMR (500 MHz, $CDCl_3$) δ 9.90 (s, 1H), 7.60 (dd, 1H, *J* = 5.0, 1.0 Hz), 7.19-7.23 (m, 1H), 7.15 (dd, 1H, *J* = 3.5, 1.0 Hz), 6.45 (s, 1H), 6.33 (s, 1H), 3.57 (t, 2H, *J* = 5.0 Hz), 3.46 (q, 2H, *J* = 7.5 Hz), 3.22 (t, 2H, *J* = 5.0 Hz), 3.13 (q, 2H, *J* = 7.5 Hz), 1.26 (t, 3H, *J* = 7.5 Hz), 1.05 (t, 3H, *J* = 7.5 Hz); ^{13}C NMR (125 MHz, $CDCl_3$) δ 188.2, 159.6, 153.8, 152.4, 143.8, 133.0, 132.4, 129.6, 128.2, 127.3, 113.1, 109.9, 106.5, 95.8, 47.8, 46.4, 45.4, 44.6, 10.6, 9.6; IR (neat, cm^{-1}) 1728, 1695, 1675, 1605, 1503, 1426, 1336; HRMS calculated for $C_{20}H_{20}N_2O_3SNa^+$ (M + Na^+): 391.0868. Found: 391.1078.

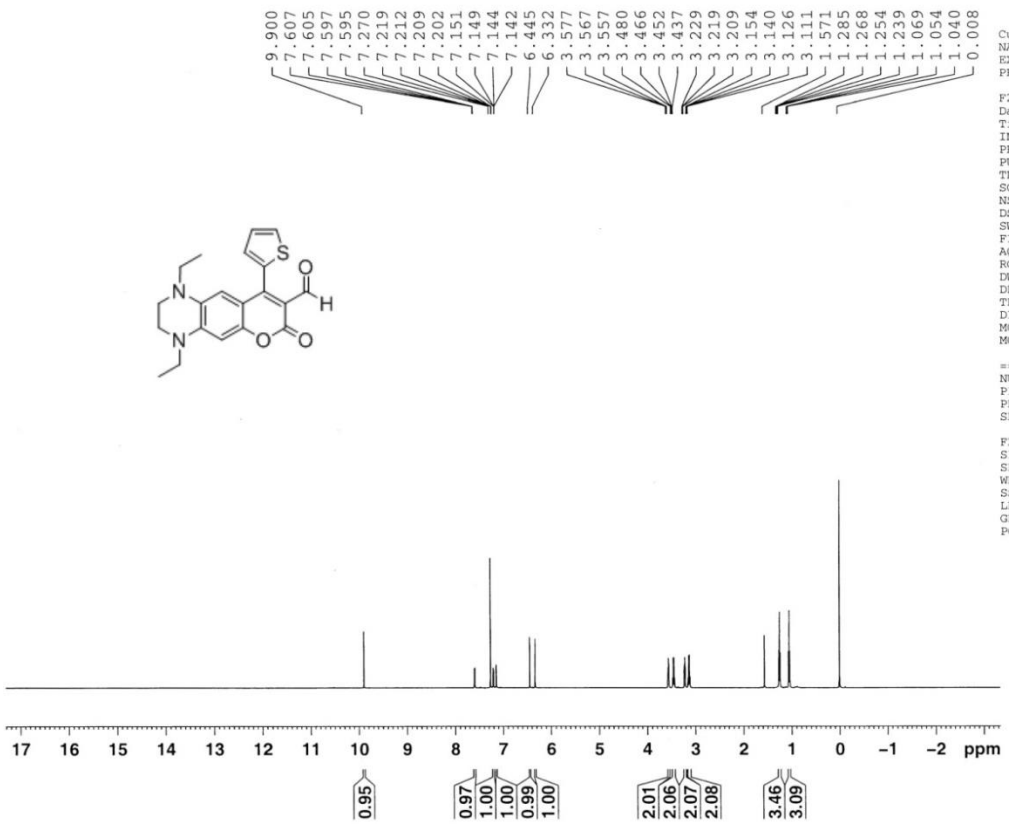
9.900
7.607
7.605
7.597
7.595
7.270
7.219
7.212
7.209
7.202
7.151
7.149
7.144
7.142
6.445
6.332
3.577
3.567
3.557
3.480
3.466
3.452
3.437
3.229
3.219
3.209
3.154
3.140
3.126
3.111
1.571
1.285
1.268
1.254
1.239
1.069
1.054
1.040
0.008
17 16 15 14 13 12 11 10 9 8 7 6 5 4 3 2 1 0 −1 −2 ppm
0.95
0.97
1.00
1.00
0.99
1.00
2.01
2.06
2.07
2.08
3.46
3.09

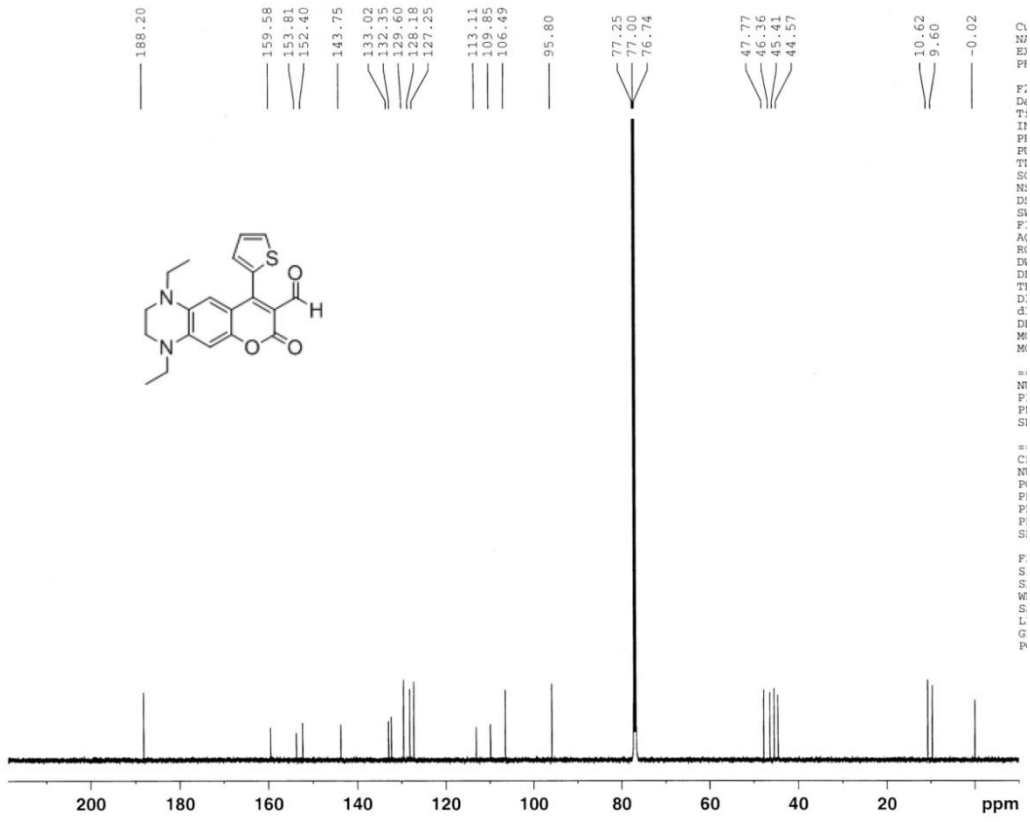
188.20
159.58
153.81
152.40
143.75
133.02
132.35
129.60
128.18
127.25
113.11
109.85
106.49
95.80
77.25
77.00
76.74
47.77
46.36
45.41
44.57
10.62
9.60
-0.02
200 180 160 140 120 100 80 60 40 20 ppm

REFERENCES

1. Bell, T. W.; Hext, N. M. *Chemical Society Reviews* **2004,** *33*, 589-598.
2. Lippincott-Schwartz, J. *Annu Rev Biochem* **2011,** *80*, 327-332.
3. (a) Bell, T. W.; Hext, N. M. Artificial Receptors for Chemosensors. In *Optical Biosensors: Present and Future*, Ligler, F. S.; Taitt, C. A. R., Eds. 2002; p 331; (b) Mohr, G. J. *Anal Bioanal Chem* **2006,** *386*, 1201-1214.
4. Wu, J.; Liu, W.; Ge, J.; Zhang, H.; Wang, P. *Chemical Society Reviews* **2011,** *40*, 3483-3495.
5. Feuster, E. K.; Glass, T. E. *J Am Chem Soc* **2003,** *125*, 16174-16175.
6. Xue, L.; Liu, C.; Jiang, H. *Org Lett* **2009,** *11*, 1655-1658.
7. Xu, Z.; Xiao, Y.; Qian, X.; Cui, J.; Cui, D. *Organic Letters* **2005,** *7*, 889-892.
8. Arimori, S.; Bosch, L. I.; Ward, C. J.; James, T. D. *Tetrahedron Letters* **2001,** *42*, 4553-4555.
9. de Silva, A. P.; Moody, T. S.; Wright, G. D. *Analyst* **2009,** *134*, 2385-2393.
10. Neelakandan, P. P.; Hariharan, M.; Ramaiah, D. *J Am Chem Soc* **2006,** *128*, 11334-11335.
11. Nolan, E. M.; Lippard, S. J. *Accounts of chemical research* **2008,** *42*, 193-203.
12. Miyawaki, A. *Annu Rev Biochem* **2011,** *80*, 357-373.
13. Lakowicz, J. R. *Principles of Fluorescence Spectroscopy*. Springer: 2007.
14. Dehmelt, L.; Bastiaens, P. I. *Nat Rev Mol Cell Biol* **2010,** *11*, 440-452.
15. Kalimuthu, P.; Abraham John, S. *Electrochimica Acta* **2011,** *56*, 2428-2432.
16. Stevens, D. R.; Schirra, C.; Becherer, U.; Rettig, J. *Front Synaptic Neurosci* **2011,** *3*, 2.
17. Borges, R.; Pereda, D.; Beltran, B.; Prunell, M.; Rodriguez, M.; Machado, J. D. *Cell Mol Neurobiol* **2010,** *30*, 1359-1364.
18. Jankowski, J. A.; Schroeder, T. J.; Ciolkowski, E. L.; Wightman, R. M. *J Biol Chem* **1993,** *268*, 14694-14700.

19. Zhang, K.; Chen, Y.; Wen, G.; Mahata, M.; Rao, F.; Fung, M. M.; Vaingankar, S.; Biswas, N.; Gayen, J. R.; Friese, R. S.; Mahata, S. K.; Hamilton, B. A.; O'Connor, D. T. *Curr Hypertens Rep* **2011,** *13*, 36-45.

20. Camacho, M.; Machado, J. D.; Alvarez, J.; Borges, R. *J Biol Chem* **2008,** *283*, 22383-22389.

21. Plattner, H.; Artalejo, A. R.; Neher, E. *The Journal of cell biology* **1997,** *139*, 1709-1717.

22. Heidelberger, R.; Waxham, M. N.; Byrne, J. H.; Roberts, J. L. *From Molecules to Networks: An Introduction to Cellular and Molecular Neuroscience*. Academic Press: 2009.

23. Cahill, A. L.; Eertmoed, A. L.; Mangoura, D.; Perlman, R. L. *Journal of neurochemistry* **1996,** *67*, 1217-1224.

24. Afework, M.; Burnstock, G. *Int J Dev Neurosci* **2005,** *23*, 567-573.

25. Gilabert, J. A.; Castejon, R.; Vargas, J. A.; Durantez, A.; Artalejo, A. R. *Cytometry* **1999,** *37*, 32-40.

26. Ciolkowski, E. L.; Cooper, B. R.; Jankowski, J. A.; Jorgenson, J. W.; Wightman, R. M. *Journal of the American Chemical Society* **1992,** *114*, 2815-2821.

27. Omiatek, D. M.; Dong, Y.; Heien, M. L.; Ewing, A. G. *ACS Chem Neurosci* **2010,** *1*, 234-245.

28. Chen, Y.; Zhang, K.; Wen, G.; Rao, F.; Sanchez, A. P.; Wang, L.; Rodriguez-Flores, J. L.; Mahata, M.; Mahata, S. K.; Waalen, J.; Ziegler, M. G.; Hamilton, B. A.; O'Connor, D. T. *Am J Hypertens* **2011,** *24*, 24-32.

29. Werner, F. M.; Covenas, R. *Int J Neurosci* **2010,** *120*, 455-470.

30. Yasuda, T.; Nakata, Y.; Choong, C. J.; Mochizuki, H. *Transl Neurodegener* **2013,** *2*, 16.

31. Chen, K. H.; Reese, E. A.; Kim, H. W.; Rapoport, S. I.; Rao, J. S. *J Alzheimers Dis* **2011,** *26*, 755-766.

32. Yanagisawa, N. *Parkinsonism & Related Disorders* **2006,** *12*, S40-S46.

33. Yao, H.; Li, S.; Tang, Y.; Chen, Y.; Chen, Y.; Lin, X. *Electrochimica Acta* **2009,** *54*, 4607-4612.

34. Crespi, F.; Croce, A. C.; Fiorani, S.; Masala, B.; Heidbreder, C.; Bottiroli, G. *J Neurosci Methods* **2004,** *140*, 67-73.

35. Siva, S.; Venkatesh, G.; Prabhu, A. A. M.; Sankaranarayanan, R.; Rajendiran, N. *Physics and Chemistry of Liquids* **2012,** *50*, 434-452.

36. Wang, H. Y.; Sun, Y.; Tang, B. *Talanta* **2002,** *57*, 899-907.

37. Slater, T. F. John Wiley & Sons: Amsterdam, 1980.

38. Okamura, H.; Tanaka, M.; Hisa, Y.; Nagatsu, I.; IBATA, Y. *Biogenic amines* **1992,** *9*, 195-204.

39. Rao, V. T.; Forrester, S. G.; Keller, K.; Prichard, R. K. *Int J Parasitol* **2011,** *41*, 249-254.

40. Chandra, S.; Wong, D. K. Y. Electrochemical Detection of Neurotransmitters at Structurally Small Electrodes. In *Nanostructured Materials for Electrochemical Biosensors*, Umasankar, Y.; Kumar, S. A.; Chen, S.-M., Eds. Nova Publishers: New York, 2009; pp 150-200.

41. Omiatek, D. M.; Bressler, A. J.; Cans, A. S.; Andrews, A. M.; Heien, M. L.; Ewing, A. G. *Sci Rep* **2013,** *3*, 1447.

42. Hashemi, P.; Dankoski, E. C.; Lama, R.; Wood, K. M.; Takmakov, P.; Wightman, R. M. *Proc Natl Acad Sci U S A* **2012,** *109*, 11510-11515.

43. Dernick, G.; Gong, L. W.; Tabares, L.; Alvarez de Toledo, G.; Lindau, M. *Nat Methods* **2005,** *2*, 699-708.

44. (a) Gubernator, N. G.; Zhang, H.; Staal, R. G.; Mosharov, E. V.; Pereira, D. B.; Yue, M.; Balsanek, V.; Vadola, P. A.; Mukherjee, B.; Edwards, R. H.; Sulzer, D.; Sames, D. *Science* **2009,** *324*, 1441-1444; (b) Lee, M.; Gubernator, N. G.; Sulzer, D.; Sames, D. *Journal of the American Chemical Society* **2010,** *132*, 8828-8830; (c) Rodriguez, P. C.; Pereira, D. B.; Borgkvist, A.; Wong, M. Y.; Barnard, C.; Sonders, M. S.; Zhang, H.; Sames, D.; Sulzer, D. *Proc Natl Acad Sci U S A* **2013,** *110*, 870-875.

45. Ki, H. A.; Naoghare, P. K.; Oh, B. K.; Choi, J. W.; Song, J. M. *Anal Biochem* **2009,** *388*, 23-27.

46. Walsh, R.; DeRosa, M. C. *Biochem Biophys Res Commun* **2009,** *388*, 732-735.

47. Tainaka, K.; Hasegawa, T.; Fukuda, M.; Nakano, S.; Fujieda, N.; Morii, T. *Nucleic Acids Symp Ser (Oxf)* **2008**, 201-202.

48. Hoss, W.; Smiley, C. *J Neurosci Res* **1977,** *3*, 249-256.

49. Kolusheva, S.; Molt, O.; Herm, M.; Schrader, T.; Jelinek, R. *J Am Chem Soc* **2005,** *127*, 10000-10001.

50. Helene, C.; Dimicoli, J. L.; Brun, F. *Biochemistry* **1971,** *10*, 3802-3809.

51. Annoni, C.; Nakata, E.; Tamura, T.; Liew, F. F.; Nakano, S.; Gelmi, M. L.; Morii, T. *Org Biomol Chem* **2012,** *10*, 8767-8769.

52. Yuan, J.; Wen, D.; Gaponik, N.; Eychmuller, A. *Angew Chem Int Ed Engl* **2013,** *52*, 976-979.

53. Dsouza, R. N.; Pischel, U.; Nau, W. M. *Chem Rev* **2011,** *111*, 7941-7980.

54. Kim, Y.-J. *Journal of Materials Science* **2013,** *48*, 3486-3493.

55. Reviriego, F.; Navarro, P.; Garcia-Espana, E.; Albelda, M. T.; Frias, J. C.; Domenech, A.; Yunta, M. J.; Costa, R.; Orti, E. *Org Lett* **2008,** *10*, 5099-5102.

56. Bracamonte, A. G.; Veglia, A. V. *Talanta* **2011,** *83*, 1006-1013.

57. Miskolczy, Z.; Biczok, L.; Megyesi, M.; Jablonkai, I. *J Phys Chem B* **2009,** *113*, 1645-1651.

58. Jun, E. J.; Liu, H.; Choi, J. Y.; Lee, J. Y.; Yoon, J. *Sensors and Actuators B: Chemical* **2013,** *176*, 611-617.

59. Secor, K. E.; Glass, T. E. *Org Lett* **2004,** *6*, 3727-3730.

60. Klockow, J. L.; Hettie, K. S.; Glass, T. E. *ACS Chem Neurosci* **2013**.

61. Hettie, K. S.; Liu, X.; Gillis, K. D.; Glass, T. E. *ACS Chem Neurosci* **2013,** *4*, 918-923.

62. Moro, M. A.; Lopez, M. G.; Gandia, L.; Michelena, P.; Garcia, A. G. *Anal Biochem* **1990,** *185*, 243-248.

63. Yang, Y.; Craig, T. J.; Chen, X.; Ciufo, L. F.; Takahashi, M.; Morgan, A.; Gillis, K. D. *J Gen Physiol* **2007,** *129*, 233-244.

64. Rasband, W. S. *Imagej* , U.S. National Institutes of Health, Bethesda, Maryland. http://imagej.nih.gov/ij/.

65. Kobayashi, T.; Urano, Y.; Kamiya, M.; Ueno, T.; Kojima, H.; Nagano, T. *J Am Chem Soc* **2007,** *129*, 6696-6697.

66. Miura, T.; Urano, Y.; Tanaka, K.; Nagano, T.; Ohkubo, K.; Fukuzumi, S. *J Am Chem Soc* **2003,** *125*, 8666-8671.

67. Urano, Y.; Kamiya, M.; Kanda, K.; Ueno, T.; Hirose, K.; Nagano, T. *J Am Chem Soc* **2005,** *127*, 4888-4894.

68. Shieh, P.; Hangauer, M. J.; Bertozzi, C. R. *J Am Chem Soc* **2012,** *134*, 17428-17431.

69. Ueno, T.; Urano, Y.; Setsukinai, K.; Takakusa, H.; Kojima, H.; Kikuchi, K.; Ohkubo, K.; Fukuzumi, S.; Nagano, T. *J Am Chem Soc* **2004,** *126*, 14079-14085.

70. Mineno, T.; Ueno, T.; Urano, Y.; Kojima, H.; Nagano, T. *Org Lett* **2006,** *8*, 5963-5966.

71. Sunahara, H.; Urano, Y.; Kojima, H.; Nagano, T. *J Am Chem Soc* **2007,** *129*, 5597-5604.

72. Secor, K.; Plante, J.; Avetta, C.; Glass, T. *Journal of Materials Chemistry* **2005,** *15*, 4073-4077.

73. Burger, P. M.; Mehl, E.; Cameron, P. L.; Maycox, P. R.; Baumert, M.; Lottspeich, F.; De Camilli, P.; Jahn, R. *Neuron* **1989,** *3*, 715-720.

74. Riveros, N.; Fiedler, J.; Lagos, N.; Munoz, C.; Orrego, F. *Brain Res* **1986,** *386*, 405-408.

75. Schenck, S.; Wojcik, S. M.; Brose, N.; Takamori, S. *Nat Neurosci* **2009,** *12*, 156-162.

76. Mendez-Hernandez, D. D.; Tarakeshwar, P.; Gust, D.; Moore, T. A.; Moore, A. L.; Mujica, V. *J Mol Model* **2013,** *19*, 2845-2848.

77. Wu, L.; Burgess, K. *J Org Chem* **2008,** *73*, 8711-8718.

78. Yu, C.; Jiao, L.; Yin, H.; Zhou, J.; Pang, W.; Wu, Y.; Wang, Z.; Yang, G.; Hao, E. *European Journal of Organic Chemistry* **2011,** *2011*, 5460-5468.

79. Chen, Y.; Wan, L.; Zhang, D.; Bian, Y.; Jiang, J. *Photochem Photobiol Sci* **2011,** *10*, 1030-1038.

80. Yuan, L.; Lin, W.; Zheng, K.; He, L.; Huang, W. *Chem Soc Rev* **2013,** *42*, 622-661.

81. Escobedo, J. O.; Rusin, O.; Lim, S.; Strongin, R. M. *Curr Opin Chem Biol* **2010,** *14*, 64-70.

82. Hilderbrand, S. A.; Weissleder, R. *Current Opinion in Chemical Biology* **2010,** *14*, 71-79.

83. Oushiki, D.; Kojima, H.; Terai, T.; Arita, M.; Hanaoka, K.; Urano, Y.; Nagano, T. *J Am Chem Soc* **2010,** *132*, 2795-2801.

84. Filip, M.; Iordache, S.; Săftoiu, A.; Ciurea, T. *World journal of gastroenterology: WJG* **2011,** *17*, 9.

85. Monici, M. *Biotechnol Annu Rev* **2005,** *11*, 227-256.

86. Vinegoni, C.; Botnaru, I.; Aikawa, E.; Calfon, M. A.; Iwamoto, Y.; Folco, E. J.; Ntziachristos, V.; Weissleder, R.; Libby, P.; Jaffer, F. A. *Science Translational Medicine* **2011,** *3*, 84ra45.

87. Pansare, V. J.; Hejazi, S.; Faenza, W. J.; Prud'homme, R. K. *Chemistry of Materials* **2012,** *24*, 812-827.

88. Zhang, M. Y.; Beyer, C. E. *J Pharm Biomed Anal* **2006,** *40*, 492-499.

89. Yoshitake, T.; Kehr, J.; Todoroki, K.; Nohta, H.; Yamaguchi, M. *Biomed Chromatogr* **2006,** *20*, 267-281.

90. Wang, F.; Wu, Y.; Lu, K.; Ye, B. *Electrochimica Acta* **2013,** *87*, 756-762.

91. Liu, M.; Xiang, J.; Zhou, J.; Ding, H. *Journal of Electroanalytical Chemistry* **2010,** *640*, 1-7.

92. Hengstenberg, A.; Blöchl, A.; Dietzel, I. D.; Schuhmann, W. *Angewandte Chemie International Edition* **2001,** *40*, 905-908.

93. Wallingford, R. A.; Ewing, A. G. *Analytical chemistry* **1989,** *61*, 98-100.

94. (a) Stehouwer, J. S.; Goodman, M. M. *J Labelled Comp Radiopharm* **2013,** *56*, 114-119; (b) Paterson, L. M.; Kornum, B. R.; Nutt, D. J.; Pike, V. W.; Knudsen, G. M. *Med Res Rev* **2013,** *33*, 54-111.

95. Looger, L. L.; Griesbeck, O. *Curr Opin Neurobiol* **2012,** *22*, 18-23.

96. (a) Maiti, S.; Shear, J. B.; Williams, R. M.; Zipfel, W. R.; Webb, W. W. *Science* **1997,** *275*, 530-532; (b) Balaji, J.; Desai, R.; Kaushalya, S. K.; Eaton, M. J.; Maiti, S. *J Neurochem* **2005,** *95*, 1217-1226.

97. Chauveau, J.; Fert, V.; Morel, A. M.; Delaage, M. A. *Clinical Chemistry* **1991,** *37*, 1178-1184.

98. Adler, M.; Wacker, R.; Booltink, E.; Manz, B.; Niemeyer, C. M. *Nature Methods* **2005,** *2*, 147-149.

99. Kim, Y.; Swager, T. M. *Macromolecules* **2006,** *39*, 5177-5179.

100. Jagtap, A. R.; Satam, V. S.; Rajule, R. N.; Kanetkar, V. R. *Dyes and Pigments* **2009,** *82*, 84-89.

VITA

Kenneth Hettie was born in New Hartford, New York in 1978. He moved to Texas at a young age and grew up just outside of San Antonio. He decided to pursue studies in biochemistry and philosophy at Trinity University. After receiving his degrees in 2002, he attended law school at Seton Hall University and worked for a short time as an analytical chemist in industry. In 2006, he began graduate studies at the University of Missouri – Columbia and worked with Dr. Timothy Glass designing and synthesizing fluorescent sensors for biological analytes. After defending his thesis, he plans to commence postdoctoral studies with Dr. Eric Kool at Stanford University and later become a professor and principal investigator in academia.